UNIVERSITÀ DEGLI STUDI DI MILANO

DOTTORATO DI RICERCA IN SCIENZE FARMACEUTICHE
CICLO XXXVIII
DIPARTIMENTO DI SCIENZE FARMACEUTICHE

NANOSUSPENSIONS-BASED ORAL DELIVERY PLATFORMS - NANODPS

Settore CHEM-08/A - Tecnologia, socioeconomia e normativa dei medicinali e dei prodotti per il benessere e per la salute

Tesi redatta con il contributo finanziario dell'Unione europea - Next Generation EU e Novartis Pharma AG
CUP n. G43C22002470004

Erasmo Ragucci
Matr. R13946
ORCID n.0009-0000-8534-175X

TUTOR: Prof.ssa Lucia Zema

CO-TUTOR: Prof.ssa Alice Melocchi

TUTOR NOVARTIS PHARMA AG: Dott. Mauro Serratoni

COORDINATORE DEL DOTTORATO: Chiar.mo Prof. Giulio Vistoli

A.A. 2024-2025

Table of contents

Introduction page 1

Aim and structure of the thesis page 7

Chapter I

Part I

Feasibility of hot melt extrusion in converting water-based nanosuspensions into solid dosage forms page 27

Part II

Development of a predictive model for converting Nanosuspensions into solid dosage forms via hot melt extrusion page 62

Chapter II

Part I

Manual wet granulation as a laboratory-scale strategy for converting aqueous nanosuspensions into granules page 97

Part II

Twin-screw wet granulation: a novel continuous manufacturing approach for solidifying nanosuspensions page 123

Conclusions page 160

Acknowledgements page 164

Introduction

Over the past decade, advancements in *in silico* drug discovery methods, such as high-throughput screening approaches (*i.e.,* artificial intelligence, machine learning), computational and combinatorial chemistry, genomics, and proteomics approaches, have led to a sharp rise in the identification of new chemical entities (NCEs) [1-3]. These are often considered interesting drug candidates by modelling scientists because of their peculiar features, including strong affinity for target receptors and superior pharmacological activity.

Most of NCEs are either designed for or would significantly benefit from oral administration, which is preferable for its superior patients' compliance and comparatively lower manufacturing and administration costs. As a further confirmation, oral products are those with the greatest number of shares in the current pharmaceutical market, which makes the development of novel orally administered dosage forms containing NCEs an interesting and moderate-risk source of revenue for pharmaceutical companies. Indeed, upon oral intake, the main limiting step for drug absorption and thus for achieving effective concentrations in the bloodstream, aside from permeability, is represented by its rate of dissolution in the gastrointestinal (GI) fluids [4, 5].

Many NCEs exhibit physicochemical properties that include significant solubility limitations. Indeed, the molecule optimization process has guided the selection of candidates having high potency and selectivity towards their biological target, which could result in a high molecular weight, stable crystal lattice implying some degree of hydrophobicity (*i.e.,* high logP), making them poorly water-soluble compounds. These aspects could even hinder researchers from pursuing further development steps, as relevant finished products could hardly reach the pharmaceutical market. Despite their promising pharmacological profiles and potential therapeutic benefits, approximately 40% of NCEs have been discontinued during either early or late development stages due to their poor aqueous solubility and resulting low bioavailability [1, 6, 7].

Within this framework, different enabling strategies have been pursued to address the above-mentioned solubility and bioavailability issues. The more conventional approaches for instance involved: salt formation, use of co-solvent and surfactants, creation of pro-drugs, complexation with cyclodextrins, co-crystallization, manufacturing of amorphous solid dispersion, formulation into emulsions and

microemulsions. Although these approaches have achieved moderate success, emphasized the rising interest towards the identification of innovative and more efficient solutions that can be in principle applied to the majority of NCEs [8-15].

A significant step forward in this respect has been the increasing awareness of the benefits associated with the application of nanotechnology-based formulation strategies to poorly soluble drugs [16-19]. Indeed, it has enhanced the likelihood of transitioning high-risk drug candidates from the discovery phase through formulation and ultimately to clinical application, effectively addressing limitations inherent in earlier methodologies.

Among these strategies, nano-sizing poorly soluble active ingredients (*i.e.,* reducing their particle size to a 10–1000 nm range by maintaining the crystallinity) with the attainment of a nanosuspension (NSs) was preliminarily demonstrated an effective approach, allowing to attain a marked increase in the powder surface area which, as indicated by the Noyes-Whitney dissolution model, would result in an improved dissolution rate and bioavailability [20-24].

In addition to enhancing oral bioavailability through improved solubility and dissolution rate, drug nanoparticles exhibit a broad spectrum of advantageous properties [25]. For instance, the relatively large surface area nanosized drug are provided with would facilitate adhesiveness to different surfaces (*i.e.,* cells, membranes). This property can potentially extend their gastrointestinal residence, thus providing a longer time for relevant dissolution and absorption. The administration of nano-sized drugs was also shown to reduce inter-subject variability and differences between fasted and fed states, minimizing the impact of the so-called food effect, ultimately improving efficacy and safety of the treatment [2, 9, 26]. Furthermore, nano-sizing would enhance the saturation solubility by significantly decreasing the thickness of the diffusion layer surrounding the drug particles, thereby accelerating the diffusion rate of dissolved molecules [27]. Reducing particle size to the nanoscale improves passive targeting, allowing the resulting nanoparticles to more effectively navigate and accumulate in specific tissues or cells. Finally, it might also allow to achieve higher drug loading.

In this context, there is a growing interest in assessing both the feasibility and the effects of reducing drug particle size to the nano-range, especially when dealing with

drug candidates encountering formulative challenges, such as high dosage requirements, low aqueous solubility coupled with large molecular weight and elevated melting point, inability to form salt, and ultimately high lipophilic nature. This is particularly relevant when scientists deal with active ingredients belonging to classes II and IV of the Biopharmaceutical Classification System (BCS), which include molecules that are challenging in terms of solubility [28-30].

From a composition standpoint, NSs are nano-dispersed solid-liquid (S/L) systems consisting of submicron colloidal drug particles in a crystalline solid-phase state, which are dispersed in an aqueous medium and maintained by a range of different excipients, such as ionic surfactants or non-ionic polymers. The former enables nanoparticle surface charging, *i.e.* generating repulsive electrostatic forces between similarly charged particles, and lowers surface free energy by reducing the interfacial tension between the solid particle and the aqueous medium. Non-ionic polymers confer colloidal stability through a dual mechanism: firstly, being absorbed onto the surface of nanoparticles and extending hydrophilic chains, they establish a steric barrier that hinders particle growth and effectively preserves the nanoscale dimensions; secondly, by increasing the viscosity of the dispersion medium, they limit Brownian motion and reduce the frequency of interparticle collisions. Therefore, a rational combination of such excipients can provide a synergistic mechanism of stabilization, thereby preserving a uniform dispersion of nanoparticles. This approach effectively prevents particles from aggregation or sedimentation phenomena from attractive interparticle forces (*e.g.,* Van der Waals interaction) [31-33].

In terms of NS manufacturing, both “top-down” and “bottom-up” technologies were proposed. While the former relies on the application of mechanical stress (*i.e.,* milling, high-pressure homogenization, microfluidization, co-grinding) to a coarse suspension, thus reducing large drug particles to a smaller dimension, the latter consists of a controlled condensation/aggregation of particles from a molecular dispersed state (*i.e.,* solvent-antisolvent method, supercritical fluid process, liquid emulsion technique). The manufacturing methods might have a marked impact on the formation and stability of NSs, and thus on their overall performance. Although in “top-down” techniques no hazardous solvents are involved, the process could generate an elevated amount of

heat, which could degrade or compromise the processing of thermosensitive drugs. In addition, crystal defects and amorphization of specific regions would occur due to high surface energetics involved during such processes, which overall may impair the physical and chemical stability of the resulting NSs. On the other hand, “bottom-up” processes generally entail the use of organic solvents, which are challenging to remove and whose residues may lead to formulation instability, *e.g.* formation of unstable polymorphs, hydrates, and solvates. Moreover, the peculiar rod-shaped particles, resulting from unique directional growth typically involved in these methodologies, may impact the physical stability of the NSs [34-36].

Being a water-based liquid system and irrespective of the manufacturing method used, NSs are also accompanied by major challenges, intended as physical and chemical instability phenomena. Indeed, the large surface area of the drug particles generates high total surface energy and, consequently, the surface free energy, leading to a thermodynamically unstable system. Therefore, drug nanoparticles are more prone to agglomerate, minimizing the surface energy, but leading to unfavourable physical issues for NSs, including sedimentation or creaming (*i.e.,* depending on particles' relative density within the formulation medium), crystal growth (*i.e.,* Ostwald ripening), and inconsistent dosing. Moreover, the primary concern associated with crystalline state transitions lies in the potential transformation between amorphous and crystalline forms.

High-energy input processes, which include both “top-down" and “bottom-up” manufacturing techniques, often lead to the formation of partially or fully amorphous NSs, which are thermodynamically unstable and tend to recrystallize over time into the more stable, low-energy crystalline state. Consequently, it would be particularly hard to ensure that the size of the drug particles would remain stable at the nano-scale level upon long-term storage [37-39].

Although chemical instability is generally less frequent, as it is inherently dependent on the specific molecular structure of the active compound, in specific cases, the presence of specific functional groups and their associated reactivity pathways dictates the susceptibility of each molecule to degradation. For instance, ester and amide moieties are particularly prone to hydrolytic degradation, whereas amino functionalities are often vulnerable to oxidative degradation processes. At the same

time, being NSs water-based products, microbial growth and contamination might occur, which cannot be prevented by simply adding preservatives to the formulation, as they are well-known for destabilizing NSs due to their liquid nature [40-46].

Despite the above-mentioned challenges, NSs are raising a lot of attention in the drug delivery field, an appeal that is further strengthened by their simple composition, minimal excipient requirements, and ease of manufacturing as well as of scale-up up [47-49]. Moreover, they become to be proposed as intermediates for the manufacturing of solid drug products. Indeed, transforming NSs into more convenient oral solid products would be highly advantageous, for instance to improve relevant stability and handling. Moreover, transforming NSs into solid products could be integrated into industrial manufacturing processes, offering improved stability during transport and storage, and supporting large-scale production [30, 40, 48, 50]. At the same time, this approach may also improve compliance among patients who typically avoid liquid products, while offering potential benefits for manufacturing and supply chain costs. This way, it would also be possible to widen and promote the applications of nano-based formulations into late development and commercial stages, which is still a hard-to-reach goal, especially when the parenteral administration route is involved. To enable the conversion from liquid NS to a monolithic solid dosage form in which nanocrystals are embedded, different methodologies and processing strategies have been applied in the literature, such as spray- and freeze-drying, fluid-bed coating, granulation, pelletization, extrusion, and printing [51-59].

Aim and structure of the thesis

Technological approaches to transform NSs into solid oral dosage forms (*e.g.,* powder, granules, pellets, capsules, tablets, and films) focus on preserving the original nanometric characteristics of the drug and bioavailability advantages achieved, while allowing flexibility in formulation design as well as dosing, stability over the product shelf-life, and improved compliance [30, 40, 48, 50].

In the current scientific literature, powders are extensively investigated when testing the feasibility of converting NSs into more stable, solid dosage forms. This choice probably relies on powder versatility, ease of processing, and ability to be further formulated into more complex products such as tablets, capsules, or granules even being the base for drug delivery systems (DDSs) development. However, the selection of the proper drying process has a pivotal role, as it can lead to undesirable criticisms. Therefore, NSs based on thermostable drugs are typically converted into dry powders using techniques such as spray-drying or fluidized bed drying, whereas freeze-drying and vacuum drying are more appropriate for formulations with thermosensitive compounds. Indeed, consisting of the atomization and solvent evaporation of a liquid feed by means of a nozzle and heated air, spray drying represents a flexible, continuous, one-step process extensively investigated for converting liquid NSs into dried particles. Notably, it enables precise control over critical quality attributes, such as particle size distribution, morphology, density, and residual moisture content, through the optimization of formulation composition and process parameters. Despite its effectiveness in transforming nanosuspensions into powders, this method presents several challenges, including possible degradation of thermolabile drugs, particle agglomeration, and high energy demand.

On the other hand, lyophilization constitutes a valuable process when dealing with thermolabile drugs. It involves the removal of solvents from a frozen solution or suspension under vacuum *via* sublimation, while preserving the structural integrity of the product. This process enhances stability over long-term storage and yields highly porous systems having low moisture content, which can be rapidly reconstituted upon the addition of an appropriate amount of aqueous media. While effective, this manufacturing technique is associated with significant constraints, being not only time- and energy-consuming, but also costly, limiting its scalability. Moreover, freezing and desiccation stresses involved during the process can compromise

nanoparticles' stability and promote agglomeration. To minimize these effects, primary drying must be conducted below the collapse temperature, and cryoprotectants should be incorporated prior to lyophilization to enhance stability.

Overall, although spray- and freeze-drying are the most commonly employed strategies to address NSs solidification, resulting powders often exhibit poor flowability and hygroscopicity constraints, which lead to significant challenges in the downstream processing leading to the final dosage forms (*e.g.,* tablets and capsules) [60-65]

Recently, the idea of exploring alternative processes for converting NS into solid products has started to populate the scientific literature, with scientists testing their direct incorporation into multiparticulate systems (*i.e.,* pellets, granules, sugar beads) or their use as functional coatings, depending on the targeted dosage form and performance [66-71]. Indeed, granulation and pelletization processes, as well as fluidized bed coating, represent attractive strategies to bridge the advantages of nanotechnology with those associated with multi-particulate solid dosage forms, opening new avenues for the development of patient-tailored drug delivery systems. Indeed, multi-particulate systems are inherently characterized by numerous benefits, including minimized risk of dose dumping and gastric emptying dependence, as well as shorter gastric residence time. Furthermore, they contribute to minimizing interindividual variability in gastrointestinal transit, promote a more uniform drug distribution in the GI tract that helps mitigate local irritation, enhance bioavailability, lower systemic toxicity, and support more predictable pharmacokinetic profiles. In addition, these systems demonstrate excellent physicochemical and technological properties when compared to spray-dried or lyophilized powders, including high stability, favourable flow characteristics, ease of dose handling, low hygroscopicity, and elevated bulk density, all of which contribute to improved performance across a range of pharmaceutical applications. Indeed, multi-particulate products can be administered as such or further formulated into other dosage forms such as capsules or tablets.

From the manufacturing point of view, several techniques, such as extrusion-spheronization, powder layering, spray-granulation, twin-screw granulation, shear-

granulation, and melt extrusion, can be used to transform NSs into solid multi-particulate products [72-79].

Based on the above-mentioned premises, the purpose of this PhD project was to combine solubility enhancement provided by NSs with relevant transformation in cost-saving and higher stability products having patient-compliant administration mode, *i.e.* to be orally administered. Besides the manufacturing of immediate release (IR) dosage forms, the project also aims at using NSs for the preparation of drug delivery systems (DDSs) intended to modulate the release performance of the active ingredient conveyed based on specific therapeutic as well as patient needs (*e.g.,* prolonged release). The project started in collaboration with Novartis Pharma AG, Basel, and benefited from the support, expertise, and know-how of the Materials Science Unit of their Pharmaceutical and Development Department (PHAD).

The initial phase of the research focused on selecting a model drug substance that could significantly take advantage of enhanced dissolution rate, and consequently improved bioavailability, through particle size reduction to the nanoscale. During this ideation phase, an extensive screening of over one hundred compounds was carried out, based on a set of pre-defined criteria, which were solubility, melting point, pKa, high occupation exposure limits, existing scientific background regarding the production of relevant NSs, and market presence. This structured approach led to the creation of a database to support the rational selection of the most suitable candidate for manufacturing the mock case study NS. Taking also into account the experience of the Novartis research team, the weakly basic compound Cinnarizine (CN) was selected as a model active for further testing. Indeed, CN has been extensively investigated by the particle engineering scientists of the team as a reference poorly water-soluble active pharmaceutical ingredient (API) [45]. CN is a highly lipophilic (*i.e.,* logP = 5.71) weak base (pKa_1 = 1.95, pKa_2 = 7.47) active compound, with a poor aqueous solubility (0.75 mg/mL), a melting point (T_m) of 118-122 °C, and currently formulated in marketed products as tablets and capsules. Moreover, based on the spectrum of pharmacological action, it needs to be administered 2-3 times a day in a 25-75 mg dosing range [80].

The production stage of the CN-based NS was demanded to the Novartis research team, targeting an API concentration of 10%. Based on previous experience, a "top-down" process was employed, entailing a wet-media milling equipment and the setting

of already tested and consolidated operating process parameters [28]. Initially, a stabilizer screening was carried out: D-alpha-tocopheryl polyethylene glycol 1000 succinate (TPGS), hydroxypropyl methylcellulose (HPMC) 603, and Kollidon® VA 64 alone or in combination with anionic surfactants (*i.e.,* dioctyl sulfosuccinate sodium salt and sodium lauryl sulphate) were considered, testing the resulting NS for key quality parameters (*e.g.,* particle size distribution, viscosity and microscopically). From this pre-formulation study, a TPGS-based NS was selected as the proper case study, eliminating the other investigated stabilizers due to instability issues (*i.e.,* coarse particles leading to sedimentation and high viscosity). More in detail, TPGS was selected for its amphiphilic nature, high physical stability, and low toxicity, which make it particularly suitable for nanostructured formulations. Its additional properties, such as P-glycoprotein inhibition, antioxidant activity, and solubilizing capacity, further contribute to its effectiveness as a stabilizing agent in oral drug delivery systems [81].

A thorough physical-chemical and biological characterization of the CN NS was deemed the first essential step of the work, also to ensure quality, stability, and performance of all the subsequent research steps. Given the critical influence of the particle size, morphology, crystallinity, and dissolution behaviour on the bioavailability of CN, a multi-technique approach was adopted. This choice allowed gaining a comprehensive understanding of the NS properties and verifying the absence of undesired instability while processing.

A comprehensive physicochemical characterization of the CN NS was performed to establish reference data for subsequent formulation studies. Particle size analysis and zeta potential measurements provided information on the nanocrystals' dimensional distribution and surface charge, which are critical parameters for predicting stability and processing behaviour, indicating a relatively uniform size distribution and a stable system. Differential Scanning Calorimetry (DSC) allowed the identification of the thermal signature of both CN and the stabilizer (*i.e.,* TPGS), serving as a reference for monitoring potential alterations during downstream processing. Morphological assessment by Scanning Electron Microscopy (SEM) enabled the visualization of particle shapes and size heterogeneity, providing insight into the potential packing, aggregation, and distribution of particles in downstream solid formulations.

Spectroscopic techniques, including confocal Raman microscopy (CRM) and Fourier-Transform Infrared (FTIR) spectroscopy, were employed to identify molecular fingerprints of the formulation components and to verify the absence of major chemical interactions or amorphization. In addition, biorelevant dissolution testing was conducted to establish a baseline performance of the CN NS, providing a benchmark for evaluating whether the nanocrystalline advantages, such as enhanced dissolution rate, were maintained upon conversion into solid dosage forms. Finally, preliminary in vitro assays using Caco-2 monolayers confirmed the suitability of the NS for subsequent biological investigations, ensuring non-cytotoxic concentrations and supporting its potential for oral bioavailability enhancement.

Proceeding with the ideation phase on a more solid basis, several solidification strategies were considered to enable the CN-NS conversion into oral dosage forms, ranging from conventional methods widely employed in the pharmaceutical industry to more innovative and emerging technologies. To this end, both extrusion-based (*e.g.,* Hot Melt Extrusion, HME) and spray-based (*e.g.,* Wet Granulation, WG) techniques were identified as particularly promising, owing to the specific advantages they offer in terms of formulation flexibility, scalability, and compatibility with continuous manufacturing. These techniques were selected not only based on their technological relevance but also considering the prior expertise acquired by the research group in which this Ph.D. project was performed. Their established applicability to a broad range of formulations and their capability to produce versatile solid dosage forms, *i.e.* either targeting IR or modified release (MR) products, further supported their selection for feasibility studies. During the subsequent Lab and Feasibility phases, HME and WG were the technologies explored for transforming the NS. Initially, a systematic screening of various polymeric carriers was manually carried out to identify the most suitable excipients to be used in the solidification process prior to switching to a larger manufacturing platform. HME is notable for not needing organic solvents, reducing processing and drying time, supporting continuous manufacturing, enabling simple scale-up, and facilitating prolonged-release drug delivery due to its high-density matrix. However, the high processing temperatures, shear forces, and energy input involved in HME impose constraints on the selection of thermally and mechanically stable APIs and excipients, which may limit its applicability in certain cases [82, 83].

On the other hand, wet granulation (WG) was deemed as "a must-have technique" to be investigated. Starting from a limited amount of material, lab-scale WG was initially performed to broaden the range of polymers to be tested for the manufacturing of granules, which could serve as an intermediate that could be further processed to attain tablets.

The work done led to a deep understanding of the limitations as well as the strengths relevant to the two previously mentioned techniques. More in detail, in the case of HME, the selection of suitable carriers was carried out by considering various properties, such as their solubility, which would influence the release performance of the resulting HME prototypes, their potential for hot-processability, and their compatibility with the thermal properties of CN. The latter aspect proved particularly challenging due to the low melting point of the selected API (approximately 120 °C), which needed to remain crystalline to preserve the properties of the starting NS. The study served as a proof-of-concept for the feasibility of using HME for converting NSs into multi-particulate solid dosage forms, showing both immediate and modified release profiles. The results confirmed HME as a versatile platform suitable for both small- and large-scale applications, enabling a single-step conversion process compatible with continuous manufacturing. In particular, the study demonstrated the potential of polymethacrylate-based polymers (*i.e.,* various grades of Eudragit®) in hot processing as a platform capable of preserving the nano-crystalline properties of the NS. On the other hand, being a preliminary qualitative screening study, it became evident that there was also a need to quantify the actual amount of API that remained in its original crystalline form *versus* the fraction that had dissolved into the carrier. As a result, the need for a more rational, model-based approach (*i.e.,* predictive modelling), to anticipate the solid-state interactions between the drug compound and the selected polymers, allowing a more accurate estimation of the suitable processing conditions turned out to be evident. This awareness prompted a collaboration with the research groups of the Institute for Particle Technology (iPAT), the Center of Pharmaceutical Engineering (PVZ), and the Institute of Pharmaceutical Technology and Biopharmaceutics at Technische Universität Braunschweig (Germany), aimed at building a predictive model. The latter was applied to the same class of polymers previously selected (*i.e.,* Eudragit® RL and RS) but using naproxen (NAP) as an

alternative model compound, to overcome the limitations encountered with the low melting CN. Indeed, NAP is a hydrophobic (*i.e.,* logP 3.18) weak acid (*i.e.,* pKa = 4.15) poorly soluble drug (*i.e.,* 0.016 mg/mL), and it has a T_m of 152-154 [84]. In this part of the project, the experimental phase began with the development of a predictive model in the form of a temperature-concentration phase diagram. The objective was to predict the behaviour of NAP in various polymers when subjected to different hot-processing techniques. To build this model, the Gordon-Taylor equation for glass transition temperature (T_g) line and an empirical equation for solid-liquid equilibrium curve modeling were employed, using specifically designed DSC-based thermal analysis protocols. In order to establish a comparative reference, a NAP-containing NS was produced and characterized in terms of its particle size distribution, revealing a monodisperse colloidal system. Multiple hot-processing techniques were evaluated, including vacuum compression molding (VCM) and hot-melt extrusion (HME), using two extruders differing in production scale (Haake™ MiniLab II, Thermo Fisher Scientific, Milan, Italy; the ZSE 12 HP-PH-40D (Leistritz Extrusionstechnik GmbH, Nürnberg, Germany). Through extensive qualitative and quantitative characterization of the resulting solid systems, including thermal analysis (*i.e.,* differential scanning calorimetry), imaging analysis (*i.e.,* CRM and SEM), and Raman spectroscopy, it was possible to demonstrate the potential of the predictive model in assessing the physical stability of both nano- and micro-sized NAP within the polymeric matrices. This approach provided essential guidance for rational decision-making, such as the selection of optimal processing conditions to preserve the desired crystalline fraction, as well as for identifying the most robust formulations suitable for subsequent scale-up and hot-processing.

In parallel, WG was also explored as an alternative strategy for the NSs solidification, to attain solid dosage forms able to preserve the critical quality attributes of the original formulations containing CN. In this context, polymers with moisture-adsorbing properties were included due to their specific physical-chemical characteristics, which allowed the system to tolerate high liquid loads without negatively affecting nanocrystal size or dissolution performance, while also maintaining the physical-technological properties of the resulting products. This approach was proven effective

in attaining multi-particulate systems preserving particle size, thermal stability, and rapid dissolution performance of the starting CN NS. Subsequently, to enable the translation of this process into an industrial-scale continuous manufacturing setting, particular attention was paid to the formulation design, which was specifically tailored to meet the requirements of a twin-screw wet granulation (TSWG) process. This part of the project was carried out entirely within the facilities of the Novartis Pharma AG (Basel), under the supervision of the Materials Science Unit team and of the Continuous Manufacturing team, who kindly provided access to the equipment for the execution of the experimental activities. Formulations were further optimized by combining soluble fillers, commonly used in wet granulation process (*i.e.,* lactose and mannitol), with insoluble excipients (*i.e.,* hydrated colloidal silicon dioxide, partially pregelatinized maize starch) capable of efficiently managing liquid absorption under high-shear, high-throughput conditions. In this regard, a lab-scale TSWG platform was investigated as a novel and scalable continuous manufacturing strategy for the solidification of NSs. The process was based on a dry binder addition approach. To support the development with a rational approach, a Design of Experiments (DoE) strategy was implemented using a full factorial design (2^3). This allowed systematic investigation of both formulation and process parameters, ensuring robustness, reproducibility, and in-depth process understanding. Overall, the downstream processing of the model NS through TSWG was successfully demonstrated. The process showed strong adaptability to various production scales, ranging from early-phase clinical development to large-scale manufacturing, while preserving the biopharmaceutical advantages of the original nanosuspension.

All the results reported in the thesis have already been disclosed, *i.e.* published, submitted for publication, or presented in the form of poster communications to international conferences.

The data and results obtained throughout the course of this research will be presented in this doctoral thesis according to the following sequence, which reflects the logical progression of the experimental work, the development of the formulations, and the underlying scientific rationale. This structure has been designed to guide the reader

through the key phases of the project, from initial screening activities to more advanced experimental investigations:

Chapter I

- Feasibility of hot melt extrusion in converting water-based nanosuspensions into solid dosage forms (*Part I*);
- Development of a predictive model for converting Nanosuspensions into solid dosage forms via hot melt extrusion (*Part II*).

Chapter II

- Manual wet granulation as a laboratory-scale strategy for converting aqueous nanosuspensions into granules (*Part I*);
- Twin-screw wet granulation: a novel continuous manufacturing approach for solidifying nanosuspensions (*Part II*).

References

1. E. Ahire, S. Thakkar, M. Darshanwad, and M. Misra, "Parenteral nanosuspensions: a brief review from solubility enhancement to more novel and specific applications," Sep. 01, 2018, *Chinese Academy of Medical Sciences*. doi: 10.1016/j.apsb.2018.07.011.
2. S. Jacob, A. B. Nair, and J. Shah, "Emerging role of nanosuspensions in drug delivery systems," Jan. 15, 2020, *BioMed Central Ltd.* doi: 10.1186/s40824-020-0184-8.
3. C. Sarkar *et al.*, "Artificial Intelligence and Machine Learning Technology Driven Modern Drug Discovery and Development," Feb. 01, 2023, *MDPI*. doi: 10.3390/ijms24032026.
4. N. Rasenack and B. W. Müller, "Micron-Size Drug Particles: Common and Novel Micronization Techniques," 2004. doi: 10.1081/PDT-120027417.
5. Stegemann Sven, Moreton Chris, Svanbäck Sami, Box Karl, Motte Geneviève, and Paudel Amrit, "Trends in oral small-molecule drug discovery and product development based on product launches before and after the Rule of Five," *Drug Discov Today*, vol. 28, no. 2, Feb. 2023, doi: https://doi.org/10.1016/j.drudis.2022.103344.
6. Y. Lu, Y. Li, and W. Wu, "Injected nanocrystals for targeted drug delivery," Mar. 01, 2016, *Chinese Academy of Medical Sciences*. doi: 10.1016/j.apsb.2015.11.005.
7. R. Shegokar and R. H. Müller, "Nanocrystals: Industrially feasible multifunctional formulation technology for poorly soluble actives," Oct. 2010. doi: 10.1016/j.ijpharm.2010.07.044.
8. B. Xie, Y. Liu, X. Li, P. Yang, and W. He, "Solubilization techniques used for poorly water-soluble drugs," Nov. 01, 2024, *Chinese Academy of Medical Sciences*. doi: 10.1016/j.apsb.2024.08.027.
9. E. Merisko-Liversidge and G. G. Liversidge, "Nanosizing for oral and parenteral drug delivery: A perspective on formulating poorly-water soluble compounds using wet media milling technology," 2011. doi: 10.1016/j.addr.2010.12.007.

10. K. T. Savjani, A. K. Gajjar, and J. K. Savjani, "Drug Solubility: Importance and Enhancement Techniques," *ISRN Pharm*, vol. 2012, pp. 1–10, Jul. 2012, doi: 10.5402/2012/195727.
11. A. T. M. Serajuddin, "Salt formation to improve drug solubility," Jul. 30, 2007. doi: 10.1016/j.addr.2007.05.010.
12. D. H. Jornada, G. F. Dos Santos Fernandes, D. E. Chiba, T. R. F. De Melo, J. L. Dos Santos, and M. C. Chung, "The prodrug approach: A successful tool for improving drug solubility," Jan. 01, 2016, *MDPI AG*. doi: 10.3390/molecules21010042.
13. K. U. Khan, M. U. Minhas, S. F. Badshah, M. Suhail, A. Ahmad, and S. Ijaz, "Overview of nanoparticulate strategies for solubility enhancement of poorly soluble drugs," Feb. 15, 2022, *Elsevier Inc.* doi: 10.1016/j.lfs.2022.120301.
14. G. Kuminek, F. Cao, A. Bahia de Oliveira da Rocha, S. Gonçalves Cardoso, and N. Rodríguez-Hornedo, "Cocrystals to facilitate delivery of poorly soluble compounds beyond-rule-of-5," Jun. 01, 2016, *Elsevier B.V.* doi: 10.1016/j.addr.2016.04.022.
15. S. V. Bhujbal *et al.*, "Pharmaceutical amorphous solid dispersion: A review of manufacturing strategies," Aug. 01, 2021, *Chinese Academy of Medical Sciences*. doi: 10.1016/j.apsb.2021.05.014.
16. S. Verma, Y. Lan, R. Gokhale, and D. J. Burgess, "Quality by design approach to understand the process of nanosuspension preparation," *Int J Pharm*, vol. 377, no. 1–2, pp. 185–198, Jul. 2009, doi: 10.1016/j.ijpharm.2009.05.006.
17. V. Patel and Y. Agrawal, "Nanosuspension: An approach to enhance solubility of drugs," *J Adv Pharm Technol Res*, vol. 2, no. 2, p. 81, 2011, doi: 10.4103/2231-4040.82950.
18. E. Merisko-Liversidge, G. G. Liversidge, and E. R. Cooper, "Nanosizing: A formulation approach for poorly-water-soluble compounds," 2003. doi: 10.1016/S0928-0987(02)00251-8.
19. P. Lakshmi and G. A. Kumar, "NANOSUSPENSION TECHNOLOGY: A REVIEW."

20. S. M. Dizaj, Z. Vazifehasl, S. Salatin, K. Adibkia, and Y. Javadzadeh, “Nanosizing of drugs: Effect on dissolution rate,” 2015.
21. Noyes Arthur A. and Wihtney Willis R., “Per cent. 2 1. 7 7 THE RATE OF SOLUTION OF SOLID SUBSTANCES IN THEIR OWN SOLUTIONS,” *ournal of the American Chemical Society*, no. 19, pp. 930–934, Oct. 1897.
22. S. Goel, M. Sachdeva, and V. Agarwal, “Nanosuspension Technology: Recent Patents on Drug Delivery and their Characterizations,” *Recent Pat Drug Deliv Formul*, vol. 13, no. 2, pp. 91–104, Jun. 2019, doi: 10.2174/1872211313666190614151615.
23. J. Chingunpituk, “Nanosuspension Technology for Drug Delivery,” 2007.
24. S. P. Jadhav, S. K. Singh, and H. S. Chawra, “Review on Nanosuspension as a Novel Method for Solubility and Bioavailability Enhancement of Poorly Soluble Drugs,” *Advances in Pharmacology and Pharmacy*, vol. 11, no. 2, pp. 117–130, Apr. 2023, doi: 10.13189/app.2023.110204.
25. M. Sousa De Almeida, E. Susnik, B. Drasler, P. Taladriz-Blanco, A. Petri-Fink, and B. Rothen-Rutishauser, “Understanding nanoparticle endocytosis to improve targeting strategies in nanomedicine,” May 07, 2021, *Royal Society of Chemistry*. doi: 10.1039/d0cs01127d.
26. S. G. Pınar, H. Canpınar, Ç. Tan, and N. Çelebi, “A new nanosuspension prepared with wet milling method for oral delivery of highly variable drug Cyclosporine A: development, optimization and in vivo evaluation,” *European Journal of Pharmaceutical Sciences*, vol. 171, Apr. 2022, doi: 10.1016/j.ejps.2022.106123.
27. M. Bisrat and C. Nyström, “Physicochemical aspects of drug release. VIII. The relation between particle size and surface specific dissolution rate in agitated suspensions,” *Int J Pharm*, vol. 47, pp. 223–231, 1988.
28. A. Bitterlich *et al.*, “Process parameter dependent growth phenomena of naproxen nanosuspension manufactured by wet media milling,” *European Journal of Pharmaceutics and Biopharmaceutics*, vol. 92, pp. 171–179, 2015, doi: 10.1016/j.ejpb.2015.02.031.
29. G. L. Amidon, H. Lennernäs, V. P. Shah, and J. R. Crison, “A theoretical basis for a biopharmaceutic drug classification: the correlation of in vitro

drug product dissolution and in vivo bioavailability," *Pharm Res*, vol. 12, 1995.

30. S. Jacob, F. S. Kather, S. H. S. Boddu, M. Attimarad, and A. B. Nair, "Nanosuspension Innovations: Expanding Horizons in Drug Delivery Techniques," Jan. 01, 2025, *Multidisciplinary Digital Publishing Institute (MDPI)*. doi: 10.3390/pharmaceutics17010136.
31. H. T. Phan and A. J. Haes, "What Does Nanoparticle Stability Mean? HHS Public Access," *J Phys Chem C Nanomater Interfaces*, vol. 123, no. 27, pp. 16495–16507, 2019, doi: 10.1021/acs.jpcc.
32. B. E. Rabinow, "Nanosuspensions in drug delivery," Sep. 2004. doi: 10.1038/nrd1494.
33. Y. Ma, Z. Cong, P. Gao, and Y. Wang, "Nanosuspensions technology as a master key for nature products drug delivery and In vivo fate," Jun. 01, 2023, *Elsevier B.V.* doi: 10.1016/j.ejps.2023.106425.
34. S. Verma, R. Gokhale, and D. J. Burgess, "A comparative study of top-down and bottom-up approaches for the preparation of micro/nanosuspensions," *Int J Pharm*, vol. 380, no. 1–2, pp. 216–222, Oct. 2009, doi: 10.1016/j.ijpharm.2009.07.005.
35. K. V. Mahesh, S. K. Singh, and M. Gulati, "A comparative study of top-down and bottom-up approaches for the preparation of nanosuspensions of glipizide," *Powder Technol*, vol. 256, pp. 436–449, 2014, doi: 10.1016/j.powtec.2014.02.011.
36. R. H. Müller, S. Gohla, and C. M. Keck, "State of the art of nanocrystals - Special features, production, nanotoxicology aspects and intracellular delivery," May 2011. doi: 10.1016/j.ejpb.2011.01.007.
37. R. Kodipyaka and S. Govindu, "Recent Trends in Top-Down Technologies for the Preparation of Nanosuspensions," Apr. 01, 2025, *Association of Pharmaceutical Teachers of India*. doi: 10.5530/ijper.20256434.
38. B. Van Eerdenbrugh, G. Van den Mooter, and P. Augustijns, "Top-down production of drug nanocrystals: Nanosuspension stabilization, miniaturization and transformation into solid products," Nov. 19, 2008. doi: 10.1016/j.ijpharm.2008.07.023.

39. A. Ahmadi Tehrani, M. M. Omranpoor, A. Vatanara, M. Seyedabadi, and V. Ramezani, "Formation of nanosuspensions in bottom-up approach: theories and optimization," Jun. 01, 2019, *Springer*. doi: 10.1007/s40199-018-00235-2.
40. M. Malamatari, S. Somavarapu, K. M. G. Taylor, and G. Buckton, "Solidification of nanosuspensions for the production of solid oral dosage forms and inhalable dry powders," Mar. 03, 2016, *Taylor and Francis Ltd*. doi: 10.1517/17425247.2016.1142524.
41. S. Verma, S. Kumar, R. Gokhale, and D. J. Burgess, "Physical stability of nanosuspensions: Investigation of the role of stabilizers on Ostwald ripening," *Int J Pharm*, vol. 406, no. 1–2, pp. 145–152, Mar. 2011, doi: 10.1016/j.ijpharm.2010.12.027.
42. A. Tuomela, J. Hirvonen, and L. Peltonen, "Stabilizing agents for drug nanocrystals: Effect on bioavailability," May 20, 2016, *MDPI AG*. doi: 10.3390/pharmaceutics8020016.
43. Y. Wang, Y. Zheng, L. Zhang, Q. Wang, and D. Zhang, "Stability of nanosuspensions in drug delivery," 2013, *Elsevier B.V.* doi: 10.1016/j.jconrel.2013.08.006.
44. D. R. Ely, R. Edwin García, and M. Thommes, "Ostwald-Freundlich diffusion-limited dissolution kinetics of nanoparticles," *Powder Technol*, vol. 257, pp. 120–123, 2014, doi: 10.1016/j.powtec.2014.01.095.
45. A. Bitterlich *et al.*, "Challenges in nanogrinding of active pharmaceutical ingredients," *Chem Eng Technol*, vol. 37, no. 5, pp. 840–846, 2014, doi: 10.1002/ceat.201300697.
46. L. Wu, J. Zhang, and W. Watanabe, "Physical and chemical stability of drug nanoparticles," May 30, 2011. doi: 10.1016/j.addr.2011.02.001.
47. R. BAZAK, M. HOURI, S. EL ACHY, W. HUSSEIN, and T. REFAAT, "Passive targeting of nanoparticles to cancer: A comprehensive review of the literature," *Mol Clin Oncol*, vol. 2, no. 6, pp. 904–908, Nov. 2014, doi: 10.3892/mco.2014.356.

48. V. P. Chavda, D. A. Vaghela, H. K. Solanki, P. C. Balar, S. Modi, and N. R. Gogoi, "Nanosuspensions: A new era of targeted therapeutics," Mar. 01, 2025, *Editions de Sante*. doi: 10.1016/j.jddst.2025.106613.
49. K. B. Sutradhar, S. Khatun, and I. P. Luna, "Increasing possibilities of nanosuspension," 2013. doi: 10.1155/2013/346581.
50. V. P. Chavda, D. A. Vaghela, H. K. Solanki, P. C. Balar, S. Modi, and N. R. Gogoi, "Nanosuspensions: A new era of targeted therapeutics," Mar. 01, 2025, *Editions de Sante*. doi: 10.1016/j.jddst.2025.106613.
51. R. M. Hanwate, R. H. Babu, A. A. Wadhave, and V. Mishra, "Advancements in Nanosuspension Technology for Drug Delivery," 2025, *Springer Nature*. doi: 10.1007/s44174-025-00368-4.
52. M. V. Chaubal and C. Popescu, "Conversion of nanosuspensions into dry powders by spray drying: A case study," *Pharm Res*, vol. 25, no. 10, pp. 2302–2308, Oct. 2008, doi: 10.1007/s11095-008-9625-0.
53. M. Wewers *et al.*, "Evaluation of the Formulation Parameter-Dependent Redispersibility of API Nanoparticles from Fluid Bed Granules," *Pharmaceutics*, vol. 14, no. 8, Aug. 2022, doi: 10.3390/pharmaceutics14081688.
54. N. Anup, S. Thakkar, and M. Misra, "Formulation of olanzapine nanosuspension based orally disintegrating tablets (ODT); comparative evaluation of lyophilization and electrospraying process as solidification techniques," *Advanced Powder Technology*, vol. 29, no. 8, pp. 1913–1924, Aug. 2018, doi: 10.1016/j.apt.2018.05.003.
55. R. Baumgartner, A. Eitzlmayr, N. Matsko, C. Tetyczka, J. Khinast, and E. Roblegg, "Nano-extrusion: A promising tool for continuous manufacturing of solid nano-formulations," *Int J Pharm*, vol. 477, no. 1, pp. 1–11, 2014, doi: 10.1016/j.ijpharm.2014.10.008.
56. J. Khinast, R. Baumgartner, and E. Roblegg, "Nano-extrusion: A one-step process for manufacturing of solid nanoparticle formulations directly from the liquid phase," *AAPS PharmSciTech*, vol. 14, no. 2, pp. 601–604, Jun. 2013, doi: 10.1208/s12249-013-9946-0.

57. S. Ubgade, V. Kilor, V. Bahekar, and A. Ittadwar, "Formulation development of immediate release pellets of tadalafil: Solidification approach for nanosuspension," *International Journal of Applied Pharmaceutics*, vol. 11, no. 4, pp. 124–131, Jul. 2019, doi: 10.22159/ijap.2019v11i4.32331.
58. G. Germini and L. Peltonen, "3d printing of drug nanocrystals for film formulations," *Molecules*, vol. 26, no. 13, Jul. 2021, doi: 10.3390/molecules26133941.
59. E. Mutylo, O. Navrátil, A. Waněk, F. Šembera, and F. Štěpánek, "Formulation of minitablets with personalised dissolution profile by fluid-bed granulation of drug nanosuspensions," *Int J Pharm*, vol. 669, Jan. 2025, doi: 10.1016/j.ijpharm.2024.125013.
60. W. He, Y. Lu, J. Qi, L. Chen, L. Yin, and W. Wu, "Formulating food protein-stabilized indomethacin nanosuspensions into pellets by fluid-bed coating technology: Physical characterization, redispersibility, and dissolution," *Int J Nanomedicine*, vol. 8, pp. 3119–3128, Aug. 2013, doi: 10.2147/IJN.S46207.
61. N. O. Chung, M. K. Lee, and J. Lee, "Mechanism of freeze-drying drug nanosuspensions," *Int J Pharm*, vol. 437, no. 1–2, pp. 42–50, Nov. 2012, doi: 10.1016/j.ijpharm.2012.07.068.
62. E. Jakubowska, M. Bielejewski, B. Milanowski, and J. Lulek, "Freeze-drying of drug nanosuspension– study of formulation and processing factors for the optimization and characterization of redispersible cilostazol nanocrystals," *J Drug Deliv Sci Technol*, vol. 74, Aug. 2022, doi: 10.1016/j.jddst.2022.103528.
63. F. Kesisoglou, S. Panmai, and Y. Wu, "Nanosizing - Oral formulation development and biopharmaceutical evaluation," Jul. 30, 2007. doi: 10.1016/j.addr.2007.05.003.
64. M. A. Rahman, M. Mujahid, A. Hussain, and Z. Iqbal, "Development and pharmacokinetic evaluation of spray-dried self-nanoemulsifying drug delivery system of sertraline," *J Pharm Investig*, vol. 47, no. 4, pp. 325–333, Jul. 2017, doi: 10.1007/s40005-016-0263-y.

65. F. Sahnen, J. P. Kamps, and K. Langer, “Conversion of indomethacin nanosuspensions into solid dosage forms via fluid bed granulation and compaction,” *European Journal of Pharmaceutics and Biopharmaceutics*, vol. 154, pp. 89–97, Sep. 2020, doi: 10.1016/j.ejpb.2020.06.020.
66. K. Y. Wan, J. Weng, S. N. Wong, P. C. L. Kwok, S. F. Chow, and A. H. L. Chow, “Converting nanosuspension into inhalable and redispersible nanoparticles by combined in-situ thermal gelation and spray drying,” *European Journal of Pharmaceutics and Biopharmaceutics*, vol. 149, pp. 238–247, Apr. 2020, doi: 10.1016/j.ejpb.2020.02.010.
67. S. G. Pınar, A. N. Oktay, A. E. Karaküçük, and N. Çelebi, “Formulation Strategies of Nanosuspensions for Various Administration Routes,” May 01, 2023, *MDPI*. doi: 10.3390/pharmaceutics15051520.
68. E. H. Tan, J. Parmentier, A. Low, and J. P. Möschwitzer, “Downstream drug product processing of itraconazole nanosuspension: Factors influencing tablet material properties and dissolution of compacted nanosuspension-layered sugar beads,” *Int J Pharm*, vol. 532, no. 1, pp. 131–138, Oct. 2017, doi: 10.1016/j.ijpharm.2017.08.107.
69. N. C. Patel and H. A. Patel, “A Recent Solidification Approach for Nanosuspension: Formulation, Optimisation and Evaluation of Canagliflozin Immediate Release Pellets,” *Folia Med (Plovdiv)*, vol. 64, no. 3, pp. 488–500, 2022, doi: 10.3897/folmed.64.e68866.
70. M. R. P. Rao, R. V. Godbole, S. G. Borate, S. Mahajan, and T. Gangwal, “Nanosuspension coated multiparticulates for controlled delivery of albendazole,” *Drug Dev Ind Pharm*, vol. 47, no. 3, pp. 367–376, 2021, doi: 10.1080/03639045.2021.1879830.
71. B. N. Tran *et al.*, “Solidifying Fenofibrate Nanocrystal Suspension: A Scalable Approach via Granulation Method,” *J Nanomater*, vol. 2023, 2023, doi: 10.1155/2023/1672030.
72. G. J. Vergote *et al.*, “An oral controlled release matrix pellet formulation containing nanocrystalline ketoprofen,” 2001. [Online]. Available: www.elsevier.com/locate/ijpharm

73. I. Aghrbi, V. Fülöp, G. Jakab, N. Kállai-Szabó, E. Balogh, and I. Antal, "Nanosuspension with improved saturated solubility and dissolution rate of cilostazol and effect of solidification on stability," *J Drug Deliv Sci Technol*, vol. 61, Feb. 2021, doi: 10.1016/j.jddst.2020.102165.
74. V. Braig, C. Konnerth, W. Peukert, and G. Lee, "Enhanced dissolution of naproxen from pure-drug, crystalline nanoparticles: A case study formulated into spray-dried granules and compressed tablets," *Int J Pharm*, vol. 554, pp. 54–60, Jan. 2019, doi: 10.1016/j.ijpharm.2018.09.069.
75. B. Y. Gajera, D. A. Shah, and R. H. Dave, "Investigating a Novel Hot Melt Extrusion-Based Drying Technique to Solidify an Amorphous Nanosuspension Using Design of Experiment Methodology," *AAPS PharmSciTech*, vol. 19, no. 8, pp. 3778–3790, Nov. 2018, doi: 10.1208/s12249-018-1189-7.
76. L. Horster, A. Bernhardt, K. Kiehm, and K. Langer, "Conversion of PLGA nanoparticle suspensions into solid dosage forms via fluid bed granulation and tableting," *European Journal of Pharmaceutics and Biopharmaceutics*, vol. 134, pp. 77–87, Jan. 2019, doi: 10.1016/j.ejpb.2018.11.011.
77. P. Kayaert, M. Anné, and G. Van Den Mooter, "Bead layering as a process to stabilize nanosuspensions: Influence of drug hydrophobicity on nanocrystal reagglomeration following in-vitro release from sugar beads," *Journal of Pharmacy and Pharmacology*, vol. 63, no. 11, pp. 1446–1453, Nov. 2011, doi: 10.1111/j.2042-7158.2011.01351.x.
78. M. Li *et al.*, "Impact of matrix surface area on griseofulvin release from extrudates prepared via nanoextrusion," *Pharmaceutics*, vol. 13, no. 7, Jul. 2021, doi: 10.3390/pharmaceutics13071036.
79. J. Möschwitzer and R. H. Müller, "Spray coated pellets as carrier system for mucoadhesive drug nanocrystals," *European Journal of Pharmaceutics and Biopharmaceutics*, vol. 62, no. 3, pp. 282–287, Apr. 2006, doi: 10.1016/j.ejpb.2005.09.005.
80. K. Wening and J. Breitkreutz, "Oral drug delivery in personalized medicine: Unmet needs and novel approaches," Feb. 14, 2011. doi: 10.1016/j.ijpharm.2010.11.001.

81. S. Raghuvanshi and K. Pathak, “Recent Advances in Delivery Systems and Therapeutics of Cinnarizine: A Poorly Water Soluble Drug with Absorption Window in Stomach,” *J Drug Deliv*, vol. 2014, pp. 1–15, Nov. 2014, doi: 10.1155/2014/479246.
82. A. K. Mehata *et al.*, “Vitamin E TPGS-Based Nanomedicine, Nanotheranostics, and Targeted Drug Delivery: Past, Present, and Future,” Mar. 01, 2023, *MDPI*. doi: 10.3390/pharmaceutics15030722.
83. M. Maniruzzaman, J. S. Boateng, M. J. Snowden, and D. Douroumis, “A Review of Hot-Melt Extrusion: Process Technology to Pharmaceutical Products,” *ISRN Pharm*, vol. 2012, 2012, doi: 10.5402/2012/436763.
84. S. Tambe, D. Jain, Y. Agarwal, and P. Amin, “Hot-melt extrusion: Highlighting recent advances in pharmaceutical applications,” Jun. 01, 2021, *Editions de Sante*. doi: 10.1016/j.jddst.2021.102452.

Chapter I - Part I

The content of Chapter I - Part I has already been published in: Pharmaceutics **2025**, 17(5), 662; https://doi.org/10.3390/pharmaceutics17050662

Feasibility of Hot Melt Extrusion in Converting Water-Based Nanosuspensions into Solid Dosage Forms

Abstract

Aim: In addition to numerous benefits provided by nanosuspensions (NSs) (*e.g.,* enhanced saturation solubility, increased area for interaction with fluids), they suffer from major stability, handling and compliance issues. To overcome these challenges, we evaluated the feasibility of hot melt extrusion (HME) in transforming a cinnarizine-based NS, selected as a case study, into granules for oral intake. **Methods:** Thermoplastic polymers, in principle compatible with the thermal behavior of the selected drug and characterized by different interaction mechanisms with aqueous fluids, were used as carriers to absorb the NS and were processed by HME. **Results**: The extruded granules pointed out good physio-technological characteristics, a drug content > 85% with coefficient of variation (CV) < 5% and tunable in vitro performance coherent with the polymeric carriers they were composed of. Particle size as well as the solid state of cinnarizine was checked using several analytical techniques in combination (*e.g.,* DSC, SEM, FT-IR, Raman). Depending on the composition of the granules, and specifically for formulations processed below 85 °C, the drug was found to remain crystalline and in the desired nanoscale. **Conclusions:** HME turned out to be a versatile process to transform, in a single-step, NSs into multi-particulate solid products for oral administration showing a variety of release profiles.

Keywords: hot melt extrusion; nanosuspension; granules; immediate release; modified release

1. Introduction

In recent years, the advent of digital technologies, such as artificial intelligence, machine learning and high-throughput screening methods, has led to the development of numerous new chemical entities (NCEs) having a high affinity for the biological target and enhanced pharmacological activity [1–3]. In this field, major efforts were devoted to the development of solid products for oral administration, like tablets and capsules, containing such NCEs, to ensure high patient compliance and low manufacturing costs, thus facilitating their spread in the pharmaceutical market [4,5]. However, due to their relatively large molecular weight as well as chemical structures, many NCEs present permeability issues through the gastrointestinal (GI) membranes and poor solubility in the GI fluids, which could affect absorption and bioavailability upon oral intake [6,7].

To counteract solubility constraints, nano-sizing poorly soluble drugs, resulting in the attainment of NSs, has been widely investigated [8–10].

NSs are submicron colloidal, heterogeneous, aqueous dispersions of practically insoluble active ingredients with a particle size in the 1–1000 nm range, which are stabilized in their crystalline state by different excipients, such as surfactants and thickening agents [11]. They can be attained through top-down or bottom-up methods, the former relying on the application of mechanical stress, while the latter on a controlled condensation/aggregation of particles from a molecular dispersion [12]. Overall, NSs are characterized by many advantages such as *i)* enhanced specific surface area of the drug bulk and improved saturation solubility [13], which would result in a faster dissolution rate according to the Noyes–Whitney dissolution model [14], *ii)* greater surface of interaction of drug particles with the solvent [15] and *iii)* enhanced mucoadhesion, increasing their GI residence and thus the time available to complete the dissolution process [1]. However, they are also characterized by physical and chemical stability issues, resulting, for instance, in sedimentation, aggregation, solid-state transformation, dimensional alteration, and crystal growth [10,16,17].

To reduce these phenomena, removing water and transforming NSs into more convenient solid products, without losing the advantages related to the presence of the drug at the nano-scale, would be fundamental. As a first stage, researchers tested well-established spray-drying and freeze-drying technologies on NSs, improving their

stability and handling [18–23]. However, such traditional drying methods suffer from high energy consumption and long processing times, representing only the preliminary step in the manufacturing of a solid dosage form. On the other hand, attaining the final medicinal products taking advantage of the so-called continuous manufacturing approach has recently raised a lot of interest [24–28]. Indeed, it was demonstrated a suitable way to increase manufacturing efficiency as well as production rate while reducing expenses per unit, especially if coupled with real-time quality controls. In this respect, hot melt extrusion (HME) using Soluplus™ as the polymeric carrier was tested as an alternative and single-step process to transform NSs into solid products and was named nano-extrusion [29–31]. Indeed, hot-processing and particularly HME has recently emerged as a promising and versatile technology [31–36], not only towards the manufacturing of solid dispersions, but also to attain a variety of delivery systems (*e.g.,* granules, capsules, pellets, tablets, rings, implants, inserts), ranging from immediate to modified release, and intended for diverse administration routes.

Based on the above-mentioned considerations, in this work we intended to widen the range of formulations undergoing HME to directly transform a water-based NS into solid dosage forms for oral intake. More in detail, HME was carried out to manufacture, in a one-step process, multi-particulate systems (*i.e.,* granules) starting from a cinnarizine-containing NS (CN NS), which was employed as a noteworthy case study. Indeed, CN not only has a challenge of thermal behavior (*i.e.,* relatively low melting temperature, T_m) but could also represent a model compound for the class II of the Biopharmaceutical Classification Systems (BCSs), in which many NCEs fall [37]. For the sake of versatility, polymeric formulations in a diverse range of release performances (*i.e.,* immediate and prolonged release, targeted release to specific sites of the GI tract) were evaluated.

2. Materials and Methods

2.1. Materials

In this study, we used polyethylene oxides (**PEO**s) with different molecular weights (Sentry POLYOX™ WSR N10 LEO NF, **PEO N10**; Sentry POLYOX™ 303 LEO NF, **PEO 303**; Iff, Milan, Italy); polymethacrylates (Eudragit® RL PO, **Eu RL**;

Eudragit® RS PO, **Eu RS**; Eudragit® E PO, **Eu E**; Evonik, Essen, Germany); glycerol (**GLY**; A.C.E.F., Milan, Italy); polyethylene glycol 8000 (**PEG**; Clariant Masterbatches, Milan, Italy); triethyl citrate (**TEC**; Sigma Aldrich, Milan, Italy); sodium starch glycolate (EXPLOTAB® CLV, **EXP**; JRS PHARMA, Rosenber, Germany); hydrated dextrates (EMDEX®, **EMD**; JRS PHARMA, Rosenber, Germany); glycerol (**GLY**; Pharmagel, Lodi, Italy); hydroxypropyl methylcellulose (Pharmacoat® 603; Shin-Etsu Chemical Co., Tokyo, Japan); copovidone (Kollidon® VA 64, BASF SE, Ludwigshafen, Germany); dioctyl sulfosuccinate sodium salt (Sigma Aldrich, Darmstadt, Germany); sodium lauryl sulphate (Carl Roth, Karlsruhe, Germay); potassium dihydrogen phosphate (KH_2PO_4) (VWR, Milan, Italy); potassium monohydrogen phosphate (K_2HPO_4) (VWR, Milan, Italy); methanol (VWR, Milan, Italy); HCl (VWR, Milan, Italy); sodium cloride (NaCl) (VWR, Milan, Italy); epoxy resin (Araldite®, Velcro Brand, Deinze, Belgium).

CN NS was kindly supplied by Novartis Pharma AG (Basel, Switzerland) and contained d-a-tocopheryl polyethylene glycol 1000 succinate (TPGS, Sigma-Aldrich, Basel, Switzerland) as a steric stabilizer [38]. CN is a highly lipophilic BCS Class II drug, having a highly pH dependent solubility (0.29 mg/mL at pH 2, 0.017 mg/mL at pH 5, and 0.002 mg/mL at pH > 6.5) and T_m of 118–122 °C [39,40]. CN NS was manufactured by Novartis Pharma AG, according to previous studies [32].

2.2. Methods

2.2.1. Preparation of the CN NS

CN NS was attained via wet media milling (WMM), starting from a stabilized raw aqueous suspension (4:35:1, drug:water:stabilizer in *w*/*w*). Initially, stabilizers screening was carried out by Novartis Pharma AG (Basel, Switzerland). TPGS, hydroxypropyl methylcellulose and Kollidon® VA 64 alone or in combination with anionic surfactants (*i.e.,* dioctyl sulfosuccinate sodium salt and sodium lauryl sulphate) were considered, testing the resulting NS for key quality parameters (*e.g.,* particle size distribution, viscosity and microscopically), as before described [17,41]. From this pre-formulation study, the TPGS-containing NS resulted in the most promising candidate. With respect to the preparation of the stabilized raw aqueous suspension, 2.5% *w*/*w* TPGS was first dissolved in bidistilled water. Then, micronized CN powder

(10% *w*/*w*) was dispersed within the stabilizer solution (magnetic stirring for about 12 h), until a homogeneous suspension was obtained. The latter underwent WMM using an agitator bead mill (DELTAVITA® 15-300, Netzsch, Selb, Germany) equipped with 600 mL silicon carbide milling chamber and yttria zirconia beads of 0.1 mm in diameter (mass = 1547 g; ρ_{bulk} = 3.58 g/cm^3, Netzsch, Selb, Germany). The chamber was filled up to 80%. The pumping rotation speed was set at 30–80 rpm (13–33 L/h), while the mill rotation speed was 10 m/s. The temperature of the suspension was kept constant at the inlet (13 °C) and at the outlet (18 °C) of the milling chamber and the total processing time was around 6 h. The total mass of the CN NS manufactured via different batches was 2.5 kg (each batch size = 1 kg).

2.2.2. Particle Size (Z-Average) and Polydispersity Index (PdI) via Dynamic Light Scattering (DLS)

Z-average and PdI of CN nanoparticles (n = 3) were measured using Zetasizer nano ZSP (Malvern Panalytical Ltd., Milan, Italy). Before the analysis, samples were diluted (1:100) using a 0.1 mM NaCl solution and equilibrated for 120 s to ensure proper conditioning. The temperature was set at 25 °C and each analysis involved 10 measurements (100 s duration each).

The stability of the CN NS, stored in a refrigerator (VWR, Basel, Switzerland; 3 ± 1 °C), was checked measuring the Z-average and PdI at pre-established time periods (*i.e.,* up to 18 months).

2.2.3. Drug Content

CN content (n = 3) was determined using high-performance liquid chromatography (HPLC; HP 1100 ChemStations, Agilent Technologies, Milan, Italy). The latter was equipped with an UV-Vis detector and a reverse-phase column L-column (InertClone ODS, 150 × 4.6 mm 5 µm ODS(3) 100 Å, Phenomenex Inc., Aschaffenburg, Germany), maintained at 30 °C. The mobile phase, *i.e.* mixture of methanol and pH 3.5 phosphate buffer [42] in water for HPLC (70:30, *v*/*v*), was filtered before use (0.45 µm membrane filter) and pumped at a flow rate of 1 mL/min at 30 °C. The time of the run was set at 10 min. The sample to be evaluated (25 mg) was initially dispersed in 15 mL of mobile phase and then ultrasonicated at 25 °C for 30 min to ensure complete CN dissolution. The resulting liquid was filtered through a 0.22 µm syringe filter and

transferred into a HPLC vial kept at 30 °C, from which 10 µL were automatically injected into the HPLC system for being assayed spectrophotometrically (retention time = 4.7 min, λ = 250 nm). The CN content was calculated using a purposely built calibration curve in the 0.25–500 µg/mL range ($y = 33.581x + 5.0951$, $R^2 = 0.9998$).

2.2.4. Differential Scanning Calorimetry (DSC)

Thermal analysis was carried out by DSC (DSC Discovery, TA Instruments, Milan, Italy; DSC Stare System 1, Mettler-Toledo, Milan, Italy). Samples were accurately weighed (3–7 mg) and tested in sealed and pierced aluminium pans. The analysis was performed under a nitrogen atmosphere (N_2 80 mL/min), setting a single heating ramp (25 °C to 200 °C, rate 10 °C/min). To test the CN NS, the latter was oven dried (40 °C, 8 h; VWR, Milan, Italy) before performing the analysis.

2.2.5. HME

HME was performed in a twin-screw extruder (Haake™ MiniLab II, Thermo Fisher Scientific, Milan, Italy), equipped with counter-rotating conical screws and a rod-shaped die (custom-made in aluminum ø = 1.80 mm) [43,44]. The mixtures to be tested were prepared in a mortar and manually fed into the barrel of the equipment. The extrudability of placebo formulations was first assessed to identify suitable operating conditions, as described in the Results and Discussion section. Specifically, the process was performed setting different excipient-wise temperatures along the barrel, which were selected based on literature findings and preliminary DSC experiments), while the screw speed was modified in real-time to avoid any increase of the torque above 200 N·cm. During manufacturing, extruded rods were manually pulled out of the die, discarding the first and the last parts attained. Then, they were manually cut into 1.8 × 2 mm granules, which were checked for weight (analytical balance BP211, Sartorius, Milan, Italy) height and diameter (digital caliper, Milan, Italy) before being stored in a static oven at 40 °C (VWR, Milan, Italy).

2.2.6. Fourier-Transform Infrared (FT-IR) Spectroscopy

FT-IR analyses were carried out using an FT-IR Spectrometer (Spectrum One, Perkin Elmer, Rodgau, Germany), operating in the spectral region between 4000 and 650

cm^{-1}. The data were analyzed by transmittance technique with 32 scansions and 4 cm^{-1} resolution.

2.2.7. Confocal Raman Microscopy (CRM)

An Alpha 300 R confocal imaging system (WITec, Ulm, Germany) was used to collect both Raman spectra and relevant maps. The excitation wavelength of 532 nm, with a laser intensity of 12–15 mW, was provided by an Nd:YAG laser (WITec, Ulm, Germany). Offset correction was performed for each study by calibration against a silicate substrate. The hyperspectral grating was G1: 600 g/mm, BLZ 500.00 nm, with a spectral center at 2100 cm^{-1}. Scans were performed with an integration time of 50–100 ms using the WITec TrueSurface; an Mk3 extension with real-time large area topographic imaging module microscope was equipped with a Zeiss LD Plan-Neofluar 63× NA 0.75 objective (Zeiss, Oberkochen, Germany). For each sample, three fragments were randomly selected, embedded in epoxy resin, and kept at least for 24 h at room temperature to allow the resin to harden. The resulting resin blocks were cut using an ultra-microtome (Leica EM UC6, Wetzlar, Germany) to obtain level block cross-sections. Initially, large-area scans were acquired at low resolution (lateral 10 μm) to gain an overview of the spatial distribution and localization of the extrudate components. Subsequently, focused high-resolution area scans were carried out at 400 × 300 μm^2 with a lateral resolution of 1 μm, and at 100 × 100 μm^2 with a lateral resolution of 0.5 μm. Hyperspectral data processing, including offset, cosmic ray removal, baseline correction, spectral filter application, average spectral extraction and spectral map deconvolution was performed using WITec Project SIX Plus 6.2 software. The corresponding intensity maps were calculated by the application of WITec TrueComponent Analysis and thresholding. Reference material spectra, including those of CN and polymeric carriers, were obtained by single spectral measurements whereby characteristic peaks for each species were defined for hyperspectral processing.

2.2.8. Scanning Electron Microscopy (SEM)

Following surface chemical modification by gold plasma evaporation (~8 nm), SEM images were acquired (SEM GEMINI 300, Carl Zeiss AG, Jena, Germany) using an accelerating voltage of 4.0 kV and setting ~6 mm as the working distance. For the CN

NS, 5 µL was filtered (0.2 µm Nucleopore Track Etch membrane, Sigma Aldrich, Schnelldorf, Germany) and washed with 50 µL of ultrapure water before chemical modification.

2.2.9. In Vitro Performance

In vitro performance (n = 3) was evaluated in an acidic buffer (pH 1.2) using a USP Apparatus 4 (Sotax, Allschwil, Switzerland) equipped with cells for powder/granules, in which samples of 25 ± 2 mg were inserted before starting the test. The apparatus was operated in an open configuration, *i.e.* having a continuous flow of fresh media into the cells (8 mL/min) and automatic sampling of the latter at pre-established time points (5 mL every 5 min). The fluids collected were then analyzed via HPLC following the procedure described in 2.2.3 Drug content. Data were expressed as percentage of drug dissolved with respect to the actual drug content.

3. Results and Discussion

3.1. Selection of Polymeric Carriers

The main target of the present work was to demonstrate the possibility of using the HME technique to transform, in a single step, a model NS into solid units. These should maintain the initial advantageous characteristic of the NS (*i.e.,* the selected drug in the crystalline state, with the desired nano-scale particle size distribution), while being able to provide a range of release patterns. In this respect, the first part of the investigation was focused on the selection of carriers suitable for HME and with a potential towards both immediate and modified release. Overall, extrudability of the formulations was deemed the pivot of the research, being the thermal behavior of the selected drug (and thus its stability at the processing temperatures involved) and that of the polymers both crucial for making the transformation feasible [33]. For this reason, T_m, glass transition (T_g) and degradation temperatures of all the materials in use were carefully considered [34]. In this respect, identifying suitable polymeric carriers was particularly challenging in view of the low CN T_m. To avoid amorphization and to obtain a nanocrystal solid dispersion, HME temperatures should be kept to at least 20–30 °C below the drug melting point [35,36]. At the same time, proper processing generally requires operating at a minimum of 20 °C above the T_g of the polymeric carrier. For this reason, only polymers known to be extruded at

temperatures ≤ 100 °C were included in the screening. Willing to attain final products characterized by both immediate (IR) and prolonged release (PR) profiles, polymers with different interaction mechanism with aqueous fluids were considered. In this respect, HME already demonstrated being a versatile technology, able to process a wide range of materials [32,45,46]. Based on the above-mentioned considerations, details on the polymeric carriers selected for the work are reported below:

- **EXP:** it shows a thermoplastic behavior under thermo-mechanical activation and in the presence of water and of another plasticizer, such as GLY, to avoid relevant retrogradation [47]. After either HME or injection molding, it still maintains the ability to disintegrate.
- **PEO N10 and 303:** non-ionic thermoplastic homopolymers of ethylene oxide having T_m < 75 °C. They are soluble in water, with swelling capacity dependent on the molecular weight. They could thus be used for the development of both IR and swellable/erodible PR-release systems [48–50].
- **PEG:** highly hydrophilic soluble polymer characterized by low T_m (around 60 °C), which is mainly used for the production of solid dispersions and IR systems [51];
- **Eu RS, RL and E:** thermoplastic polymethacrylates with different thermal and solubility characteristics [45,52]. More into detail, Eu E is a cationic copolymer soluble in acidic media (up to pH 5.0) with a T_g of about 48 °C. Eu RL and Eu RS are insoluble cationic polymers sharing the same molecular structure but differing in the content of ammonium functional groups. This results in diverse permeability properties, with T_g values around 70 and 67 °C, respectively.
- **EMD:** water-soluble and lactose-free materials composed of glucose monohydrate and different polysaccharides derived from starch, showing a hot-processing aptitude similar to the latter [26,43].

3.2. Blend Preparation and HME Trials

To assess the potential of HME for the intended target, the high amount of water of the NS represented a key aspect towards the hot-processability of the selected carriers. In this respect, the work was further challenged by the availability of a lab-scale equipment with a very short barrel. This represented a major constraint. Indeed, the operator was forced to incorporate the desired load of CN (and thus the associated NS

volume) gradually into the polymeric carrier (*i.e.,* by repeating the wetting, kneading and drying steps several times) before loading the formulation into the extruder. First trials were performed on samples composed of the sole polymer, eventually plasticized, to rule out the capability of the various formulations towards water (used as a mock-up of the CN NS) incorporation. The pre-test consisted of wetting the selected polymers with the same amount of water contained in a 100 mg/g NS aliquot. This way, it was possible to estimate the number of granulation drying (40 °C) steps needed to avoid the formation of a paste that cannot be fed into the extruder. Overall, complete loading of the liquid took from 1 to 6 repeated stages, depending on the polymeric carrier considered. After addition of the proper type and amount of plasticizers, which were selected based on literature data and on previous findings collected in the lab, formulations underwent HME. The operating conditions set are reported in Table 1. These were selected considering the aspect of the extruded rods at the die and to avoid any temperature increase over 100 °C, which might have caused CN amorphization.

Table 1. HME parameters relevant to different formulations.

Formulation		**HME Conditions**			**Granulation-Oven Drying Steps, n°**
Polymeric Carrier	**Plasticizer, % on the Dry Carrier**	**T, °C**	**Screw Speed, rpm**	**Max Torque Recorded, N·cm**	
EXP	10% H_2O and 15% GLY	90	35	150	1
PEO N10	-	80	30	15	5
PEO 303	-	100	15	90	2
PEG	-	50–55	15	85	6
Eu RL	10% TEC	80	15	90	2
Eu RS	15% TEC	85	30	15	2
Eu E	5% TEC	80	30	30	2
EMD	10% GLY	50	30	40	6

Placebo extrudates showing either a non-uniform shape/diameter or characterized by extreme brittleness were discarded (*i.e.,* EXP- and EMD-based ones). Then, drug-containing formulations were prepared by using either the CN micronized powder (*i.e.,* reference extruded products manufactured for comparison purposes) or the CN NS, targeting a 10% *w*/*w* drug load in the final products. The granulation-drying steps and the operating conditions optimized for placebo formulations were employed.

The CN NS contained nanoparticles of ~500 nm with a PdI of 0.4 and was demonstrated dimensionally stable over time (Figure 1a). The thermal analysis of oven-dried aliquots of the NS highlighted the presence of two endothermic peaks, being the first related to the TPGS stabilizer (T_m = 40.44 °C) and the second sharp one ascribed to the CN melting (T_m = 117.04 °C) (Figure 1b) [53,54]. SEM was also performed to obtain a comprehensive morphological overview of the NS (Figure 1c) [55]. CN nanocrystals were characterized by two distinct shapes, *i.e.* cylindrical and ellipsoidal-spherical geometries, and resulted dimensionally polydisperse. Indeed, cylindrical needle-like particles, having a length between 0.4 and 4 μm, co-existed with rare spherical in-shape nanocrystals characterized by smaller dimensions (between 100 and 500 nm).

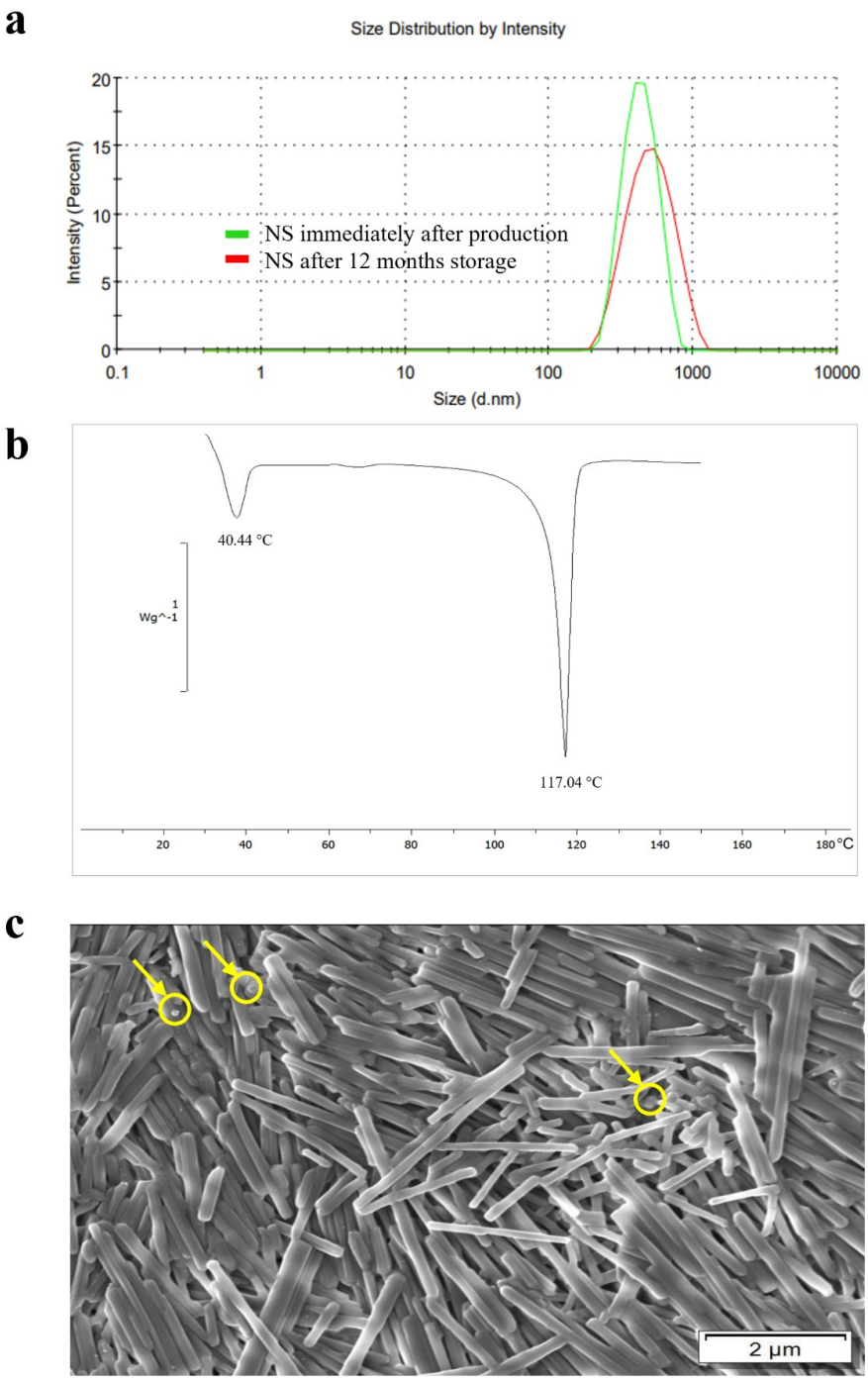

Figure 1. (**a**) Particle size and distribution of CN attained by DLS at different storage times together with the relevant (**b**) DSC thermogram and (**c**) SEM image showing the cylindrical and ellipsoidal-spherical (in yellow circles) geometries of CN nanoparticles.

3.3. Granule Characterization

All the granules attained, both placebo and CN-containing ones, showed an analogous aspect and homogeneous dimensional characteristics. The drug load was always higher than 85% (CV < 5%), highlighting a good processability of the formulations investigated, intended as good dispersibility of the nanocrystals in the wet mass during the initial granulation step and then in the molten formulation undergoing HME. Micro-scale insights on the extruded products were then obtained taking advantage of Raman confocal microscopy. Furthermore, in vitro performance of the finished granules was consistent with the characteristics of the polymeric carriers they were composed of [52,56] and was confirmed after 12 months of storage. Focusing on PEO N10-, PEG-, and Eu E-based IR units, the whole amount of drug was dissolved within 30 min (data reported in the subsequent chapters). On the other hand, all the PR carriers investigated were able to slow down drug release, with 100%, 25%, and <1% of CN released after 2 h of testing when dealing with PEO 303, Eu RL and Eu RS, respectively (Figure 2). Ensuring proper control of the release rate of CN, which is a poorly soluble drug, from PR multi-particulate systems could be especially challenging when the drug is loaded into the system as a NS (*i.e.,* a form intrinsically endowed with a higher solubility and dissolution rate in view of the particle size reduction up to the nanoscale). Indeed, in PR systems, the release rate must be controlled by the characteristics of the formulation (*e.g.,* permeability through the inert matrix or through the polymeric network of the swelled one) and not unintentionally determined by the very low tendency to dissolve of the conveyed drug.

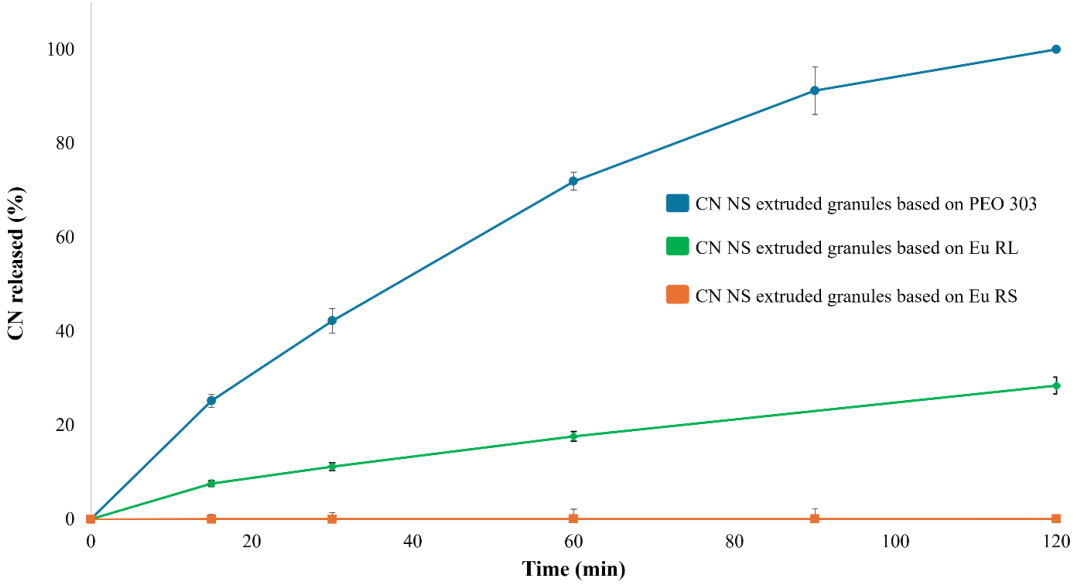

Figure 2. Release profiles (USP Apparatus 4 equipped with cells for powder/granules, acidic buffer pH 1.2 flowing at 8 mL/min, 5 mL of fluid sampled every 5 min) relevant to PR granules having different composition.

Several analytical techniques were employed to assess whether the CN nanocrystals remained dispersed within the HME granules. More into detail, by determining diagnostic peaks relevant to different molecular entities included in the specimens, FT-IR analysis helped in preliminarily verifying the composition of the sample. The presence of CN was associated with an intense band at 963 cm^{-1}, due to the =C─H bending within a double bond in trans configuration (Figure 3). In parallel, bands known for being characteristic of different polymer structures were ruled out. By way of example, the FT-IR spectra of formulations based on PEG and PEO N10 are reported in Figure 3 [57,58]. To complement the above-mentioned data, confocal Raman microscopy was selected as a suitable imaging approach to gain a deeper understanding of CN-polymeric carrier interactions and drug distribution within the polymer matrix. In particular, CN reference spectra were selected from the Novartis database, with spectral filters centred at 90, 119 and 218 cm^{-1} (lattice vibration frequencies), 1002 cm^{-1} (aromatic ring), 1597 cm^{-1} (aromatic ring) and 1654 cm^{-1} (C=C, double bond of the lateral chain) [59]. More specifically, the presence of characteristic shoulders in the diagnostic peaks at the lattice vibration frequencies were correlated to the presence of crystalline CN. On the other hand, based on previous

literature findings [60], excipient spectral extraction was determined using filters centred at:

- 363 cm^{-1} (C-O-C bending vibration), 1481 cm^{-1} (CH_2 bending), 2846 cm^{-1} (symmetric stretching of CH_2 in a saturated bond) and 2887 cm^{-1} (OH stretching) for PEO N10, PEO 303 and PEG 8000 (oxyethylene group CH_2-CH_2-O-);
- 1450 cm^{-1} (CH_2 methylene group), 1726 cm^{-1} (C=O stretching of the carbonyl group of ester function) and 2948 cm^{-1} (symmetric and asymmetric stretching of C-H in methyl and methylene functions) for Eu polymers;
- 866 cm^{-1}, 1739 cm^{-1} and 2940 cm^{-1} for TEC;
- 844 cm^{-1}, 1751 $cm^{-1}$and 2886 cm^{-1} for TPGS.

DSC and SEM analyses were employed to gain a further confirmation on the FT-IR results, particularly regarding the possibility that the HME process might have caused CN amorphization or had an impact on morphology, size and distribution of the drug nanocrystals within the polymeric matrices. In this respect, illustrative results, *i.e.* those useful to deepen the peculiarities of the various case studies investigated, are briefly presented in the following paragraphs.

3.3.1. PEG

Raman spectra collected from different areas of PEG-based granules were useful in appreciating the spatial distribution of the two main molecular entities identified (Figure 4a): *i)* an extruded homogeneous matrix, in which CN was mainly dispersed into the polymeric carrier (*i.e.,* blue sample area 1 in Figure 4b), and *ii)* well-demarcated PEG enclosures (*i.e.,* yellow sample area 2 in Figure 4b). The presence of the latter was attributed to an inadequate melting of the polymer, probably as a consequence of the limited residence time of the formulation within the barrel of the lab-scale equipment available, coupled with a too low extrusion temperature.

Although the slight presence of the shoulders of diagnostic peaks at the lattice vibration frequencies in the CN spectra may inform about the presence of undefined quantities of crystalline CN, the DSC profile (Figure 4c) was only characterized by *i)* in the presence of an endothermic sharp peak (T_m = 64.42 °C), which can be ascribed to the polymeric carrier melting point and *ii)* in the absence of peculiar CN endothermic peaks, suggesting amorphization of the majority of CN in the granules. Analogous profiles were obtained with the reference extruded specimens containing

CN powder as such , supporting the hypothesis of drug dissolution in the molten PEG. This result was in agreement with initial assessments of CN compatibility with different polymers carried out by DSC. Accordingly, the release performance of both extruded products (in acidic buffer, pH 1.2) was quite similar (Figure 4d). Only a slight difference could be noticed at the very beginning of the experiment. Indeed, after 3 min of testing, the amount of CN dissolved from the NS-based products was 15% greater than that relevant to samples containing the micronized drug powder.

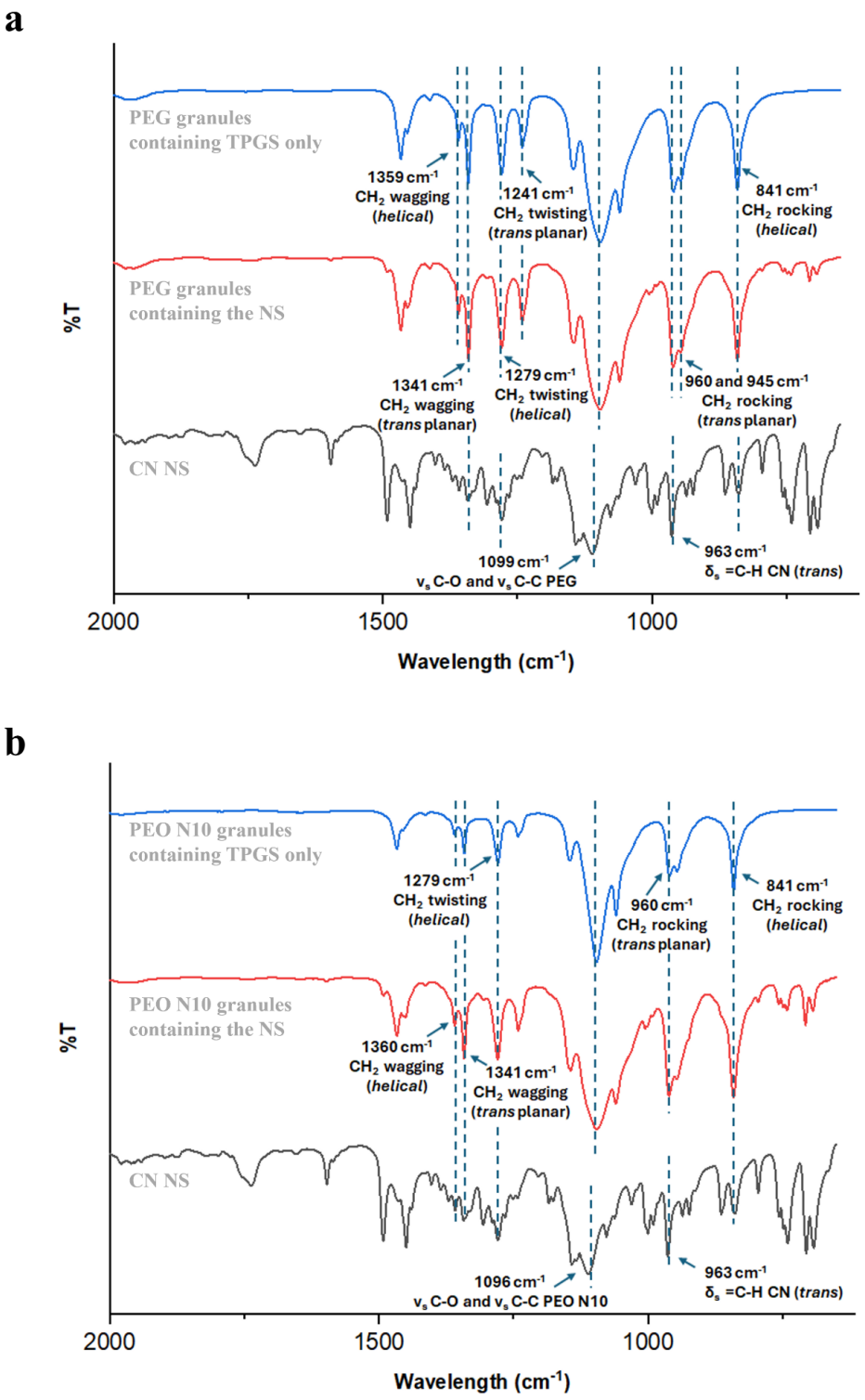

Figure 3. FT-IR spectra of (**a**) PEG- and (**b**) PEO N10-based granules.

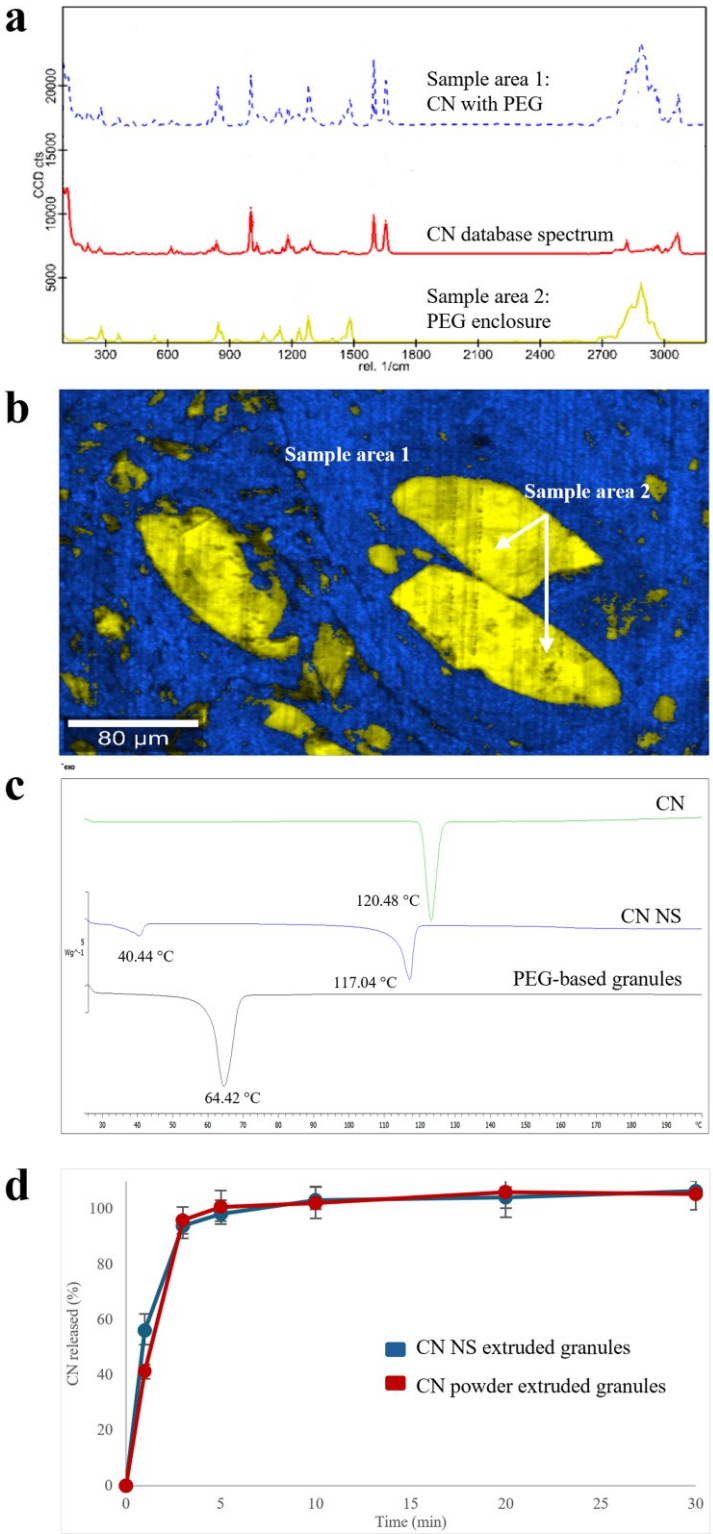

Figure 4. (**a**) Raman spectra, (**b**) Raman molecular map, (**c**) DSC thermograms and (**d**) release profiles (USP Apparatus 4 equipped with cells for powder/granules, acidic buffer pH 1.2 flowing at 8 mL/min, 5 mL of fluid sampled every 5 min) relevant to PEG-based products.

3.3.2. PEO N10

Focusing on Raman spectra of samples based on low-molecular weight PEO, areas with different composition could be identified (Figure 5a,b): a homogeneous polymeric matrix containing amorphous CN (*i.e.,* blue sample area 1), in which spots of almost pure crystalline drug (*i.e.,* red sample area 3) or of polymeric matrix very highly concentrated in CN (*i.e.,* violet sample area 2) were randomly dispersed. The dissolution performance was coherent with the above-mentioned composition. Indeed, extruded granules containing CN NS were characterized by a faster dissolution rate with respect to the reference samples containing CN powder as such (Figure 5c), even in a poorly discriminating media for the drug of interest, such as the acidic buffer pH 1.2 (*i.e.,* a media in which drug solubility is relatively high). Also in this case, the CN amorphous quote was associated with dissolution of the drug in the polymer. In this respect, to increase the amount of crystalline matter within the product, it would be necessary to extrude the formulation at temperatures largely below drug T_m. However, this was hard to achieve due to the high polymer melt viscosity at lower temperatures with respect to those employed.

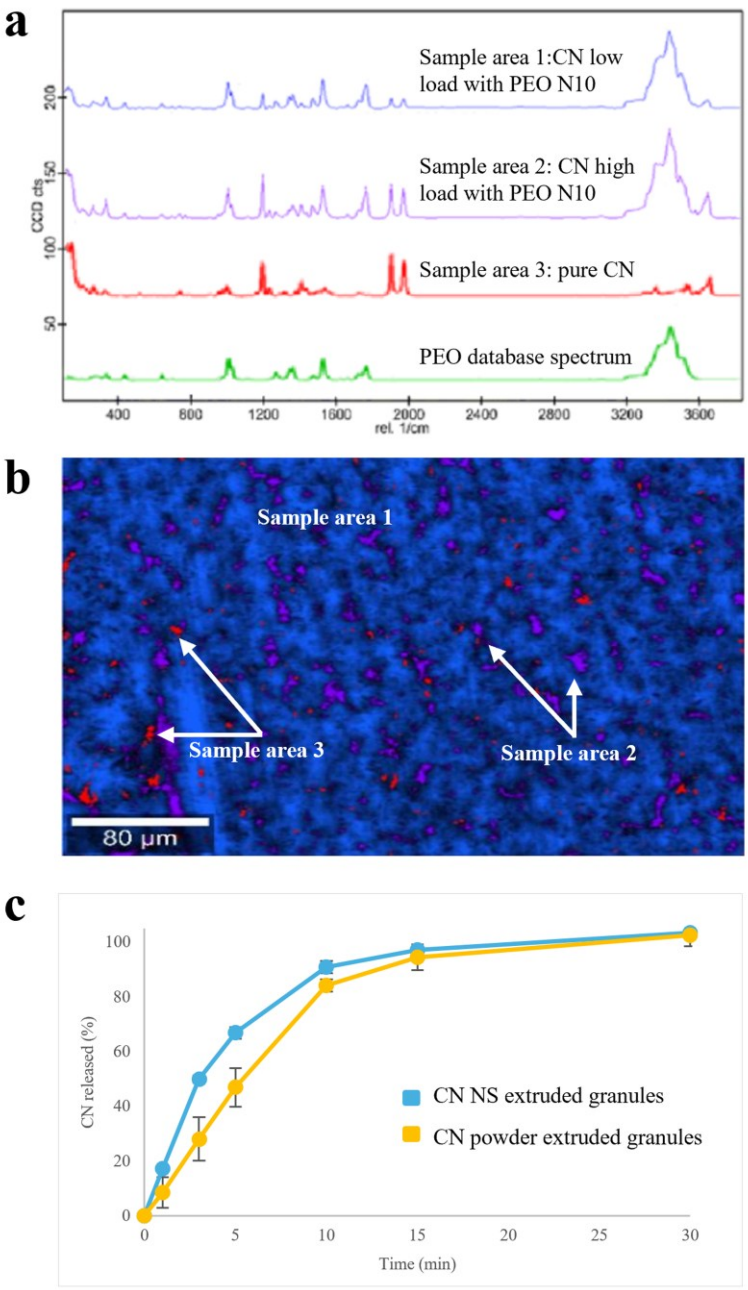

Figure 5. (**a**) Raman spectra, (**b**) Raman molecular map and (**c**) release profiles (USP Apparatus 4 equipped with cells for powder/granules, acidic buffer pH 1.2 flowing at 8 mL/min, 5 mL of fluid sampled every 5 min) relevant to PEO N10-based granules.

3.3.3. PEO 303

A high molecular weight PEO (*i.e.,* PEO 303), which is widely employed in the formulation of swellable/erodible PR matrices, was also screened. Focusing on Raman data, areas in which CN was embedded within the PEO matrix (*i.e.,* blue sample area 1 in Figure 6a,b) could be highlighted, the latter surrounding well-demarcated and segregated enclosures with a predominant polymeric composition (*i.e.,* green sample area 2 in Figure 6a,b). Although the presence of shoulders of diagnostic peaks at the lattice vibration frequencies in the CN spectra may alert to the presence of undefined quantities of crystalline CN, the absence of the endothermic peak corresponding to CN melting in DSC profiles indicated its quantitative amorphization (Figure 6c). Working temperatures for this high molecular weight PEO turned out especially critical. In fact, the 100 °C set during HME failed in ensuring complete melting of the polymer, but caused CN dissolution.

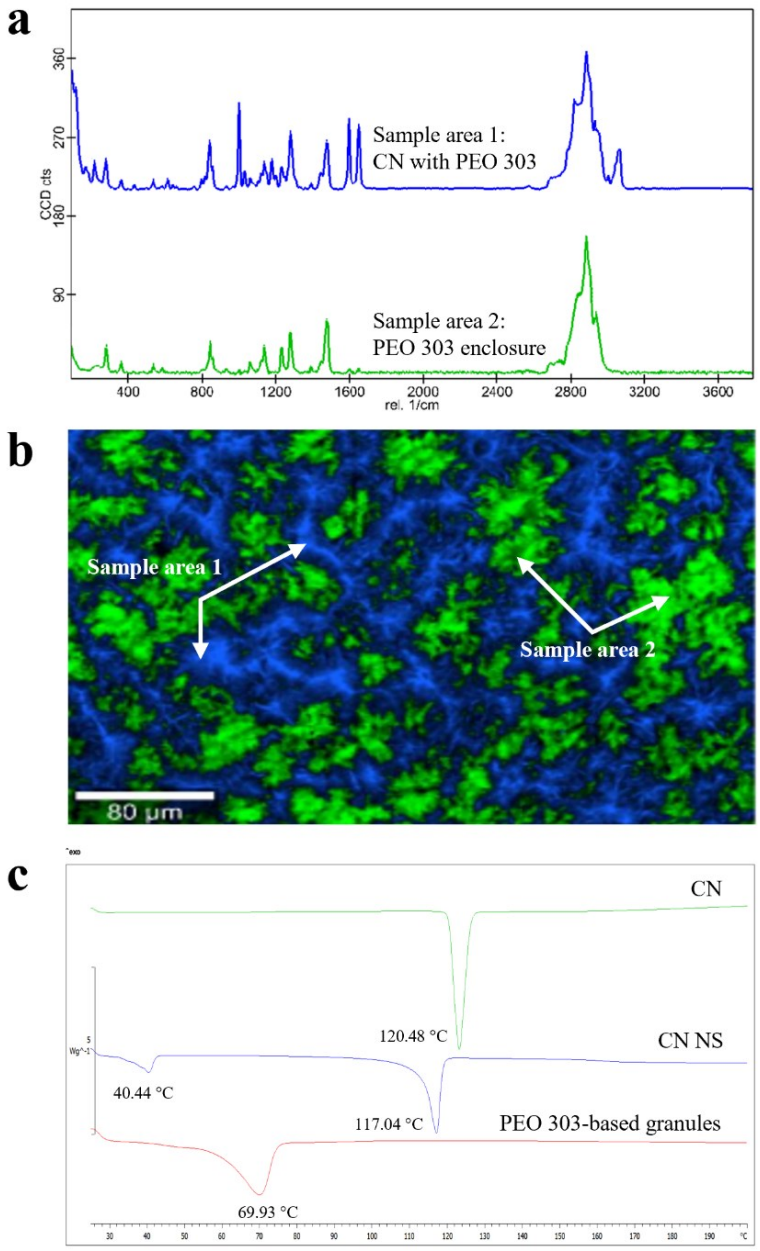

Figure 6. (**a**) Raman molecular map, (**b**) Raman spectra and (**c**) DSC thermograms of PEO 303-based granules.

3.3.4. Eu RS, Eu RL and Eu E

High-resolution Raman analysis of Eu-based extruded products pointed out a spatial distribution of pure crystalline CN entities into the different polymethacrylate-based carriers. More specifically, there were three diverse scenarios.

In Eu-RS-based granules, finely and randomly dispersed regions of pure CN were observed, which were immersed in the pure polymeric carrier (*i.e.,* red and yellow

sample areas 1 and 2, respectively, in Figure 7a,b). To better clarify the solid state of CN spots within the polymer, SEM images were also acquired. Interestingly, the images of the sample cross-section showed elongated pore clusters with a butterfly-like pattern, in the walls of which CN crystals could be appreciated via appropriate magnification (Figure 7d). Individually, these crystalline entities measured up to 0.5–1.0 μm. On the other hand, the presence of the pores could be associated with rapid drying of residues of the liquid fraction of the CN NS. These large pores being randomly dispersed within the matrix could be ascribed to CN NS fractions whose aqueous part was not properly mixed with the polymer and was dried too fast during HME (Figure 7c).

In the case of Eu RL-based granules, Raman findings revealed two main molecular entities: a crystal CN dispersion in the polymer (*i.e.,* blue sample area 1 in Figure 8a,b) with Eu RL enclosures having a length of ~1–340 μm (*i.e.,* orange sample area 2 in Figure 8a,b). As previously discussed for PEG- and PEO 303-based units, pure unaltered polymeric regions in polymethacrylate-based samples could be ascribed to the low residence time of the formulations in the lab-scale extruder employed, which did not allow a complete phase transition at the selected temperature and plasticizing conditions. This was not the case of Eu E-based products. In fact, the Raman analysis pointed out an intimate dispersion of CN in the polymer (*i.e.,* blue sample area 1 in Figure 9a,b) but with enclosures of pure crystalline drug (*i.e.,* red sample area 2 in Figure 9a,b).

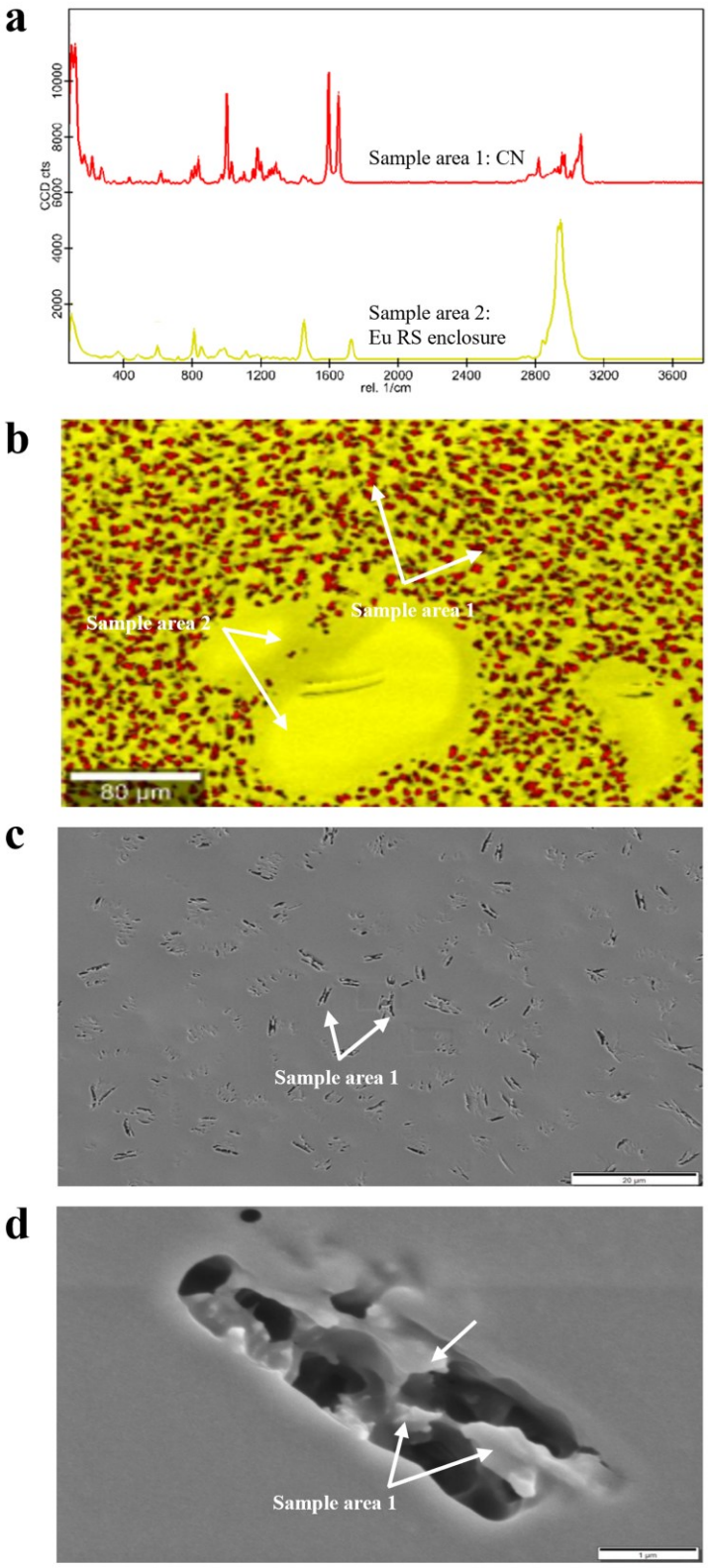

Figure 7. (**a**) Raman spectra, (**b**) Raman molecular map and (**c**,**d**) SEM images, at different magnifications, of Eu RS-based granules.

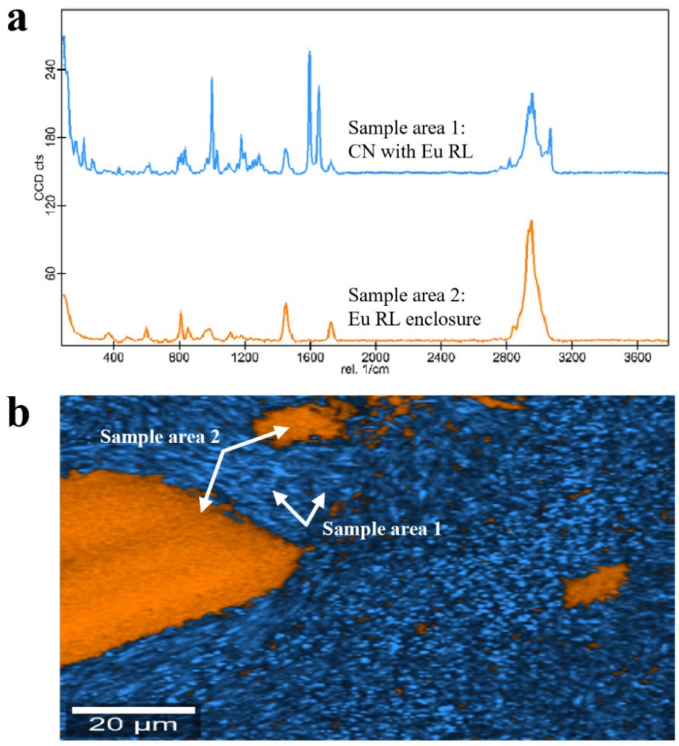

Figure 8. (**a**) Raman spectra and (**b**) Raman molecular map of Eu RL-based granules.

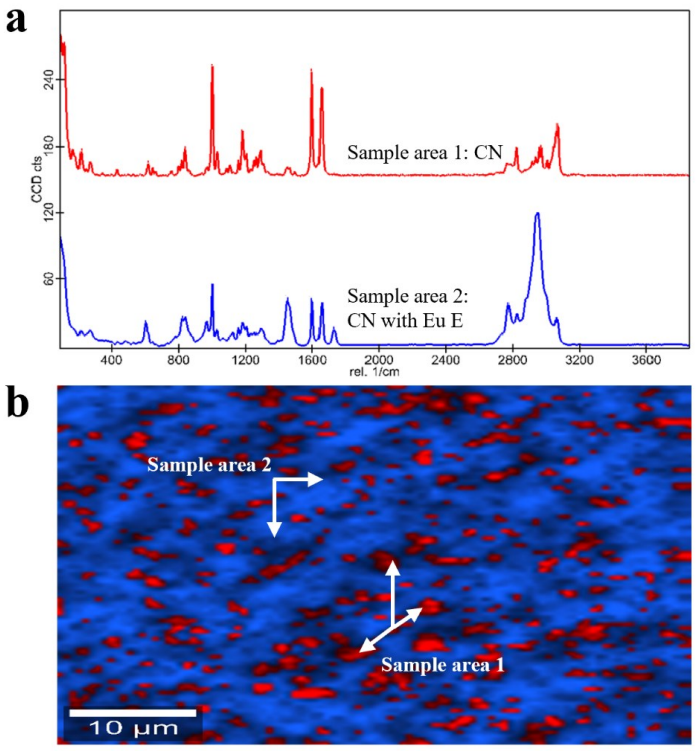

Figure 9. (**a**) Raman spectra and (**b**) Raman molecular map of Eu E-based granules.

4. Conclusions

This work represented a proof-of-concept study on the feasibility of HME in manufacturing multi-particulate systems for oral intake having a variety of release behavior, starting from a NS based on CN, a BCS class II model drug. In a wider perspective, this work further confirmed the versatility of HME for both small-scale manufacturing, as required by clinical trials testing the potential of NCEs, and for large-scale processing. Indeed, it was demonstrated a useful technology to turn NSs into solid products in a single step, thus being compatible with continuous manufacturing, while enabling the attainment of granules with both IR and PR performances. Compared with what was already available in the scientific literature, this research contributed to widen the numerosity and type of polymeric carriers that can be employed for processing NSs via HME. As CN represented a quite demanding model drug in view of its thermal behavior, it was challenging to attain granules containing the unmodified nanocrystals and equally interesting to identify the conditions under which CN dissolved and amorphized into the carrier. In this respect, the combination of the different analytical techniques used in the work was also proven fundamental in deepening the understanding of the products' micro-structure.

References

1. Jacob, S.; Nair, A.B.; Shah, J. Emerging role of nanosuspensions in drug delivery systems. *Biomater. Res.* **2020**, *24*, 3. https://doi.org/10.1186/s40824-020-0184-8.
2. Kesisoglou, F.; Panmai, S.; Wu, Y. Nanosizing—Oral formulation development and biopharmaceutical evaluation. *Adv. Drug Deliv. Rev.* **2007**, *59*, 631–644. https://doi.org/10.1016/j.addr.2007.05.003.
3. Merisko-Liversidge, E.; Liversidge, G.G. Nanosizing for oral and parenteral drug delivery: A perspective on formulating poorly-water soluble compounds using wet media milling technology. *Adv. Drug Deliv. Rev.* **2011**, *63*, 427–440. https://doi.org/10.1016/j.addr.2010.12.007.
4. Alqahtani, M.S.; Kazi, M.; Alsenaidy, M.A.; Ahmad, M.Z. Advances in oral drug delivery. *Front. Pharmacol.* **2021**, *12*, 618411. https://doi.org/10.3389/fphar.2021.618411.
5. Lou, J.; Duan, H.; Qin, Q.; Teng, Z.; Gan, F.; Zhou, X.; Zhou, X. Advances in oral drug delivery systems: Challenges and opportunities. *Pharmaceutics* **2023**, *15*, 484. https://doi.org/10.3390/pharmaceutics15020484.
6. Liu, J.; Tu, L.; Cheng, M.; Feng, J.; Jin, Y. Mechanisms for oral absorption enhancement of drugs by nanocrystals. *J. Drug Deliv. Sci. Technol.* **2020**, *56*, 101607. https://doi.org/10.1016/j.jddst.2020.101607.
7. Lipinski, C.A.; Lombardo, F.; Dominy, B.W.; Feeney, P.J. Experimental and computational approaches to estimate solubility and permeability in drug discovery and development settings. *Adv. Drug Deliv. Rev.* **1997**, *23*, 3–25. https://doi.org/10.1016/S0169-409X(96)00423-1.
8. Rasenack, N.; Müller, B.W. Micron-size drug particles: Common and novel micronization techniques. *Pharm. Dev. Technol.* **2004**, *9*, 1–13. https://doi.org/10.1081/pdt-120027417.
9. Patel, V.; Agrawal, Y. Nanosuspension: An approach to enhance solubility of drugs. *J. Adv. Pharm. Technol. Res.* **2011**, *2*, 81–87. https://doi.org/10.4103/2231-4040.82950.
10. Wang, Y.; Zheng, Y.; Zhang, L.; Wang, Q.; Zhang, D. Stability of nanosuspensions in drug delivery. *J. Control. Release* **2013**, *172*, 1126–1141. https://doi.org/10.1016/j.jconrel.2013.08.006.

11. Rabinow, B.E. Nanosuspensions in drug delivery. *Nat. Rev. Drug Discov.* **2004**, *3*, 785–796. https://doi.org/10.1038/nrd1494.
12. Verma, S.; Gokhale, R.; Burgess, D.J. A comparative study of top-down and bottom-up approaches for the preparation of micro/nanosuspensions. *Int. J. Pharm.* **2009**, *380*, 216–222. https://doi.org/10.1016/j.ijpharm.2009.07.005.
13. Bisrat, M.; Nyström, C. Physicochemical aspects of drug release. VIII. The relation between particle size and surface specific dissolution rate in agitated suspensions. *Int. J. Pharm.* **1988**, *47*, 223–231. https://doi.org/10.1016/0378-5173(88)90235-9.
14. Noyes, A.A.; Whitney, W.R. The rate of solution of solid substances in their own solutions. *J. Am. Chem. Soc.* **1897**, *19*, 930–934. https://doi.org/10.1021/ja02086a003.
15. Dizaj, S.M.; Vazifehasl, Z.; Salatin, S.; Adibkia, K.; Javadzadeh, Y. Nanosizing of drugs: Effect on dissolution rate. *Res. Pharm. Sci.* **2015**, *10*, 95–108.
16. Jacob, S.; Kather, F.S.; Boddu, S.H.S.; Attimarad, M.; Nair, A.B. Nanosuspension Innovations: Expanding horizons in drug delivery techniques. *Pharmaceutics* **2025**, *17*, 136. https://doi.org/10.3390/pharmaceutics17010136.
17. Bitterlich, A.; Laabs, C.; Krautstrunk, I.; Dengler, M.; Juhnke, M.; Grandeury, A.; Bunjes, H.; Kwade, A. Process parameter dependent growth phenomena of naproxen nanosuspension manufactured by wet media milling. *Eur. J. Pharm. Biopharm.* **2015**, *92*, 171–179. https://doi.org/10.1016/j.ejpb.2015.02.031.
18. Malamatari, M.; Somavarapu, S.; Taylor, K.M.G.; Buckton, G. Solidification of nanosuspensions for the production of solid oral dosage forms and inhalable dry powders. *Expert Opin. Drug Deliv.* **2016**, *13*, 435–450. https://doi.org/10.1517/17425247.2016.1142524.
19. Van Eerdenbrugh, B.; Froyen, L.; Van Humbeeck, J.; Martens, J.A.; Augustijns, P.; Van den Mooter, G. Drying of crystalline drug nanosuspensions—The importance of surface hydrophobicity on dissolution behavior upon redispersion. *Eur. J. Pharm. Sci.* **2008**, *35*, 127–135. https://doi.org/10.1016/j.ejps.2008.06.009.
20. Wewers, M.; Czyz, S.; Finke, J.H.; John, E.; Van Eerdenbrugh, B.; Juhnke, M.; Bunjes, H.; Kwade, A. Influence of formulation parameters on redispersibility of

naproxen nanoparticles from granules produced in a fluidized bed process. *Pharmaceutics* **2020**, *12*, 363. https://doi.org/10.3390/pharmaceutics12040363.

21. Chaubal, M.V.; Popescu, C. Conversion of nanosuspensions into dry powders by spray drying: A case study. *Pharm. Res.* **2008**, *25*, 2302–2308. https://doi.org/10.1007/s11095-008-9625-0.
22. Jakubowska, E.; Bielejewski, M.; Milanowski, B.; Lulek, J. Freeze-drying of drug nanosuspension- study of formulation and processing factors for the optimization and characterization of redispersible cilostazol nanocrystals. *J. Drug Deliv. Sci. Technol.* **2022**, *74*, 103528. https://doi.org/10.1016/j.jddst.2022.103528.
23. Chung, N.O.; Lee, M.K.; Lee, J. Mechanism of freeze-drying drug nanosuspensions. *Int. J. Pharm.* **2012**, *437*, 42–50. https://doi.org/10.1016/j.ijpharm.2012.07.068.
24. Byrn, S.; Futran, M.; Thomas, H.; Jayjock, E.; Maron, N.; Meyer, R.F.; Myerson, A.S.; Thien, M.P.; Trout, B.L. Achieving continuous manufacturing for final dosage formation: Challenges and how to meet them 20–21 May 2014 continuous manufacturing symposium. *J. Pharm. Sci.* **2015**, *104*, 792–802. https://doi.org/10.1002/jps.24247.
25. Desai, P.M.; Hogan, R.C.; Brancazio, D.; Puri, V.; Jensen, K.D.; Chun, J.-H.; Myerson, A.S.; Trout, B.L. Integrated hot-melt extrusion—Injection molding continuous tablet manufacturing platform: Effects of critical process parameters and formulation attributes on product robustness and dimensional stability. *Int. J. Pharm.* **2017**, *531*, 332–342. https://doi.org/10.1016/j.ijpharm.2017.08.097.
26. Puri, V.; Brancazio, D.; Desai, P.M.; Jensen, K.D.; Chun, J.; Myerson, A.S.; Trout, B.L. Development of maltodextrin-based immediate-release tablets using an integrated twin-screw hot-melt extrusion and injection-molding continuous manufacturing process. *J. Pharm. Sci.* **2017**, *106*, 3328–3336. https://doi.org/10.1016/j.xphs.2017.06.020.
27. Maniruzzaman, M.; Nokhodchi, A. Continuous manufacturing via hot-melt extrusion and scale up: Regulatory matters. *Drug Discov. Today* **2017**, *22*, 340–351. https://doi.org/10.1016/j.drudis.2016.11.007.
28. Casati, F.; Melocchi, A.; Moutaharrik, S.; Uboldi, M.; Foppoli, A.; Maroni, A.; Zema, L.; Neut, C.; Siepmann, F.; Siepmann, J.; et al. Injection molded capsules

for colon delivery combining time-controlled and enzyme-triggered approaches. *Int. J. Mol. Sci.* **2020**, *21*, 1917. https://doi.org/10.3390/ijms21061917.

29. Gajera, B.Y.; Shah, D.A.; Dave, R.H. Investigating a novel hot melt extrusion-based drying technique to solidify an amorphous nanosuspension using design of experiment methodology. *AAPS PharmSciTech* **2018**, *19*, 3778–3790. https://doi.org/10.1208/s12249-018-1189-7.
30. Baumgartner, R.; Eitzlmayr, A.; Matsko, N.; Tetyczka, C.; Khinast, J.; Roblegg, E. Nano-extrusion: A promising tool for continuous manufacturing of solid nano-formulations. *Int. J. Pharm.* **2014**, *477*, 1–11. https://doi.org/10.1016/j.ijpharm.2014.10.008.
31. Khinast, J.; Baumgartner, R.; Roblegg, E. Nano-extrusion: A one-step process for manufacturing of solid nanoparticle formulations directly from the liquid phase. *AAPS PharmSciTech* **2013**, *14*, 601–604. https://doi.org/10.1208/s12249-013-9946-0.
32. Maniruzzaman, M.; Boateng, J.S.; Snowden, M.J.; Douroumis, D. A review of hot-melt extrusion: Process technology to pharmaceutical products. *ISRN Pharm.* **2012**, *2012*, 436763. https://doi.org/10.5402/2012/436763.
33. Thakkar, R.; Thakkar, R.; Pillai, A.; Ashour, E.A.; Repka, M.A. Systematic screening of pharmaceutical polymers for hot melt extrusion processing: A comprehensive review. *Int. J. Pharm.* **2020**, *576*, 118989. https://doi.org/10.1016/j.ijpharm.2019.118989.
34. Censi, R.; Gigliobianco, M.R.; Casadidio, C.; Di Martino, P. Hot melt extrusion: Highlighting physicochemical factors to be investigated while designing and optimizing a hot melt extrusion process. *Pharmaceutics* **2018**, *10*, 89. https://doi.org/10.3390/pharmaceutics10030089.
35. Crowley, M.M.; Zhang, F.; Repka, M.A.; Thumma, S.; Upadhye, S.B.; Battu, S.K.; McGinity, J.W.; Martin, C. Pharmaceutical applications of hot-melt extrusion: Part I. *Drug Dev. Ind. Pharm.* **2007**, *33*, 909–926. https://doi.org/10.1080/03639040701498759.
36. Alshetaili, A.; Alshahrani, S.M.; Almutairy, B.K.; Repka, M.A. Hot melt extrusion processing parameters optimization. *Processes* **2020**, *8*, 1516. https://doi.org/10.3390/pr8111516.

37. Amidon, G.L.; Lennernäs, H.; Shah, V.P.; Crison, J.R. A theoretical basis for a biopharmaceutic drug classification: The correlation of in vitro drug product dissolution and in vivo bioavailability. *Pharm. Res.* **1995**, *12*, 413–420. https://doi.org/10.1023/a:1016212804288.
38. Tuomela, A.; Hirvonen, J.; Peltonen, L. Stabilizing agents for drug nanocrystals: Effect on bioavailability. *Pharmaceutics* **2016**, *8*, 16. https://doi.org/10.3390/pharmaceutics8020016.
39. Maghsoodi, M.; Nokhodchi, A.; Azhdarzadeh Oskuei, M.; Heidari, S. Formulation of cinnarizine for stabilization of its physiologically generated supersaturation. *AAPS PharmSciTech* **2019**, *20*, 139. https://doi.org/10.1208/s12249-019-1338-7.
40. Raghuvanshi, S.; Pathak, K. Recent advances in delivery systems and therapeutics of cinnarizine: A poorly water soluble drug with absorption window in stomach. *J. Drug Deliv.* **2014**, *2014*, 479246. https://doi.org/10.1155/2014/479246.
41. Bitterlich, A.; Laabs, C.; Busmann, E.; Grandeury, A.; Juhnke, M.; Bunjes, H.; Kwade, A. Challenges in nanogrinding of active pharmaceutical ingredients. *Chem. Eng. Technol.* **2014**, *37*, 840–846. https://doi.org/10.1002/ceat.201300697.
42. Van Eerdenbrugh, B.; Vermant, J.; Martens, J.A.; Froyen, L.; Van Humbeeck, J.; Augustijns, P.; Van den Mooter, G. A screening study of surface stabilization during the production of drug nanocrystals. *J. Pharm. Sci.* **2009**, *98*, 2091–2103. https://doi.org/10.1002/jps.21563.
43. Uboldi, M.; Chiappa, A.; Pertile, M.; Piazza, A.; Tagliabue, S.; Foppoli, A.; Palugan, L.; Gazzaniga, A.; Zema, L.; Melocchi, A. Investigation on the use of fused deposition modeling for the production of IR dosage forms containing Timapiprant. *Int. J. Pharm. X* **2023**, *5*, 100152. https://doi.org/10.1016/j.ijpx.2022.100152.
44. Uboldi, M.; Pasini, C.; Pandini, S.; Baldi, F.; Briatico-Vangosa, F.; Inverardi, N.; Maroni, A.; Moutaharrik, S.; Melocchi, A.; Gazzaniga, A.; et al. Expandable drug delivery systems based on shape memory polymers: Impact of film coating on mechanical properties and release and recovery performance. *Pharmaceutics* **2022**, *14*, 2814. https://doi.org/10.3390/pharmaceutics14122814.

45. Melocchi, A.; Parietti, F.; Maroni, A.; Foppoli, A.; Gazzaniga, A.; Zema, L. Hot-melt extruded filaments based on pharmaceutical grade polymers for 3D printing by fused deposition modeling. *Int. J. Pharm.* **2016**, *509*, 255–263. https://doi.org/10.1016/j.ijpharm.2016.05.036.
46. Repka, M.A.; Battu, S.K.; Upadhye, S.B.; Thumma, S.; Crowley, M.M.; Zhang, F.; Martin, C.; McGinity, J.W. Pharmaceutical applications of hot-melt extrusion: Part II. *Drug Dev. Ind. Pharm.* **2007**, *33*, 1043–1057. https://doi.org/10.1080/03639040701525627.
47. Melocchi, A.; Loreti, G.; Del Curto, M.D.; Maroni, A.; Gazzaniga, A.; Zema, L. Evaluation of hot-melt extrusion and injection molding for continuous manufacturing of immediate-release tablets. *J. Pharm. Sci.* **2015**, *104*, 1971–1980. https://doi.org/10.1002/jps.24419.
48. Rane, M.; Tiwari, S.; Rajabi-Siahboomi, A.; Parmar, J. Application of polyethylene oxide in hydrophilic matrix tablets. *Pharm. Times* **2013**, *45*, 41–48.
49. Trotzig, C.; Abrahmsén-Alami, S.; Maurer, F.H.J. Structure and mobility in water plasticized poly(ethylene oxide). *Polymer* **2007**, *48*, 3294–3305. https://doi.org/10.1016/j.polymer.2007.03.047.
50. Vanza, J.D.; Patel, R.B.; Dave, R.R.; Patel, M.R. Polyethylene oxide and its controlled release properties in hydrophilic matrix tablets for oral administration. *Pharm. Dev. Technol.* **2020**, *25*, 1169–1187. https://doi.org/10.1080/10837450.2020.1808015.
51. Gullapalli, R.P.; Mazzitelli, C.L. Polyethylene glycols in oral and parenteral formulations—A critical review. *Int. J. Pharm.* **2015**, *496*, 219–239. https://doi.org/10.1016/j.ijpharm.2015.11.015.
52. Dos Santos, J.; da Silva, G.S.; Velho, M.C.; Beck, R.C.R. Eudragit®: A versatile family of polymers for hot melt extrusion and 3D printing processes in pharmaceutics. *Pharmaceutics* **2021**, *13*, 1424. https://doi.org/10.3390/pharmaceutics13091424.
53. Kumbhar, P.S.; Nadaf, S.; Manjappa, A.S.; Jha, N.K.; Shinde, S.S.; Chopade, S.S.; Shete, A.S.; Disouza, J.I.; Sambamoorthy, U.; Kumar, S.A. D-α-tocopheryl polyethylene glycol succinate: A review of multifarious applications in

nanomedicines. *OpenNano* **2022**, *6*, 100036. https://doi.org/10.1016/j.onano.2022.100036.

54. Repka, M.A.; Mcginity, J.W. Influence of Vitamin E TPGS on the properties of hydrophilic films produced by hot-melt extrusion. *Int. J. Pharm.* **2000**, *202*, 63–70. https://doi.org/10.1016/S0378-5173(00)00418-X.
55. Rauscher, H.; Mech, A.; Gaillard, C.; Stintz, M.; Wohlleben, W.; Weigel St Ghanem, A.; Hodoroaba, V.; Babick, F.; Mielke, J. *Towards a Review of the EC Recommendation for a Definition of the Term "Nanomaterial"*; European Union: Brussels, Belgium, 2015.
56. Cantin, O.; Siepmann, F.; Danede, F.; Willart, J.F.; Karrout, Y.; Siepmann, J. PEO hot melt extrudates for controlled drug delivery: Importance of the molecular weight. *J. Drug Deliv. Sci. Technol.* **2016**, *36*, 130–140. https://doi.org/10.1016/j.jddst.2016.09.003.
57. Ilie, C.; Stîngă, G.; Iovescu, A.; Purcar, V.; Anghel, D.F.; Donescu, D. The influence of nonionic surfactants on the carbopol-peg interpolymer complexes. *Rev. Roum. Chim.* **2010**, *55*, 409–417.
58. Yang, S.; Liu, Z.; Liu, Y.; Jiao, Y. Effect of molecular weight on conformational changes of PEO: An infrared spectroscopic analysis. *J. Mater. Sci.* **2015**, *50*, 1544–1552. https://doi.org/10.1007/s10853-014-8714-1.
59. Trivedi, J.U.; Ghalsasi, P.; Ganguly, S.; Jenepha Mary, S.J.; James, C. Raman spectroscopic study of cinnamyl-1 diphenylmethyl-4 piperazine (Cinnarizine) at high pressure. *J. Mol. Struct.* **2022**, *1253*, 132214. https://doi.org/10.1016/j.molstruc.2021.132214.
60. Sagitova, E.A.; Prokhorov, K.A.; Nikolaeva, G.Y.; Baimova, A.V.; Pashinin, P.P.; Yarysheva, A.Y.; Mendeleev, D.I. Raman analysis of polyethylene glycols and polyethylene oxides. *J. Phys. Conf. Ser.* **2018**, *999*, 012002. https://doi.org/10.1088/1742-6596/999/1/012002.

Chapter I - Part II

The content of Chapter I - Part II is currently being prepared for submission to a scientific journal.

Development of a predictive model for converting Nanosuspensions into solid dosage forms via hot melt extrusion

1. Introduction

In recent years, the discovery of new chemical entities (NCEs) has accelerated dramatically due to advances in drug discovery methods, offering unprecedented opportunities for therapeutic innovation. However, a large proportion of these molecules suffers from poor aqueous solubility, which limits their dissolution in gastrointestinal (GI) fluids and, consequently, compromises their bioavailability. These compounds often fall into Class II or IV of the Biopharmaceutical Classification System (BCS). Despite their therapeutic potential, many NCEs are discontinued during either early or late development stages mainly due to formulation challenges for enabling the desired biopharmaceutical performances. Consequently, improving the solubility and dissolution of drug candidates has become a central challenge in drug development and a key focus of formulation research [1-5]. To overcome these limitations, several formulation strategies have been explored, including salt formation, co-solvent, prodrugs, surfactant and cyclodextrin complexation, as well as co-crystallization, emulsion and microemulsion, and particle size reduction [6-12]. Among these, solid dispersions (SDs) have gained increasing attention due to their versatility and effectiveness in enhancing the solubility and bioavailability of poorly soluble drugs. Depending on the solid-state nature of the drug within the polymeric matrix, SDs can be categorized as amorphous SDs (ASDs) and crystalline SDs (CSDs) [13, 14].

ASDs have emerged as one of the most effective formulation strategies for enhancing the oral bioavailability of poorly water-soluble drug compounds. Despite their well-known advantages, their application is accompanied by several challenges. These include the requirement for specialized manufacturing techniques, the difficulty in

accurately predicting *in vivo* performance, and concerns related to physical and chemical stability over prolonged storage periods [15-17]. In response to these limitations, CSDs have been investigated as a more stable alternative, offering enhanced thermodynamic stability, superior long-term physical integrity, and improved control over crystallinity and polymorphic forms. In contrast to amorphous systems, CSDs are less prone to physical transformations during storage, reducing the risk of unexpected changes in drug performance**.** Moreover, it is well established in the modern pharmaceutical industry that reducing the crystallite size of drugs during the manufacturing process leads to notable changes in drug physical properties, particularly enhancing solubility and, consequently, bioavailability in accordance with the Noyes-Whitney model [18-21].

The successful development of SDs relies fundamentally on investigating the compatibility between the active pharmaceutical ingredient (API) and the selected polymer, ensuring the formation of a homogeneous system capable of maintaining either thermodynamic or kinetic stability over a time period relevant for pharmaceutical use. Therefore, understanding the API-polymer temperature-composition (T-C) phase diagram, *i.e.* integrating the solid-liquid equilibrium (SLE) curve with the glass-transition temperature (T_g) line, offers both a fundamental framework for solid-state interactions' evaluation and guidance for proper decision-making, *i.e.* selecting suitable processing conditions that allow the manufacturing of either ASDs or CSDs [22, 23].

The preparation of nanosuspensions (NSs) of active pharmaceutical ingredients (APIs) with bioavailability limitations mainly due to poor aqueous solubility also represents a recent and effective strategy for the development of challenging yet highly-promising therapeutic compounds. In a previous study, we demonstrated the potential of hot-melt extrusion (HME) for converting a NS of a BCS class II drug into a solid dosage form. However, a critical issue remained the selection of suitable formulation and process parameters to preserve drug nanocrystals within the final product, thereby maintaining the improved biopharmaceutical performance associated with nanosizing. Within this context, the present work aimed to develop a model to streamline the design of effective extruded products derived from nanosuspensions. The model was constructed through the generation of temperature-composition (T-C) phase diagrams,

employing a specifically designed differential scanning calorimetry (DSC)-based protocol, namely the step-wise dissolution (S-WD) method [22]. The model's suitability was evaluated for its ability to predict *i)* the solubility of a model drug (*i.e.,* naproxen, NAP) in different polymethacrylate-based polymers (*i.e.,* Eudragit® RL PO and RS PO) and *ii)* the processability of formulations containing its NS while preserving drug crystallinity, using those prepared with the micronized drug as reference systems.

2. Materials and Methods

2.1. Materials

In this study, micronized naproxen (NAP; kindly provided by Novartis Pharma AG, Basel, Switzerland; mean particle size distribution, PSD: ~ 15.2 ± 2.4 μm) was used as a poorly water-soluble model API. NAP is a highly lipophilic BCS Class II drug, having poor solubility in water (15.9 mg/L at 25°C), T_g of 5 °C, T_m of 152-155 °C [24]. Stabilizers of the NAP NS: vinylpyrrolidone–vinyl acetate copolymer (PVP/VA, Kollidon VA 64, kindly provided by BASF SE, Germany) and sodium dodecyl sulfate (SDS, Sigma Aldrich, USA). Polymethacrylates (Eudragit® RL PO, Eu RL; Eudragit® RS PO, Eu RS; kindly provided by Evonik, Essen, Germany) were used as carrier excipient/matrix formers during hot-processing.

2.2. Methods

2.2.1. Sample preparation

2.2.1.1. NS

Batches of NAP NS (500 g) were produced using a stirred media mill (MiniCer, kind loan of Netzsch Feinmahltechnik GmbH, Germany). During milling, NAP particles were electrosterically stabilized against agglomeration by PVP VA and SDS. The ratio used in the nanosuspension was 10:2.5:0.25 (NAP: PVP VA 64: SDS), with a final drug concentration of 20 wt%. The mill was operated in recirculation mode with a constant mass flow of about 35 $kg \cdot h^{-1}$. The stirrer tip speed was set to $v = 9\ m \cdot s^{-1}$, and the temperature of the suspension was kept constant at 25 ± 1 °C at the outlet of the milling chamber. Yttrium-stabilized zirconium oxide (ZrO_2) grinding media (ρ_{GM} = 6067 $kg \cdot m^{-3}$) with a mean size of $X_{50,GM}$ = 315 μm (Sigmund Lindner GmbH,

Germany) were employed. The filling ratio of the grinding chamber with the grinding media was set at ϕ_{GM} = 0.8. To achieve a sufficiently small particle size, the milling duration was set to 4h.

2.2.1.2. Powdered samples

Either micronized NAP or NAP NS was mixed (in a mortar for at least 5 min) with the selected polymethacrylate-based polymers, with the active ingredient ranging from 5 to 80 wt%. Samples prepared starting from the NS were oven dried (8h, 40°C) to remove water.

2.2.1.3. Molded samples

Disk-shaped samples (n =3, 8 mm in diameter, 1 mm in height) were molded using a vacuum compression molding system (VCM, MeltPrep GmbH, Austria). More in detail, a previously weighed amount (*i.e.,* 20-25 mg) of the desired powdered formulation was loaded into the circular chamber of the equipment. Vacuum was applied, and then the chamber was heated for 10 min, setting a constant temperature (*i.e.,* 100°C). Subsequently, the chamber was cooled, thanks to a cooling plate connected to a compressed air source, for 3 minutes. The resulting disks were carefully removed and stored in sealed plastic bags until use.

2.2.1.4. Extruded samples

Extruded specimens were prepared using two different equipment: *i)* a lab-scale extruder (Haake™ MiniLab II, Thermo Fisher Scientific, Milan, Italy), and *ii)* a pilot-scale twin-screw extruder (ZSE 12 HP-PH-40D, Leistritz Extrusionstechnik GmbH, Nürnberg, Germany). The former equipment was fed with the selected powdered formulations, while the latter allowed concurrent feeding, at different positions along the barrel, of the solid and the liquid starting materials. More in detail, the solid starting materials were polymers alone or mixed with micronized NAP, while NAP NS represented the liquid, which was directly injected into the barrel containing pure polymers.

The lab-scale extrusion process took advantage of an instrument equipped with counter-rotating conical screws and a round-shaped die (custom-made in aluminum ø = 1.80 mm). Powdered formulations were manually fed into the barrel of the equipment. Specifically, the process was performed by setting different polymer-wise temperatures of the barrel, which were chosen based on the findings resulting from the DSC-based model. Screw speed was kept constant at 20 rpm. During manufacturing, extruded rods were manually pulled out of the die, and the mid-section of the resulting rods was analyzed, assuming homogeneous and equilibrium-like process conditions for this portion. Then, they were manually cut into 1.8 × 2 mm segments, which were checked for weight (analytical balance BP211, Sartorius, Milan, Italy), height, and diameter (digital caliper, Milan, Italy) before being stored in a desiccator.

The pilot-scale HME process was performed in a co-rotating twin screw extruder (maximum torque allowance of 10 Nm per screw) equipped with a gravimetric dosing unit (K-CL-SFS-MT12, Coperion K-Tron Schweiz GmbH, Niederlenz, Switzerland) and a circular die of 2.5 mm in diameter. The screws used in this work were characterized by the presence of powder-conveying elements with a large pitch of 20 mm in the feeding section (zone 1), while kneading elements with 30° offset angles were placed before the liquid port for liquid loading. These were followed by conveying elements with different pitch lengths (zone 2-3), with side feeding of the NS occurring in zone 2. A mixing section had consecutive mixing and conveying elements (10 mm pitch length), followed by a set of kneading elements with 60° offset angles (zone 4-5). Conveying elements differing in pitch length (from 10 to 20 mm) and a degassing port (zone 7) represented the final part of the screws (zone 6-8).

The equipment barrel had nine sections (8 temperature-controlled barrel zones), individually heated with electric heaters or cooled with water. The process conditions were set to apply a progressive temperature gradient along the barrel. Specifically, the temperature was maintained at 25 °C in zone 1, increased to 75 °C in zone 2, and further raised to 100 °C in the subsequent zones (*i.e.,* zone 3-8), in order to promote gradual melting and homogeneous mixing of the material throughout the extrusion process.

The screw speed was adjusted to reach the proper processing conditions (*i.e.,* material flow, shear-mixing conditions), ranging from 30 to 100 rpm. The starting materials

(*i.e.,* polymers or PMs) were fed into zone 1 at a rate of 0.1 kg/h, while the NAP NS was side-injected into zone 2 by using a twin-roller low-flow compact pump head (Petro Gas Ausrüstungen GmbH, Berlin, Germany), connected with an injection nozzle adaptor (0.5 mm in diameter). The NS flow rate was kept constant (*i.e.,* 0.134 kg/h) based on the targeted drug load (*i.e.,* 20 wt%). The extruded rods were pulled off by a conveyor belt (Fedotec GmbH, Rickenbach, Germany) at a speed rate optimized to maintain their diameter constant. The specific mechanical energy (SME) input was calculated using the screw speed (rpm, n), the drive Torque (M_D), and the mass flow ($\dot{m}$) as follows:

$$SME = \frac{2*\pi*n*MD}{\dot{m}} \qquad \text{(Eq. 1)}$$

2.2.2. Characterization

2.2.2.1. Differential scanning calorimetry (DSC)

Thermal properties of different specimens (*i.e.,* NAP and polymers alone, NAP NS, powdered formulations, vacuum molded disks, and extrudates) were analyzed *via* DSC (DSC1, Mettler Toledo, Gießen, Germany). In particular, 5.0 ± 0.5 mg of the desired sample were weighed into a 40 µL-aluminum crucible, sealed with a perforated lid. All scans were performed under nitrogen atmosphere (N_2 50 mL/min), setting three different ramps: first heating (25°C to 170°C, β= 10 K/min), cooling (170°C to -20°C, β= 10 K/min), and second heating (-20°C to 170°C, β= 10 K/min).

Adapting a procedure previously described [22, 23], a step-wise dissolution (S-WD) method was applied to supersaturated powdered formulations (*i.e.,* containing 80 wt% of NAP either as micronized powder and as NS) for building the solid-liquid-equilibrium (SLE) curve. These samples were generally considered supersaturated as they showed well-resolved peaks of NAP recrystallization and melting in the second heating DSC profile. More in detail, the dissolution process consisted of converting the crystalline NAP into its amorphous form during the annealing time (t_a=5 min). The initial annealing temperature (T_{ai} =115 °C), considered as the solubility temperature when the S-WD method is used, was set as the lowest temperature of interest. Accordingly, the supersaturated powdered formulations tested were heated to T_{ai} at β= 10 K/min and held for t_a. Afterwards, the sample was quenched to an appropriate temperature significantly below NAP T_g (*i.e.,* -20 °C at β= 40 K/min). Following

quenching, the system was reheated (β =10 K/min) to T_{a2} [*i.e.,* $T_{a2} = (T_{ai} + 5°C)$] and held for t_a. This process was repeated, incrementing T_{ai} until reaching the final annealing temperature (T_{af} = 150 °C), considered the highest temperature of interest. An additional step was performed at T_{af} +20°C to calculate ΔH_{fus} and, consequently, the residual amount of crystalline material.

The glass-transition temperature (T_g) line was defined by fitting the experimental values obtained from DSC protocols to the Gordon-Taylor (G-T) equation:

$$T_g = \frac{w_{API} * T_{g,API} + k_{G-T} * w_{Polymer} * T_{g,Polymer}}{w_{API} + k_{G-T} * w_{Polymer}} \quad \text{(Eq. 2)}$$

given w_{API} and $w_{Polymer}$, and $T_{g,API}$ and $T_{g,Polymer}$ as the weight fraction and the glass transition temperatures of the bulk NAP and polymer, respectively. The parameter k_{G-T} was considered as an empirical term and fitted to the NAP-polymer T_g dataset.

To predict NAP thermal solubility in different Eudragit carriers, the SLE curve modelling was conducted using an empirical analytical approach:

$$T_s = -Ae^{bx} + T_m + C \quad \text{(Eq. 3)}$$

being T_s the NAP solubility temperature, T_m the pure NAP onset melting temperature, x the NAP weight fraction (wt%), and A, b, and C the fitting parameters. In this investigation, experimental solubility data were fitted to Eq. 2 without applying any constraints to the C parameter, which was estimated after optimizing A and b by setting C to zero. These parameters were obtained using the Levenberg−Marquardt algorithm.

NAP melting point (T_m) was assessed as the onset temperature of the API melting transition. The experimentally determined ΔH_{fus} (*i.e.,* -144.36 J/g, NAP; -97.94 J/g, NAP NS) was considered to further evaluate the residual crystalline fraction of each hot-processed sample, using the following equation:

$$\text{Crystalline fraction} = \left(\frac{\Delta H_{fus}\text{sample}}{\Delta H_{fus}\text{reference}}\right) \quad \text{(Eq. 4)}$$

where the relative crystalline fraction was calculated based on the amount of drug loaded into the system. Therefore, the percentages are expressed as values relative to the dosed amount. Meanwhile, glass-transition temperatures (T_g) of pure polymers and of powdered formulations containing NAP and NAP NS were considered as the

midpoint of the glass-transition event relevant to the second heating step. On the other hand, the temperature of annealing (T_a) was interpreted as the solubility temperature (T_s) when the S-WD is used.

2.2.2.2. Particle size (Z-average) and Polydispersity index (PdI) via Dynamic Light Scattering (DLS)

Z-average and PdI of NAP nanoparticles (n = 3) were measured using Zetasizer nano ZSP (Malvern Panalytical Ltd., United Kingdom). Before the analysis, samples were adequately diluted (1:100) in saturated NAP solution and equilibrated for 120 s to ensure proper temperature conditioning. Subsequently, measurements were performed at 25 °C for 180 s. Each sample was measured in triplicate, and the mean values of the z-average (z-avg.) and polydispersity index (PdI) were used as characteristic values for the nanosuspensions. For the measurements,1.59 was set as the refractive index (RI) of naproxen, as previously calculated [25].

2.2.2.3.Confocal Raman microscopy (CRM)

To obtain the molecular distribution and investigate the presence of NAP in different solid states within samples, each formulation was scanned with a confocal Raman microscope (alpha300 R; WITec GmbH, Ulm, Germany). Optical micrographs of the samples were obtained using a 10x/0.25 lens (EC EPIPLAN, Zeiss, Oberkochen, Germany). For the measurements, a laser TrueSurface Mk 3 as topography correction, and a 20×/0.50 DIC lens (EC EPIPLAN-Neofluar, Zeiss, Oberkochen, Germany) were applied. Maximum possible rectangular areas (8200x8200 μm² areas at 20x20 μm^2 resolution, discs; 2250x2250 μm² at 10x10 μm resolution, extrudates) were applied to obtain the entire samples molecular maps. After the optimization of the scan parameters, a large area scan was performed (400x300 μm² and 1500x1300 μm², discs and extrudates, respectively) at 2x2 μm resolution, applying a laser power of 25-30 mW, and an integration time of 0.01 s. Hyperspectral data processing, including offset, cosmic ray removal, baseline correction, spectral filter application, and average spectral extraction, was performed using the microscope software (Control FIVE 5.2.10.88; WITec GmbH). The corresponding intensity maps were calculated by the application of WITec TrueComponent Analysis. Reference spectral data, including

those of NAP and polymeric carriers, were obtained by single-spectrum measurements, where the characteristic diagnostic peaks for each species were defined for hyperspectral processing.

2.2.2.4.Scanning electron microscopy (SEM)

Samples for analysis were prepared on a double-sided adhesive carbon pad and sputter-coated with a gold layer of 4 nm, using a sputtering device (Balzers Union Limited, Balzers, Principality of Liechtenstein). Morphology and size of NAP particles within the specimens were assessed by SEM on a Helios G4 CX (FEI Deutschland GmbH, Frankfurt am Main, Germany) with an Everhart-Thornley detector in secondary electron mode, an acceleration voltage of 3.0 kV, a beam current of 0.1 nA, and a working distance of 4.00 mm.

3. Results and Discussion

The rationale behind creating the T-C phase diagrams was to provide a predictive framework for guiding the design of products with tailored crystalline and amorphous fractions of the selected drug. Specifically, building different diagrams allowed to identify experimental conditions suitable for obtaining samples with a sufficiently high crystalline drug fraction, by selecting an operational window that minimizes the amorphous component in favour of the crystalline one. The defined parameters, such as drug load and processing temperature, needed to minimise the amorphization of the active ingredient, while enabling effective incorporation of nanocrystals into the polymer matrix. Additionally, these conditions had to support a continuous HME process characterized by direct injection of the water-based NS into the equipment barrel.

3.1. Determination of T_g line and SLE curve construction

The construction of the model, the so-called T-C phase diagram, relied on the proper determination of its constituent curves, specifically the glass transition (T_g) line and the solid–liquid equilibrium (SLE) curve. The model was constructed using micronized NAP powder and NS-containing specimens and, to broaden the investigation, considering different polymethacrylate polymers (*i.e.,* Eu RL and Eu

RS). A benchmark reference model was established for each formulation to ensure an accurate comparison between the predicted residual crystallinity and the actual residual amount assessed *via* DSC experiments.

By way of example, the complete procedural workflow used to build the predictive model for Eu RL-based formulations, including sample preparation, DSC protocols, data fitting (*e.g.,* Gordon-Taylor eq. and the Empirical equation), and the derivation of the T_g line and SLE curve, is described in the following section.

The polymer alone and in combination with micronized NAP, with w_{NAP} fractions increasing from 5 wt% to 80 wt%, were subjected to the DSC protocol as described in Section 2.2.2.1. Overall, thermograms pointing out a complete amorphization of the loaded w_{NAP} fraction in the second heating step were considered for our purpose. Numerical results are summarized in Table 1. Notably, formulations with a drug content ranging from 40 to 80 wt% were excluded because they were characterized by a major recrystallization upon cooling. Indeed, in the second heating step, an endothermic event associated with NAP melting could be highlighted. Accordingly, the determination of a reliable T_g value was not possible. As a matter of fact, the amount of polymethacrylate polymer in the sample was not enough to inhibit NAP recrystallization on quenching. Conversely, when dealing with formulations with lower w_{NAP} fractions, the drug did not recrystallize upon cooling, allowing the identification of a reliable T_g value on the second heating cycle. Therefore, the Gordon-Taylor equation parameter, k_{G-T}, could be calculated by using the experimental T_g dataset measured for formulations containing less than 20% of NAP. Thus, it was possible to determine the T_g line, and the corresponding k_{G-T} value of 0.540 together with the relevant fitting R^2 of 0.999.

Table 1. Experimental T_g values relevant to Eu RL-based samples.

w_{API}	$w_{polymer}$	**Experimental T_g (°C)**
1	0	5
0.2	0.8	49.66
0.1	0.9	59.57
0.05	0.95	67.05
0	1	71.1

Focusing on the SLE curve modeling, the supersaturated formulation (*i.e.,* having an 80 wt% w_{NAP} fraction) underwent the S-WD protocol as discussed in Section 2.2.2.1. Step-relevant thermograms enabled a reliable correlation of the detected T_g values to their respective T_a, and they were found to gradually decrease with each dissolution step towards the highest annealing temperature tested. T_a outputs of 115 to 150 °C were selected for the S-WD method, spanning from the onset of drug-polymer interaction (*i.e.,* ~115 °C) to just below the NAP melting point. The corresponding T_g were used to calculate the associated w_{API} by rearranging the G-T equation (Table 2). Therefore, experimental solubility data (*i.e.,* T_{as} and w_{API}) were fitted to the Empirical equation, enabling the estimation of the *A*, *b*, and *C* fitting parameters and, thus, the drafting of the SLE curve.

Table 2. Experimental T_g values and corresponding calculated w_{API} relevant to each heating step (T_a) undergone by Eu RL-based samples

T_a (°C)	**Experimental T_g (°C)**	**Corresponding calculated w_{API}**
115	51.63	0.18396
120	49.18	0.21127
125	47.18	0.2344
130	44.87	0.26209
135	41.69	0.30205
140	38.46	0.34497
145	35.56	0.3857
150	30.68	0.45939

The same procedure was applied to all formulations (*i.e.,* Eu RL-NAP NS, Eu RS-NAP, and Eu RS-NAP NS), enabling the achievement of the fitted parameters describing the T_g line and SLE curves. These are reported in Table 3, together with the R^2 of relevant fitting equations.

Table 3. Fitted parameters and relevant R^2 for T_g line, and SLE curve relevant to all formulations tested

	T_g line		**SLE curve**			
	k_{G-T}	**R^2**	***A***	***b***	***C***	**R^2**
Eu RL-NAP	0.53988	0.99872	133.92764	-6.33594	0.09784	0.99403
Eu RL-NAP NS	0.57345	0.99827	152.08146	-6.36621	0.01024	0.99856
Eu RS-NAP	0.43722	0.99968	123.05111	-5.65125	0.07912	0.99274
Eu RS-NAP NS	0.42502	0.99827	158.09835	-7.39826	0.07567	0.99377

Experimental T–C phase diagrams relevant to Eu RL and Eu RS-based systems, manufactured starting from either NAP powder or relevant NS, are reported in Figure 1.

All T-C phase diagrams revealed an extensive processing window within which the investigated formulations can be processed while preserving a high amount of crystalline NAP. Based on these models and on the identification of critical process parameters, it is therefore possible to infer the expected relative proportions of amorphous and crystalline fractions, thus providing predictive insight into the solid-state composition of the resulting formulation (Table 4).

The relative proportions of amorphous and crystalline fractions were derived from the T-C phase diagram. For a given temperature and overall API concentration, the intersection with the SLE curve represented the maximum soluble fraction of the drug in the polymer (*i.e.,* the dissolved or amorphous portion). The remaining amount corresponded to the undissolved, crystalline fraction.

Based on the assumption that the mixture would contain an 80:20 w/w polymer-drug ratio rather than 100 wt% polymer, the dissolved fraction was calculated by normalizing the solubility to the polymer content. The crystalline fraction was then obtained as the difference between the total NAP loaded and the dissolved portion. To enable this calculation, the empirical equation (Eq. 3) was rearranged as a function of the drug concentration x, as follows:

$$x = \frac{1}{b}\ln\left(\frac{T_m + C - T_s}{A}\right) \qquad \text{(Eq. 5)}$$

This allowed the estimation of the NAP solubility in the polymer at any selected temperature, which in turn was used to quantify the relative amorphous and crystalline fractions.

All formulations exhibited a high degree of consistency, regardless of whether the model was constructed from micronized NAP or from the relevant NS. Nevertheless, nanocrystals showed a greater tendency to solubilize within the polymeric matrix compared to micronized powders. This behavior can likely be attributed to the greater area of interaction and to the particle size-dependent thermal stability of the nanocrystals, where the higher surface free energy could accelerate any thermal processes, rendering them thermodynamically more reactive and, consequently, more

prone to dissolution [26, 27]. In addition, the residual stabilizers inherently present in the NS-based systems (*i.e.,* PVP VA64 and SDS) may have further contributed to these effects. Although present at low concentrations, they could have enhanced the tendency of the nanocrystals to dissolve within the polymeric matrix by improving wetting, intermolecular interactions, or partial solubilization of NAP during heating.

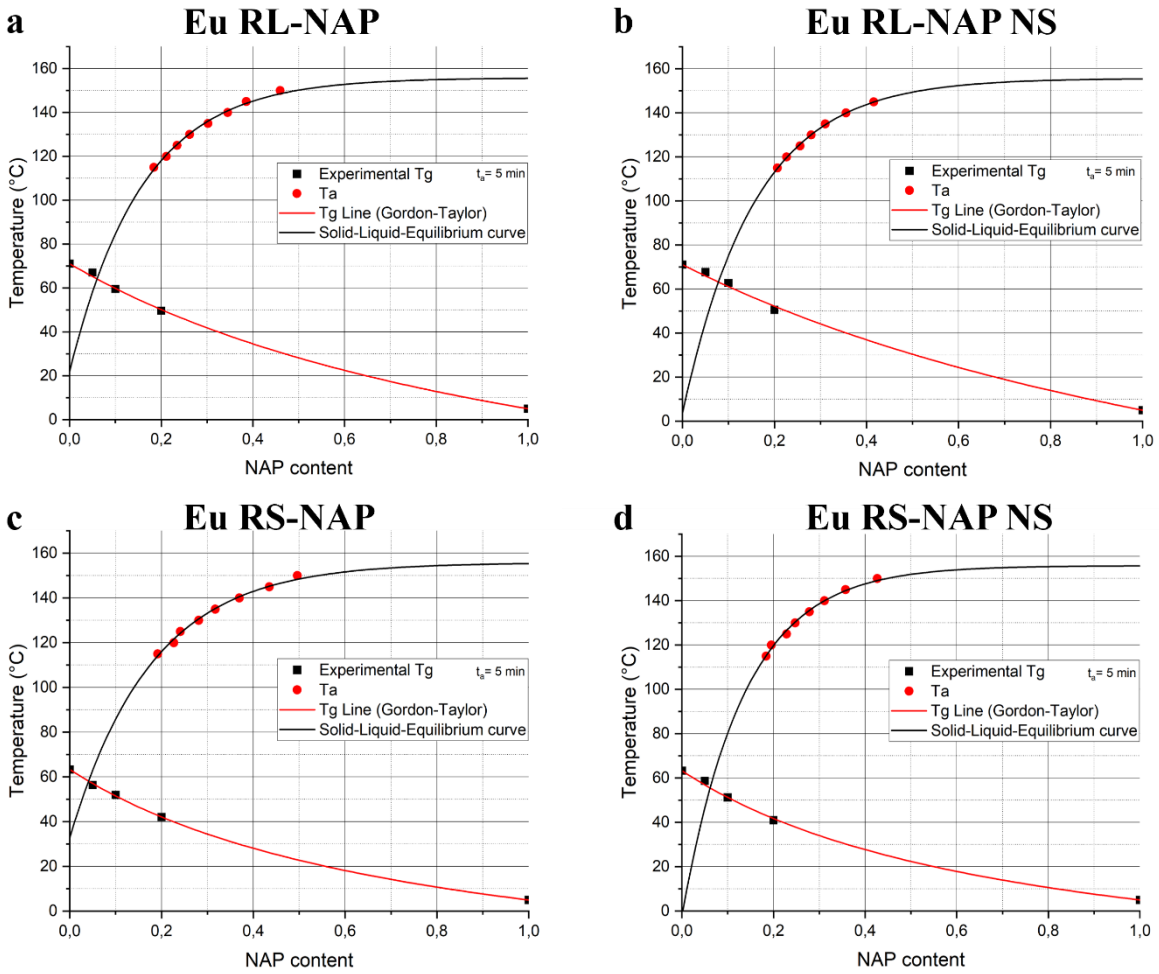

Figure 1. Experimental T–C phase diagrams relevant to (a,b) Eu RL-NAP and (c,d) Eu RS-NAP systems, manufactured starting from either (a,c) micronized NAP powder or (b,d) relevant NS.

To ensure comparability across all formulations, the selection of processing conditions, *i.e.,* taking into account all the predictive models constructed, was directed towards formulations with a targeted NAP content of 20 wt% (*i.e.,* 200 mg/g). This choice guaranteed the presence of a significant crystalline fraction, while allowing processing at a temperature of 100 °C.

Table 4. Evaluation of the expected amorphous and crystalline fractions relevant to 200 mg/g NAP-loaded systems processed at 100°C

	Amorphous fraction (mg/g)	**Crystalline fraction (mg/g)**
Eu RL-NAP	110.5	89.5
Eu RL-NAP NS	126.2	73.8
Eu RS-NAP	112.0	88.0
Eu RS-NAP NS	112.7	87.3

3.2. Application of the T-C phase diagram across different processing scales

As a step forward and to validate the previously built T-C phase diagrams, NAP-and NAP NS-containing formulations were subjected to hot-processing. Given the minimal sample requirements in terms of weight, VCM was initially employed to assess thermal properties of the drug and its residual crystallinity under the specified heating conditions (Table 5).

Table 5. Normalized ΔH_{fus} and relevant crystalline fraction values calculated based on the NAP content in the various specimens manufactured by VCM

	ΔH_{fus}, normalized (J/g)	**Crystalline fraction (mg/g)**
Eu RL-NAP	-13.75	95.3
Eu RL-NAP NS	-18.78	191.7
Eu RS-NAP	-19.03	131.8
Eu RS-NAP NS	-7.68	78.5

In addition, the static nature of VCM, which theoretically more closely resembles the conditions used in DSC experiments, makes the system more representative of the assumptions in the predictive model. In this respect, the crystalline fraction was found

to be similar to, or in some cases higher than, the expected values. This can be explained by the non-uniform and time-dependent thermal history experienced by the formulations during processing, where portions of the specimens may not reach the nominal set temperature, particularly between the disc core and its surface. Moreover, the higher-than-expected crystallinity observed in Eu RL-NAP NS (*i.e.,* 191.7 mg/g *vs* 73.8 mg/g), in contrast to Eu RS-NAP NS (*i.e.,* 78.5mg/g *vs* 87.3 mg/g), which exhibited a reliable crystallinity, can be attributed to intrinsic differences in the polymer properties. Eu RL is more permeable to water, and even the mild drying conditions employed may have induced transient plasticization of the polymer chains. This could have diminished its ability to inhibit NAP crystallization, leading to partial recrystallization during storage. In comparison, the lower water permeability of Eu RS likely preserved its stabilizing capacity, resulting in crystallinity consistent with theoretical expectations. Given that the processing procedure was identical for both polymers, these observations might suggest that the divergences arising from polymer-drug-water interactions are intrinsic to the polymer rather than from the applied methodology.

Within this framework, not all the solubilized NAP was expected to remain in the amorphous state during storage at ambient conditions, particularly when crystalline domains were already present. Indeed, these pre-existing crystals could act as nucleation sites, lowering the energy barrier for recrystallization and promoting the transformation of the amorphous fraction back into the crystalline state upon cooling [28, 29]. Upon reaching room temperature, the system therefore approached an equilibrium in which a portion of NAP recrystallized, resulting in a coexistence of amorphous and crystalline fractions. Indeed, analysis of the T-C phase diagram (Figure 1) indicated that at ambient conditions (*i.e.,* 25 °C), the intersection with the SLE curve suggested that the thermodynamically stabilized amorphous fraction was expected to be below 2 wt% (*i.e.,* ~ 4 mg/g), or essentially negligible. Consequently, the experimentally observed solid-state composition reflected not only the solubility at elevated temperatures but also the thermodynamic and kinetic factors that drove crystallization during cooling. The system can therefore be considered a partially amorphous dispersion, with residual crystalline regions embedded within the amorphous matrix.

Additionally, it is worth noting that the excipients contained in the NAP NS (*i.e.,* PVP VA 64 and SDS) might alter the apparent phase behavior. While they may increase NAP solubility at processing conditions, they could also have affected the retention of the amorphous fraction upon cooling, either promoting or limiting recrystallization. These considerations highlighted the limitations of interpreting the T-C phase diagram as a strict predictor of the final solid-state composition and underscored the importance of accounting for polymer-NAP-stabilizer interactions when evaluating the resulting formulation.

Considering the overall promising findings attained in these preliminary experiments, the extrusion process was carried out under the temperature conditions suggested by the predictive model.

3.2.1. HME

HME was performed on two different instrument scales (Haake™ MiniLab II and Leistritz Extrusionstechnik GmbH extruders). The resulting products were thoroughly characterized to deepen the dispersion of NAP within the polymer matrices, assessing and quantifying its solid state and the residual crystalline matter. Additionally, for the NAP NS-containing formulations, a morphological analysis of the surfaces was carried out to gather information on particle size and the geometry of the dispersed nanocrystals.

Before starting the trials, a comprehensive characterization of the physico-chemical quality attributes of the NAP NS was performed, providing reference benchmark data for the subsequent evaluation of the extruded samples. The NAP NS contained nanoparticles of average ~198 nm with a PdI of 0.11, demonstrating a narrow and homogeneous particle size distribution. The thermal analysis of oven-dried aliquots of the NS highlighted the presence of a single endothermic peak, related to the NAP melting point (T = 152.58 °C, ΔH_{fus} = -97.94 J/g). The observed reduction of the ΔH_{fus} in the nanosized system, compared to the micronized form of the NAP (*i.e.,* -144.36 J/g), can be rationalized by the well-established size dependence of the thermodynamic properties in nanoscale materials. Indeed, NAP particle size comminution increases the surface-to-volume ratio, resulting in a larger fraction of atoms residing at the surface. These surface species are less strongly bonded than those in the interior of the crystal, exhibiting weaker cohesive interactions that reduce the overall lattice stability,

and consequently lower the energy required for fusion. Moreover, the presence of stabilizers may have subtly contributed to these thermal responses, further promoting the thermodynamic reactivity of the nanocrystals and their propensity to undergo partial dissolution during heating.

SEM was also performed to obtain a comprehensive morphological overview of the NS (Figure 2). NAP nanocrystals appeared as slender, elongated needles, consistent with an acicular morphology, and resulted in dimensionally monodisperse nanoparticles consistent with DLS measurements. To complement the above-mentioned data, confocal Raman microscopy was selected as a suitable imaging approach to reveal the NS molecular fingerprint and, thus, when dealing with polymer-drug mixtures, to gain a deeper understanding of NAP-carrier interactions and of the drug distribution within the matrix. In particular, according to already available literature findings, Raman spectroscopy revealed a molecular fingerprint consisting of 92, 123 and 152 cm^{-1}(lattice vibration frequencies), 1397 and 1425 cm^{-1}(bending vibration of CH_3 and CH_2 groups), 1492 and 1585 cm^{-1} (aromatic ring), 1635 cm^{-1} (carboxyl acid), 2946 and 3073 cm^{-1}(stretching vibration of CH_3 and CH_2 groups) for NAP [30] as discussed in Section 3.2.1.1. (Figure 3).

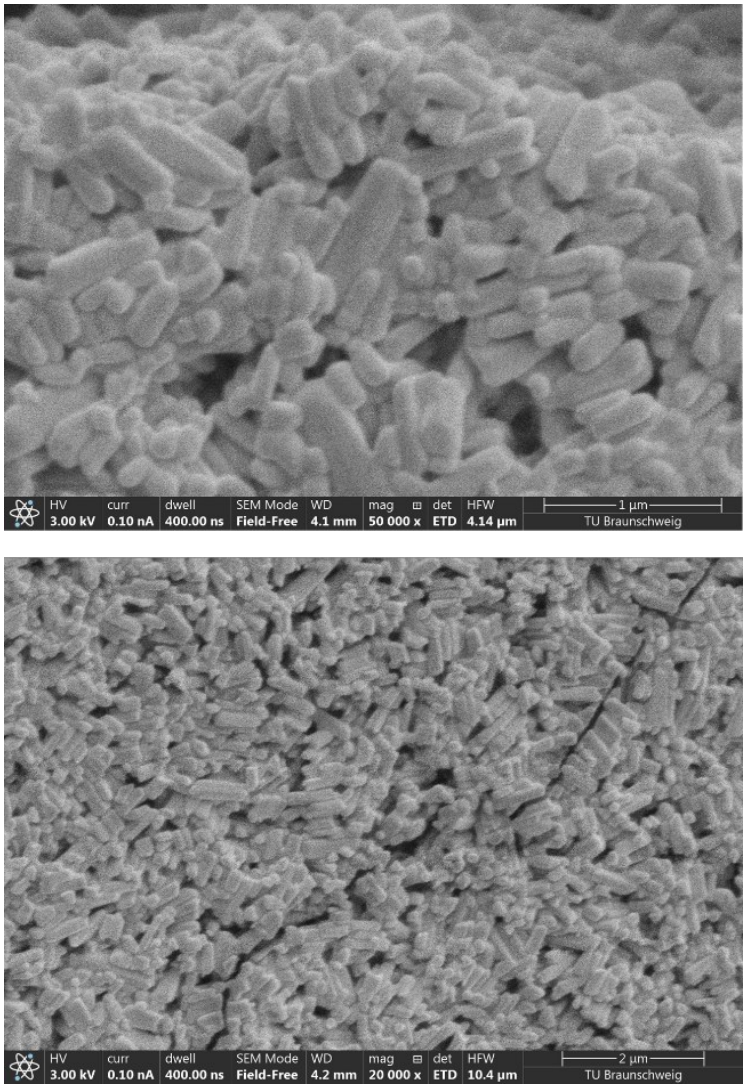

Figure 2. SEM images of oven-dried NAP NS, at different magnifications.

3.2.1.1. Eu RL- and RS-based products

Optical micrographs and Raman spectra collected from different areas of the cross-sections of extruded Eu RL-NAP extrudates showed a peculiar spatial distribution of the two main molecular entities identified (Figure 3a-c and Figure 3e-g): *i)* an extruded homogeneous matrix, in which the NAP was molecularly dispersed into the polymeric carrier (*i.e.,* blue area) surrounding *ii)* separated and homogeneously distributed crystalline NAP regions (*i.e.,* red spots). The crystalline nature of these regions was confirmed by the presence of vibrational lattice frequencies (*i.e.,* 92, 123, and 152 cm^{-1}) in the NAP spectra. Indeed, the absence of all crystallinity-related peaks in the 90–200 cm^{-1} region, together with the presence of the diagnostic NAP peaks (*i.e.,* 1397 and 1425 cm^{-1}, 1492 and 1585 cm^{-1}, and 1635 cm^{-1}), indicated that the drug was present but dispersed and solubilized within the polymer matrix. The finer distribution of the crystalline phase observed in the sample processed with the Leistritz extruder can likely result from the higher mechanical energy input and shear intensity characteristic of the larger-scale co-rotating system. These conditions would enhance mixing efficiency and may induce partial comminution of NAP crystals, leading to a more homogeneous dispersion within the polymer matrix. NS-containing extrudates exhibited a finer and more uniform distribution pattern, which may hint at the presence of retained nanoparticulate NAP homogeneously dispersed within the polymeric matrix, with a dispersity likely finer than the resolution of the analytical technique used (Figure 4a and 4d). To better clarify the solid state of NAP regions within the carriers, SEM was employed as a qualitative tool. Interestingly, images of cross and longitudinal sections of the samples showed nanocrystals with needle-like elongated geometry, dimensionally consistent with those of the original NS. In some areas, needle-like NAP particles up to 3 μm in length were also visible (Figure 4b). This phenomenon might reflect a partial solubilization of the drug followed by recrystallization during cooling, most likely resulting from the system limited capacity to effectively suppress recrystallization and subsequent crystal growth. Conversely, the SEM micrograph of the Leistritz-based extrudate revealed particles with needle-like geometries, appearing either as elongated plates or as slender elongated entities, ranging from 0.6 to 1.5 μm (Figure 4e). The comparatively larger particle size may be attributed to the continuous processing: the direct injection of the NS into the heated

barrel of the equipment already containing softened and highly viscous carrier may lead to the rapid evaporation of the aqueous medium, generating a supersaturated environment. Such thermodynamically unfavourable conditions might promote uncontrolled growth of the dispersed nanocrystals or, alternatively, partial solubilization followed by recrystallization upon cooling.

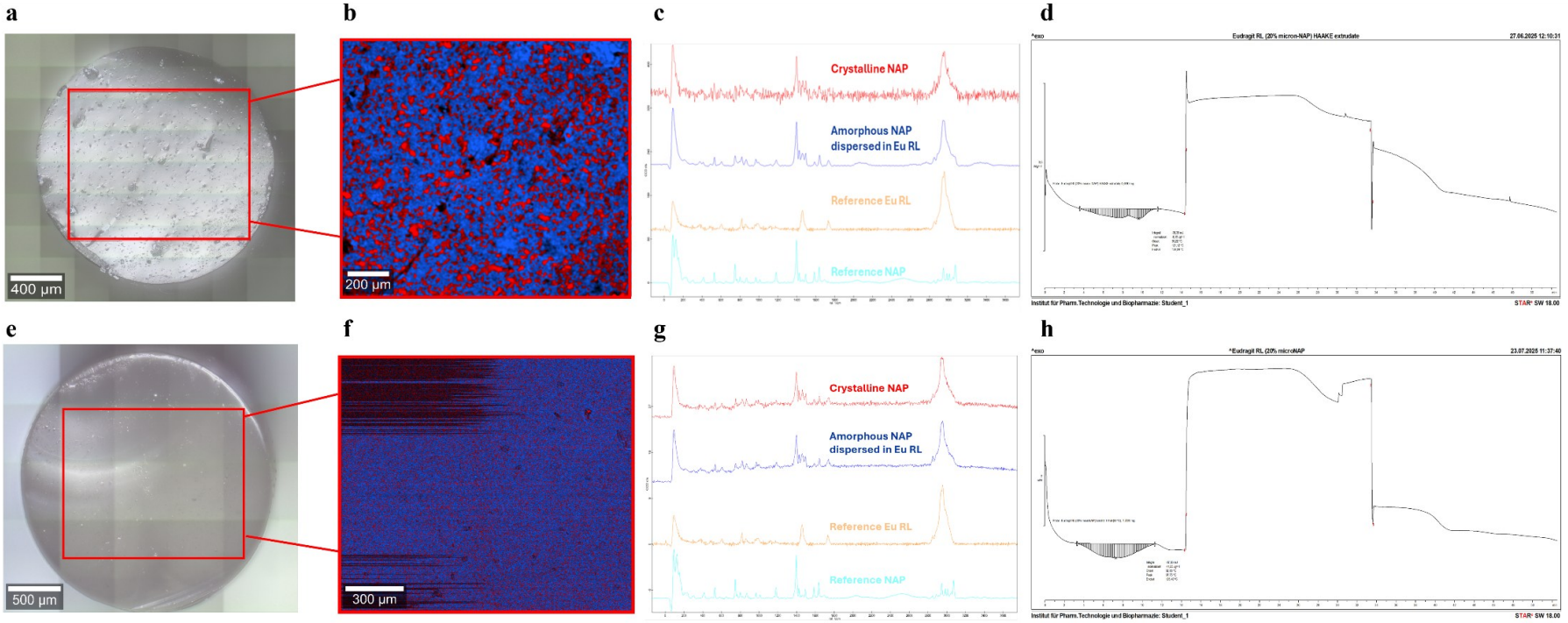

Figure 3. (a,e) Optical micrographs, (b,f) Raman molecular maps, (c,g) spectra, and (d,h) DSC thermograms of cross-sections of Eu RL-NAP extrudates manufactured using either Haake™ MiniLab II (a, b, c, d) or Leistritz Extrusions Technik GmbH (e, f, g, h) equipment, respectively.

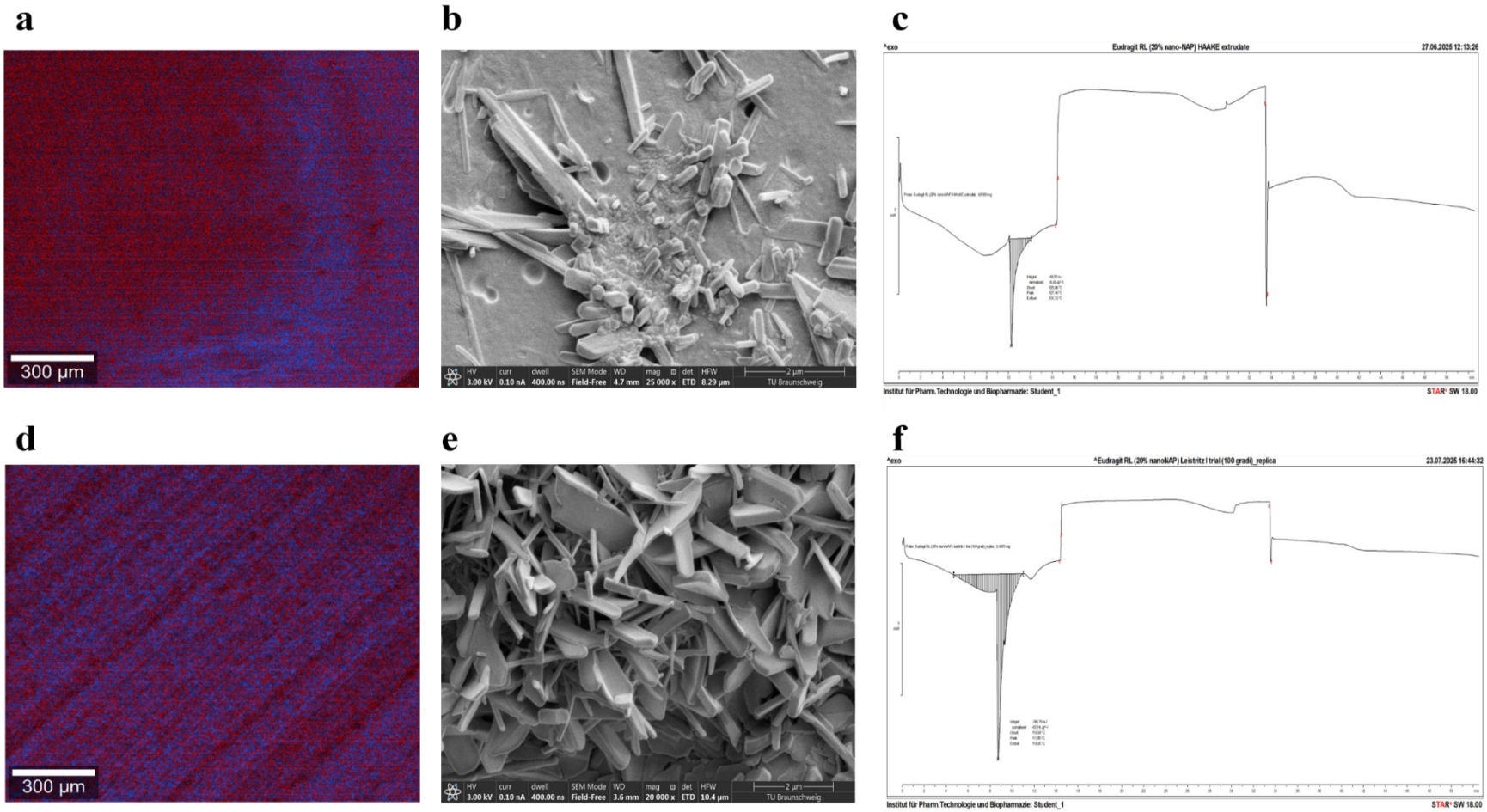

Figure 4. (a,d) Raman molecular maps, (b, e) SEM images, and (c, f) DSC thermograms of cross-sections of Eu RL-NAP extrudates manufactured using either Haake™ MiniLab II (a, b, c) or Leistritz Extrusionstechnik GmbH (e, f, g) equipment, respectively.

Stated the impact of processing conditions, it was deemed fundamental to evaluate the applicability of the predictive model by assessing the residual crystalline fraction in the extruded products. To this end, all samples were analyzed *via* DSC. All samples exhibited endothermic transitions corresponding to the melting of the crystalline NAP component embedded within the polymeric matrix. The quantification of these thermal events was performed by comparing the normalized ΔH_{fus} to that of NAP and NAP NS, respectively (Table 5).

Table 6. Normalized ΔH_{fus} and relevant crystalline fraction values calculated based on the NAP content in the various specimens.

Sample	**Manufacturing equipment**	**ΔH_{fus}, normalized (J/g)**	**Crystalline fraction (mg/g)**
Eu RL-NAP	HME, HAAKE MiniLab II	-8.19	56.7
	HME, Leistritz Extrusionstechnik GmbH	-11.23	77.8
Eu RL-NAP NS	HME, HAAKE MiniLab II	-8.42	85.9
	HME, Leistritz Extrusionstechnik GmbH	-67.19	686.0

The results confirmed that the predictive capability of the model was critically dependent on the initial preparation of the specimens. Those subjected to a drying pre-treatment, aimed at removing water, demonstrated both enhanced processability and residual crystallinity levels, results that were in close agreement with the model predictions. On the other hand, the samples prepared with micronized NAP were expected to exhibit slightly higher crystallinity (*i.e.,* 89.5 mg/g, Table 6). The observed reduction, *i.e.* 56.7 mg/g and 77.8 mg/g, could be attributed to the higher temperature levels generated during the hot-melt extrusion process, also in view of the friction and of the mechanical energy involved. This mechanical input may have promoted a greater solubilization of NAP within the polymeric matrix. The NAP NS-based extruded sample showed a slightly higher crystallinity than expected (85.9 mg/g *versus* 73.8 mg/g). This behavior may be attributed to the increased thermodynamic

instability of the drug at the nanoscale, where high-energy crystal nuclei are more prone to recrystallize during the cooling step, leading to a partial recovery of the crystalline phase [29, 31].

Conversely, the sample produced under continuous processing conditions, where the NS was directly injected into the extruder, exhibited a substantially higher amount of residual crystalline NAP than expected. The different drug dosing approach employed led to an inadequate control of the NS injection, resulting in an overloading of the latter. In fact, the crystalline content was nearly four times higher than the set concentration (*i.e.,* 686 mg/g instead of 200 mg/g), suggesting that a drastically gone-wrong process *via* demixing occurred. Moreover, water played a critical role by lowering the material temperature upon injection into the extruder, thereby further limiting the extent of NAP solubilization compared to the expected outcome. These results highlighted that a much deeper understanding and control of the process parameters would be required to prevent unacceptable effects such as drastic demixing and uncontrolled NS loading. Importantly, these deviations stem solely from the HME process under the given conditions (*i.e.,* including the influence of water) and may not indicate limits in the formulation design or in the predictive capability of the DSC method

Raman analysis performed on Eu RS-based samples pointed out a similar NAP dispersion within the polymeric matrix with respect to what was previously discussed for Eu RL. Indeed, the spatial distribution of the chemical entities detected in these samples was consistent with that previously observed (Figures 5a-c and 5e-g). These findings suggested that the processing method had a direct impact on the spatial distribution and particle size of the crystalline phase within the polymeric matrix. Furthermore, the solid state of the drug in these domains was confirmed through the presence of diagnostic lattice vibrational peaks in the Raman spectra, providing clear evidence of the retained crystallinity. Indeed, Raman spectra and relevant maps collected from NS-based samples highlighted a finer dispersion of the drug nanoparticles within the matrices (Figure 6a, 6d). Morphological and dimensional analysis of the particle population embedded within the polymer, conducted *via* SEM imaging, demonstrated that the HAAKE-based extrudate comprises regions in which spherical nanoparticles exhibit an average particle size of ~200 nm, alongside more

heterogeneous areas where elongated, plate-like particles were substantially larger, reaching up to 2.5 μm (Figure 6b). In contrast, samples obtained through the continuous HME processing revealed a population of particles with diverse morphology, including thin needle-like particles ranging from 0.5 to 1.5 μm, as well as irregularly shaped, flake-like particles reaching up to 4 μm.

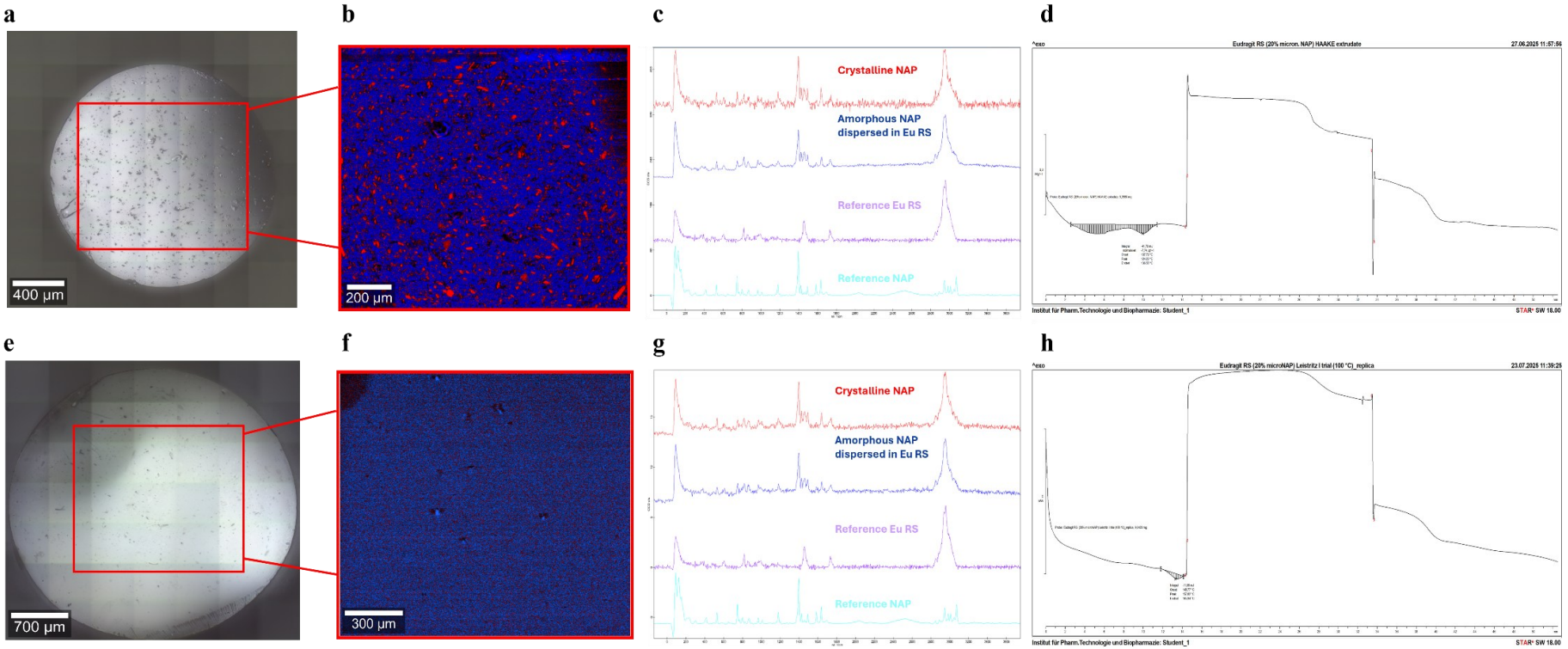

Figure 5. (a,e) Optical micrographs, (b,f) Raman molecular maps, (c,g) spectra, and (d,h) DSC thermograms of cross-sections of Eu RS-NAP extrudates manufactured using either Haake™ MiniLab II (a, b, c, d) or Leistritz Extrusionstechnik GmbH (e, f, g, h) equipment, respectively.

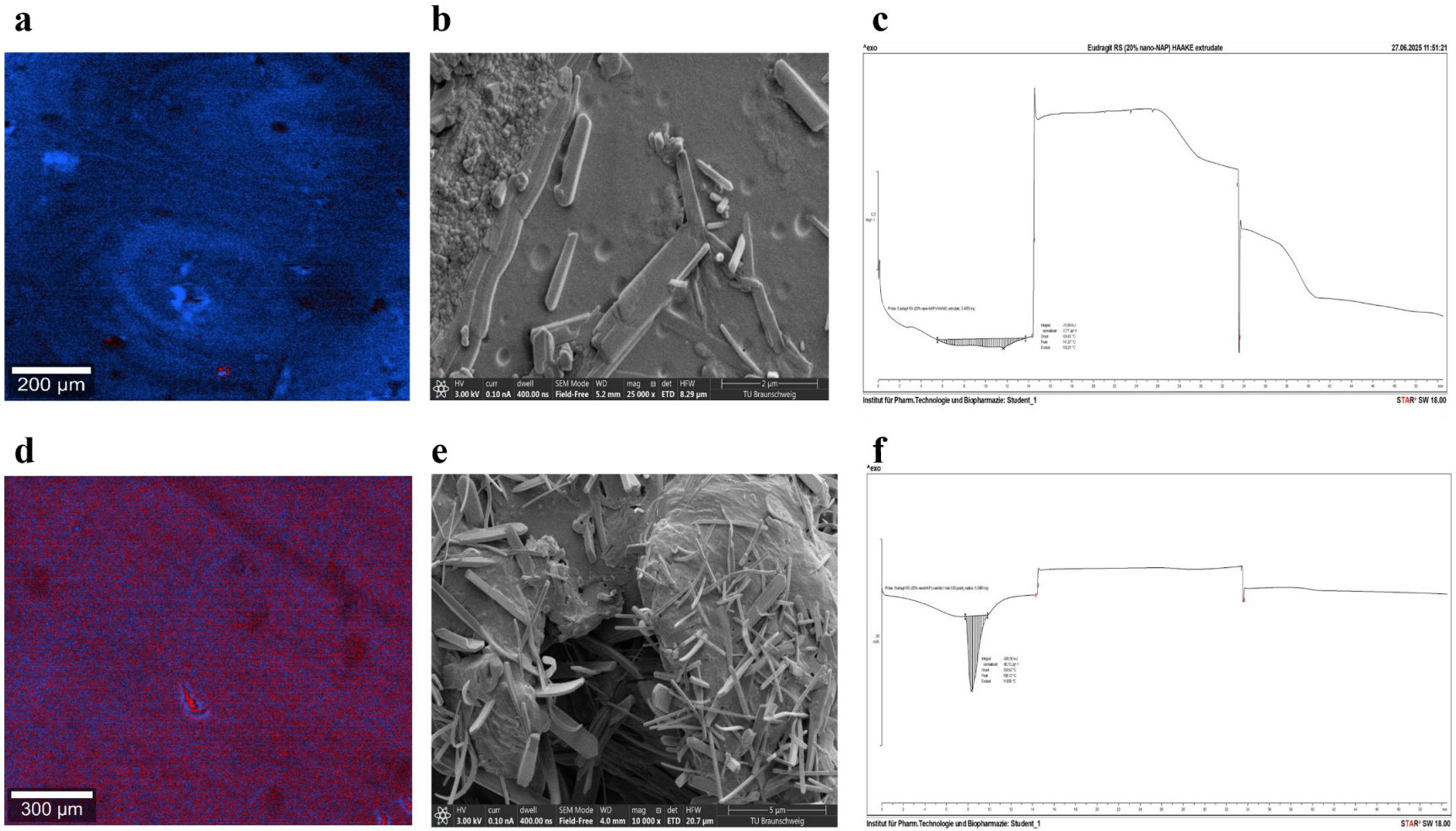

Figure 6. (a,d) Raman molecular maps, (b, e) SEM images, and (c, f) DSC thermograms of cross-sections of Eu RS-NAP extrudates manufactured using either Haake™ MiniLab II (a, b, c) or Leistritz Extrusionstechnik GmbH (e, f, g) equipment, respectively.

In this instance as well, assessing the residual crystalline fraction in the extruded products was considered essential to evaluate the applicability of the predictive model. Accordingly, DSC measurements were subsequently employed to quantify the residual crystalline fraction within the specimens. The resulting thermograms, although differing in intensity across samples, consistently displayed an endothermic event corresponding to NAP melting. This observation not only confirmed the presence of residual crystallinity but also provided insights into the relative proportion of the crystalline phase retained after processing. The quantification of these thermal events was performed by comparing the normalized ΔH_{fus} to that of NAP as such or in NS form, respectively (Table 7).

Table 7. Normalized ΔH_{fus} and relevant crystalline fraction values calculated based on the NAP content in the various specimens.

Sample	**Manufacturing equipment**	**ΔH_{fus}, normalized (J/g)**	**Cristalline fraction (mg/g)**
Eu RS-NAP	HME, HAAKE MiniLab II	-7.74	53.6
	HME, Leistritz Extrusionstechnik GmbH	-1.15	7.9
Eu RS-NAP NS	HME, HAAKE MiniLab II	-5.77	58.9
	HME, Leistritz Extrusionstechnik GmbH	-80.13	818.2

The results partially supported the predictive capability of the model, although some limitations became evident when the extrusion process was performed at a larger scale (*e.g.,* Leistritz Extrusionstechnik GmbH). In the case of samples produced with the HAAKE MiniLab II, the removal of excess water prior to processing led to a closer agreement with the model predictions, with residual crystallinity values (*i.e.,* 53.6 mg/g and 58.9 mg/g, respectively) below the expected predicted levels (*i.e.,* 88.0 mg/g and 87.3 mg/g, respectively). Although the predictive model provided valuable guidance, the lower residual crystallinity observed in extruded specimens can likely be attributed to the enhanced amorphization induced by the higher temperatures

involved during the extrusion process. Based on the calculated residual crystalline fractions, it can be inferred that the effective temperature reached by the material during processing was ~102-103 °C (*i.e.,* extrapolated from the SLE curve), which accounts for the higher degree of NAP amorphization observed. Unlike the static conditions assumed in the T-C phase diagram, extrusion involves mechanical shear, and thus higher temperatures, and rapid material flow, which can promote greater dissolution of NAP within the polymeric matrix.

In the case of larger-scale extrusion, significantly lower residual crystallinity was observed (*i.e.,* 7.9 mg/g *vs* 88 mg/g). As previously mentioned, this is likely attributable to the higher temperature reached during processing (*i.e.,* ~114 °C), which may have promoted extensive polymer chain mobility and enhanced solubilization of NAP within the matrix. Consequently, the material underwent a significantly higher degree of amorphization, resulting in residual crystallinity far below the values predicted by the T–C phase diagram. Conversely, when the process was implemented side-injecting the NS, similar limitations to those observed with Eu RL were apparent. In this case, an even higher NAP was observed (*i.e.,* 818.2 mg instead of 200 mg), further supporting the previously discussed issues related to drastic process instability.

4. Conclusions

In this work, a model grounded in the temperature-concentration (T-C) phase diagram was systematically employed to elucidate the solubility and solid-state stability of NAP, a prototypical Biopharmaceutics Classification System (BCS) Class II compound, within polymethacrylate-based carrier matrices. This model facilitated rational selection of critical formulation and processing parameters, such as drug loading and thermal input, thereby enabling the design of optimised hot-processing protocols. The validity of the predictive approach was established by experimental investigations conducted across multiple manufacturing scales, encompassing both VCM and HME platforms. The model consistently identified process conditions conducive to maximising the attainable residual crystallinity of NAP, thereby underscoring its utility as a robust tool in formulation development.

Nonetheless, the research has highlighted inherent limitations within the current modelling paradigm, particularly its inability to account for dynamic, process-dependent factors that become increasingly significant in continuous manufacturing environments. Empirical results, especially at the larger extrusion scale, revealed pronounced deviations between predicted and observed crystallinity values. These discrepancies are attributable to complex phenomena such as intensified mechanical shear, higher temperature profiles, accelerated material flow, and the physicochemical characteristics of the polymer carrier, all of which collectively enhance the amorphization of the active pharmaceutical ingredient beyond the static assumptions of the T-C phase diagram. Furthermore, process variables including specific mechanical energy input, liquid throughput, and residence time were found to exert a profound influence on the final solid-state properties of the extrudates, yet remain unaddressed by the current model.

Consequently, to advance towards a universally applicable and scalable predictive tool for hot-processing technologies, future work must focus on the integration of process analytical technologies (PAT) and advanced modelling strategies capable of capturing the interplay between formulation composition, process dynamics, and material attributes. Refinement of the model to incorporate real-time process parameters and feedback mechanisms will be essential for achieving consistent material quality and robust process control. Simultaneously, the continuous manufacturing setup should be further optimised to ensure precise material feeding, homogenous mixing, and effective thermal management, thereby facilitating reproducible product quality and seamless process integration.

In summary, this thesis has demonstrated the substantial potential of the T-C phase diagram-based model in the context of SDs design, while also delineating the challenges posed by scale-up and continuous processing. The insights gained herein lay a solid foundation for the development of next-generation predictive and control frameworks, which are imperative for the reliable and efficient translation of hot-processing technologies from laboratory to industrial scale.

References

1. S. Kumar, D. Bhargava, A. Thakkar, and S. Arora, "Critical Reviews™ in Therapeutic Drug Carrier Systems," 2013. [Online]. Available: www.begellhouse.com
2. G. L. Amidon, H. Lennernäs, V. P. Shah, and J. R. Crison, "A theoretical basis for a biopharmaceutic drug classification: the correlation of in vitro drug product dissolution and in vivo bioavailability," *Pharm Res*, vol. 12, 1995.
3. C. Sarkar *et al.*, "Artificial Intelligence and Machine Learning Technology Driven Modern Drug Discovery and Development," Feb. 01, 2023, *MDPI*. doi: 10.3390/ijms24032026.
4. S. Jacob, F. S. Kather, S. H. S. Boddu, M. Attimarad, and A. B. Nair, "Nanosuspension Innovations: Expanding Horizons in Drug Delivery Techniques," Jan. 01, 2025, *Multidisciplinary Digital Publishing Institute (MDPI)*. doi: 10.3390/pharmaceutics17010136.
5. R. Shegokar and R. H. Müller, "Nanocrystals: Industrially feasible multifunctional formulation technology for poorly soluble actives," Oct. 2010. doi: 10.1016/j.ijpharm.2010.07.044.
6. S. V. Bhujbal *et al.*, "Pharmaceutical amorphous solid dispersion: A review of manufacturing strategies," Aug. 01, 2021, *Chinese Academy of Medical Sciences*. doi: 10.1016/j.apsb.2021.05.014.
7. K. U. Khan, M. U. Minhas, S. F. Badshah, M. Suhail, A. Ahmad, and S. Ijaz, "Overview of nanoparticulate strategies for solubility enhancement of poorly soluble drugs," Feb. 15, 2022, *Elsevier Inc.* doi: 10.1016/j.lfs.2022.120301.
8. D. H. Jornada, G. F. Dos Santos Fernandes, D. E. Chiba, T. R. F. De Melo, J. L. Dos Santos, and M. C. Chung, "The prodrug approach: A successful tool for improving drug solubility," Jan. 01, 2016, *MDPI AG*. doi: 10.3390/molecules21010042.
9. E. Merisko-Liversidge, G. G. Liversidge, and E. R. Cooper, "Nanosizing: A formulation approach for poorly-water-soluble compounds," 2003. doi: 10.1016/S0928-0987(02)00251-8.

10. K. T. Savjani, A. K. Gajjar, and J. K. Savjani, “Drug Solubility: Importance and Enhancement Techniques,” *ISRN Pharm*, vol. 2012, pp. 1–10, Jul. 2012, doi: 10.5402/2012/195727.
11. A. T. M. Serajuddin, “Salt formation to improve drug solubility,” Jul. 30, 2007. doi: 10.1016/j.addr.2007.05.010.
12. B. Xie, Y. Liu, X. Li, P. Yang, and W. He, “Solubilization techniques used for poorly water-soluble drugs,” Nov. 01, 2024, *Chinese Academy of Medical Sciences*. doi: 10.1016/j.apsb.2024.08.027.
13. C. Liu *et al.*, “Oral bioavailability enhancement of β-lapachone, a poorly soluble fast crystallizer, by cocrystal, amorphous solid dispersion, and crystalline solid dispersion,” *European Journal of Pharmaceutics and Biopharmaceutics*, vol. 124, pp. 73–81, Mar. 2018, doi: 10.1016/j.ejpb.2017.12.016.
14. H. Huang, Y. Zhang, Y. Liu, Y. Guo, and C. Hu, “Influence of Intermolecular Interactions on Crystallite Size in Crystalline Solid Dispersions,” *Pharmaceutics*, vol. 15, no. 10, Oct. 2023, doi: 10.3390/pharmaceutics15102493.
15. K. Kawakami, “Modification of physicochemical characteristics of active pharmaceutical ingredients and application of supersaturatable dosage forms for improving bioavailability of poorly absorbed drugs,” May 01, 2012. doi: 10.1016/j.addr.2011.10.009.
16. K. Kawakami *et al.*, “Long-term physical stability of amorphous solid dispersions: Comparison of detection powers of common evaluation methods for spray-dried and hot-melt extruded formulations,” *J Pharm Sci*, vol. 114, no. 1, pp. 145–156, Jan. 2025, doi: 10.1016/j.xphs.2024.06.020.
17. A. Newman, G. Knipp, and G. Zografi, “Assessing the performance of amorphous solid dispersions,” 2012, *John Wiley and Sons Inc.* doi: 10.1002/jps.23031.
18. A. Mihranyan and M. Strømme, “Solubility of fractal nanoparticles,” *Surf Sci*, vol. 601, no. 2, pp. 315–319, Jan. 2007, doi: 10.1016/j.susc.2006.09.037.
19. C. Hu, Z. Liu, C. Liu, Y. Zhang, H. Fan, and F. Qian, “Improvement of Antialveolar Echinococcosis Efficacy of Albendazole by a Novel Nanocrystalline Formulation with Enhanced Oral Bioavailability,” *ACS Infect Dis*, vol. 6, no. 5, pp. 802–810, May 2020, doi: 10.1021/acsinfecdis.9b00231.

20. E. Roduner, “Size matters: Why nanomaterials are different,” *Chem Soc Rev*, vol. 35, no. 7, pp. 583–592, Jun. 2006, doi: 10.1039/b502142c.
21 C. Galli, “Experimental determination of the diffusion boundary layer width of micron and submicron particles,” *Int J Pharm*, vol. 313, no. 1–2, pp. 114–122, Apr. 2006, doi: 10.1016/j.ijpharm.2006.01.030.
22. A. Mathers, M. Pechar, F. Hassouna, and M. Fulem, “The step-wise dissolution method: An efficient DSC-based protocol for verification of predicted API–polymer compatibility,” *Int J Pharm*, vol. 648, Dec. 2023, doi: 10.1016/j.ijpharm.2023.123604.
23. A. Mathers, F. Hassouna, M. Klajmon, and M. Fulem, “Comparative Study of DSC-Based Protocols for API-Polymer Solubility Determination,” *Mol Pharm*, vol. 18, no. 4, pp. 1742–1757, Apr. 2021, doi: 10.1021/acs.molpharmaceut.0c01232.
24. A. Mathers, M. Pechar, F. Hassouna, and M. Fulem, “API solubility in semi-crystalline polymer: Kinetic and thermodynamic phase behavior of PVA-based solid dispersions,” *Int J Pharm*, vol. 623, Jul. 2022, doi: 10.1016/j.ijpharm.2022.121855.
25. M. Wewers *et al.*, “Influence of formulation parameters on redispersibility of naproxen nanoparticles from granules produced in a fluidized bed process,” *Pharmaceutics*, vol. 12, no. 4, Apr. 2020, doi: 10.3390/pharmaceutics12040363.
26. N. Zulbeari and R. Holm, “Long-term versus short-term stress physical stability assessment of pharmaceutical nano- and microsuspensions,” *Int J Pharm*, vol. 677, May 2025, doi: 10.1016/j.ijpharm.2025.125646.
27. L. Wu, J. Zhang, and W. Watanabe, “Physical and chemical stability of drug nanoparticles,” May 30, 2011. doi: 10.1016/j.addr.2011.02.001.
28. A. Kapourani, T. Tzakri, V. Valkanioti, K. N. Kontogiannopoulos, and P. Barmpalexis, “Drug crystal growth in ternary amorphous solid dispersions: Effect of surfactants and polymeric matrix-carriers,” *Int J Pharm X*, vol. 3, Dec. 2021, doi: 10.1016/j.ijpx.2021.100086.
29. X. Yao, L. Yu, and G. G. Z. Zhang, “Impact of Crystal Nuclei on Dissolution of Amorphous Drugs,” *Mol Pharm*, vol. 20, no. 3, pp. 1796–1805, Mar. 2023, doi: 10.1021/acs.molpharmaceut.2c00989.

30. B. Rojek, M. Gazda, and A. Plenis, “FTIR, Raman spectroscopy and HT-XRD in compatibility study between naproxen and excipients,” *Spectrochim Acta A Mol Biomol Spectrosc*, vol. 302, Dec. 2023, doi: 10.1016/j.saa.2023.123048.
31. A. Yusuf, A. R. Z. Almotairy, H. Henidi, O. Y. Alshehri, and M. S. Aldughaim, “Nanoparticles as Drug Delivery Systems: A Review of the Implication of Nanoparticles’ Physicochemical Properties on Responses in Biological Systems,” Apr. 01, 2023, *MDPI*. doi: 10.3390/polym15071596.

Chapter II - Part I

The content of Chapter II - Part II is currently being prepared for submission to a scientific journal

Manual wet granulation as a laboratory-scale strategy for converting aqueous nanosuspensions into granules

1. Introduction

A significant step forward in the formulation of poorly soluble drugs has been the increasing awareness of the benefits associated with the application of nanotechnology. In this context, the development of nanosuspensions (NSs) has emerged as a powerful tool to enhance the dissolution rate and improve the oral bioavailability of the molecule of interest. Nevertheless, being NSs liquid water-based systems, they present major challenges. For instance, tend to have limited long-term stability, poor handling, and entail difficulties in storage and distribution [1-5]. Therefore, developing robust strategies to transform liquid NSs into solid dosage forms has become a key objective among researchers, as this approach can significantly improve stability, simplify the supply chain, and ultimately maximize both therapeutic and commercial potential of nanosized drugs [6-9].

Wet granulation (WG) represents a versatile and widely employed technology to process large quantities of liquid formulations, which are used as the granulating liquid. In this respect, it could be advantageously employed for processing water-based NSs and transforming the latter into solid products. This process transforms fine powders into larger, uniform granules by promoting interparticulate adhesion, resulting in a cohesive wet mass that, after proper drying and screening, yields granules with improved flowability, compressibility/tabletability/compactability, and mechanical integrity. From a processing perspective, WG involves wetting, nucleation, growth by coalescence, consolidation, and attrition, during which formulation and process parameters set would ultimately impact on granule structure. The latter, and especially the particle size, morphology, moisture content, and hardness, are fundamental towards final product quality both whether granules are used as final dosage forms or as intermediates for further processing [10-13].

Based on these premises, the present work explored, at the lab scale, the feasibility of wet granulation to convert a water-based nanosuspension (NS) into granules. More

into details, the granules were produced using as the binding liquid a NS containing cinnarizine (CN NS), which served as a case study. Indeed, CN represents a model compound for the Biopharmaceutical Classification System (BCS) class II, which encompasses a large proportion of new chemical entities (NCEs) [14]. To maximize versatility, polymeric excipients showing a variety of interaction mechanisms with aqueous fluids, thus in principle being used for the formulation of products providing diverse release patterns ranging from immediate to modified release, were investigated. Resulting granules were assessed for key quality parameters considering their potential use either as final dosage forms or as intermediates for the manufacturing of tablets.

2. Materials and Methods

2.1. Materials

CN (mean particle size distribution, PSD: ~ 63.5 ± 1.2 μm) and CN NS (CN load, 10 wt%; d-a-tocopheryl polyethylene glycol 1000 succinate, TPGS, 2.5%; Z-average of ~ 350 nm and PdI of 0.4), both kindly supplied by Novartis Pharma AG (Basel, Switzerland). CN NS was manufactured and characterized as described before [15]. Excipients: sodium starch glycolate (Explotab® CLV, EXP; JRS PHARMA, Rosenber, Germany); soy polysaccharides (Emcosoy®, SP; JRS PHARMA, Rosenber, Germany); lactose monohydrate (GranuLac® 200, LT; MEGGLE, Wasserburg, Germany); polymethacrylates (Eudragit® RL PO, ERL; Eudragit® E PO, EPO; Evonik, Essen, Germany); ethylcellulose (Ethocel™ standard 10 premium, EC; Dupont, UK); hydroxypropyl methylcellulose acetate succinate (AQQAT® AS LG, HPMCAs; Shin-Etsu Chemical, Tokyo, Japan). Binders: polyvinylpyrrolidone (Kollidon® 30, PVP K-30; BASF SE, Germany); copolymer of vinylpyrrolidone and vinyl acetate 6:4 (Kollidon® VA 64, PVP/VA 64; BASF SE, Germany). Other additives: potassium dihydrogen phosphate (AnalaR NORMAPUR, KH_2PO_4; VWR CHEMICALS, Leuven, Belgium); methanol (AnalaR NORMAPUR, CH_4O; VWR CHEMICALS, Fontenay-sous-Bois, France); hydroxypropyl methylcellulose (METHOCEL™ K4M premium, HPMC K4M; Colorcon®, Harleysville, Pennsylvania, USA), magnesium stearate (Mg St; Sigma-Aldrich, Milan, Italy).

2.2. Methods

2.2.1. Particle Size (Z-Average) and Polydispersity Index (PdI) via Dynamic Light Scattering (DLS)

Z-average and PdI of CN NS (n = 3) were measured using Zetasizer Nano ZS DLS instrument (Malvern Instruments, Worcestershire, UK). Before the analysis, samples were diluted (1:100) using a saturated CN solution and equilibrated for 120 s to ensure proper conditioning. The resulting dispersions were sonicated (Ultrasonic Homogenizer UP200St, Hielscher, Germany) for 1 minute at 70% amplitude to disrupt potential aggregates and ensure proper dispersion of the nanocrystals. The temperature was set at 25 °C, and each analysis involved 10 measurements (100 s duration each). The stability of the CN NS, stored in a refrigerator (VWR, Basel, Switzerland; 3 ± 1 °C), was checked by measuring the Z-average and PdI at pre-established time periods (*i.e.,* up to 18 months).

2.2.2. Wet granulation (WG)

WG process was manually performed using pestle and mortar. More in detail, granulates were prepared using either placebo solutions or CN NS added with binders as granulation liquid. Different types (*i.e.,* PVP K-30 and PVP VA/64) and binder concentrations (*i.e.,* 2.5 wt% and 5 wt%) were tested (Table 1). The required binder amount was directly weighed (analytical balance, EWJ 600-2SM, KERN & SOHN GmbH, Balingen, Germany) into the liquid, intended as water or CN NS, and stirred until complete binder solubilization before use.

For all batches, the same quantity of granulation liquid was added progressively in small aliquots, while the powder blend was manually mixed with a pestle to ensure homogeneous wetting and distribution of the binder. This procedure was applied uniformly to placebo and NS-based formulations to achieve comparable wetting and binder content. The addition of liquid was interrupted when the target conditions were reached: *i.e.* for NS-based batches, when the intended CN loading (*i.e.,* 100 mg/g) was achieved, while for placebo batches, when the same quantity of liquid had been added to provide equivalent wetting and binder content across formulations. The wet masses were subsequently oven-dried at 40 °C for 8 h to reach constant mass.

Table 1. Formulation composition (g) of placebo and CN NS-loaded granules

		Formulation composition (g)							
Formulation code		**1a**	**2a**	**1b**	**2b**	**1aNS**	**2aNS**	**1bNS**	**2bNS**
Carrier		17.0	16.5	17.0	16.5	17.0	16.5	17.0	16.5
CN		-				2.0			
TPGS		-				0.5			
Binder	**PVP K-30**	0.5	1.0	-	-	0.5	1.0	-	-
	PVP/VA 64	-	-	0.5	1.0	-	-	0.5	1.0

2.2.3. Granules characterization

2.2.3.1. Process yield

Granules with particle size between 355 and 500 µm were selected using a vibratory sieve shaker (AS 200 basic, Retsch, Haan, Germany, time = 4 min, amplitude of sieving =5). The product yield was calculated as the percentage ratio between the amount of granulate retained on the 355 µm sieve and the total amount of granulate produced, as reported below:

$$\text{Yield (\%)} = 100 * \frac{\text{granulate weight fraction}_{355\,\mu m}}{\text{total weight of granulate produced}} \qquad \text{(Eq. 1)}$$

2.2.3.2. Bulk and Tapped Density

To assess the product density, 5 g of granules within the 355–500 µm size range were weighed and transferred into a 25 mL graduated cylinder. The apparent volume (V_0) of the uncompacted granulate was measured, calculating the bulk density (ρ) as:

$$\text{Bulk density (g/ml)} = \frac{m}{V_0} \qquad \text{(Eq. 2)}$$

Tapped density was then determined according to Method 1 described in the European Pharmacopoeia (XI Ed., 2.9.34). The 25 mL cylinder containing the granules was placed in a tapping volumeter (Stampf Volumeter Stav2003, JEL, Gemini, Netherlands). The products underwent an additional 240 taps, and the final volume (V_f, corresponding to V_{250}) was recorded. Tapped density was calculated as:

$$\text{Tapped density (g/ml)} = \frac{m}{V_f} \qquad \text{(Eq. 3)}$$

2.2.3.3. Flowability

Granule flowability (Eur. Ph. XI Ed., 2.9.36) was evaluated by calculating the compressibility index (CI) and the Hausner ratio (RH), according to the following equations:

$$\text{CI (\%)} = 100 * \frac{V_0 - V_f}{V_0} \qquad \text{(Eq. 4)}$$

2.2.3.4. Friability

Friability of granules having a particle size between 355 and 500 µm was assessed using a testing procedure adapted from the European Pharmacopoeia (XI Ed., 2.9.7, Method B). In particular, 4 g of granules were accurately weighed (analytical balance, EWJ 600-2SM, KERN & SOHN GmbH, Balingen, Germany) directly into a glass

container and then sealed. Then the container was inserted in a turbula mixer (Turbula T2C, Willy A. Bachofen WAB, Switzerland) and subjected to horizontal oscillations for 2 minutes at a constant frequency of 200 oscillations/min. After the experiment, the granules were sieved using a pre-calibrated set of sieves (*i.e.,* 500 µm, 355 µm, and the collecting base), mounted on a vibratory sieve shaker (AS 200 basic, Retsch, Germany). Sieving was performed for 1 min at an amplitude of 4. The fraction retained on the 355 µm sieve was collected and weighed with (CKE 16K0.05, KERN & SOHN, Germany). Friability was calculated as the percentage ratio between the mass loss and the initial granule mass, as follows:

$$\text{Friability (\%)} = 100 * \frac{m_1 - m_2}{m_1} \qquad \text{(Eq. 5)}$$

where m_1 is the initial mass of granules, and m_2 is the final mass after sieving.

2.2.3.5. Particle size

Particle size analysis (n=3) of the selected granulates was measured using a laser diffraction particle size analyzer (Mastersizer 3000, Malvern Instrument, Malvern, UK) equipped with a dry powder disperser (Aero S). The mean particle size (D_{50}) and the corresponding standard deviation (SD) were subsequently calculated.

2.2.3.6. Drug content

CN content (n = 3) was determined using high-performance liquid chromatography (HPLC; HP 1100 ChemStations, Agilent Technologies, Milan, Italy). The latter was equipped with an UV-Vis detector and a reverse-phase column L-column (InertClone ODS, 150 × 4.6 mm 5 µm ODS (3) 100 Å, Phenomenex Inc., Aschaffenburg, Germany), maintained at 30 °C. The mobile phase (*i.e.,* mixture of methanol and pH 3.5 phosphate buffer in water for HPLC;70:30 *v*/*v*) was filtered before use (0.45 µm membrane filter) and pumped at a flow rate of 1 mL/min at 30 °C. The time of the run was set at 10 min. The sample to be evaluated (25 mg) was initially dispersed in 15 mL of mobile phase and then ultrasonicated at 25 °C for 30 min to ensure complete CN dissolution. The resulting liquid was filtered through a 0.22 µm syringe filter and transferred into an HPLC vial kept at 30 °C, from which 10 µL were automatically injected into the HPLC system for being assayed spectrophotometrically (retention time = 4.7 min, λ = 250 nm). The CN content was calculated using a purposely built

calibration curve in the 0.25–500 µg/mL range (y = 33.581x + 5.0951, R^2 = 0.9998). The percentage CN content was calculated as the ratio between the experimentally measured load and a normalized reference value. The latter was calculated taking into account the actual drug content in the CN NS (92.62 µg/mL).

2.2.3.7. *In vitro* performance

Dissolution performance (n = 3) was evaluated *in vitro* using HCl 0.1N (pH 1.2) as the medium and by assembling a small-scale dissolution test ensuring sink conditions. Samples of 25 mg ± 2 mg were dispersed in 15 mL of acidic buffer, maintained at a constant temperature of 25°C, and stirred (300 rpm) by means of a magnetic stir bar. At pre-determined time points (*i.e.,* 1, 3, 5, 10, and 15 min), 1 mL of the dissolution media was withdrawn and filtered through a 0.22 µm syringe filter and replaced with fresh medium to maintain the sink conditions. CN was quantified by HPLC, as described in Section 2.2.3.6. Data were expressed as a percentage of the drug dissolved with respect to the actual drug content.

2.2.3.8. Nanocrystals redispersibility

Nanocrystals redispersibility (n =3) was measured *via* dynamic light scattering (DLS), using a Zetasizer Nano ZS DLS instrument (Malvern Instruments, Worcestershire, UK). Samples were dispersed in a saturated CN solution (200 rpm), and the resulting dispersions were sonicated (Ultrasonic Homogenizer UP200St, Hielscher, Germany) for 1 min at 70% amplitude to separate finer excipient particles from the drug nanocrystals. Z-average (z-avg.) and polydispersity index (PdI) were used as characteristic values for differentiating the redispersibility ability from the tested granules. Data were compared to the original NS dimension through the redispersibility index (RDI) [16]. RDI was calculated (Eq. 6) by normalizing the mean particle size of the redispersed nanocrystals (z-avg.redisp) to the mean NS particle size (z-avg.orig):

$$RDI = \frac{\text{z-avg.redisp}}{\text{z-avg.orig}} \qquad \text{(Eq. 6)}$$

2.2.4. Mini-tablets production

EC2bNS-based granules (355–500 μm particle size) were blended with an external phase consisting of HPMC K4M and/or Mg St, as reported in Table 2.

Table 2. Mini-tablets compositions (w/w %)

	EC2bNS mini-tablet	**EC2bNS-HPMC K4M mini-tablet**
Granulate (%)	98.5	49.25
Mg St (%)	1.5	
HPMC K4M (%)	0	49.25

The resulting blends were processed by means of a rotary tablet press (AM-8S, Officine Ronchi, Cinisello Balsamo, Italy) equipped with 4 mm round punches. When dealing with formulations based on granules and Mg St only, compression forces were set to approximately 5 kN, to obtain tablets with a nominal weight of 25.0 mg and a crushing strength in the 15-20 N range. For tablets containing HPMC K4M in the external phase, a compression force of ~5 kN was applied, resulting in products having a nominal weight of 25.0 mg and a crushing strength <5 N.

2.2.5. Mini-tablets characterization

Mini-tablets (n=10) were characterized for mass uniformity (CRYSTAL 500, Gibertini, Milan, Italy), thickness (Mitutoyo CD-15CP, Andover, UK), and hardness (crash tester, Erweka GmbH, Langen, Germany). Drug load and dissolution performance were determined as reported in Section 2.2.3.6. and 2.2.3.7., respectively. However, for the dissolution performance, the selected time points differed from those previously employed when testing granules and were: 15, 30, 60, 90, and 120 min.

3. Results

3.1. Binder and polymeric carrier selection

In this feasibility study, the WG technique was selected as a flexible strategy for converting liquid NSs into solid intermediates at the lab scale. This method was considered appropriate prior to exploring larger-scale equipment, such as high-shear mixers, particularly considering the limited volume of NS available and the intent to conduct a preliminary screening of various carriers.

Using NSs as the wetting solution for granulation required careful selection of binders, as they may cause instability, such as drug aggregation and sedimentation. To this end, two hydrophilic binders (*i.e.,* PVP K-30 and PVP/VA 64) were tested at 2.5 wt% and 5 wt% for the preparation of CN NS wetting solutions. Particle size analysis check-control of the NS was performed immediately after binder addition and repeated after 24 h (Table 3). Interestingly, the presence of the selected type and amount of binders did not impact the CN NS dimensional characteristics (Table 3).

Table 3. Z-average and PdI relevant to the modified NS (*i.e.,* upon the addition of different binders at increasing concentrations), tested at different times

		Dimensional analysis	**T_0 ± SD**	**T_{24h} ± SD**
PVP K-30 (1)	**2.5 wt% (a)**	**Z-Ave**	346.37 ± 0.50	347.73 ± 5.16
		PdI	0.181 ± 0.026	0.259 ± 0.015
	5 wt% (b)	**Z-Ave**	353.40 ± 1.01	350.27 ± 2.90
		PdI	0.176 ± 0.008	0.297 ± 0.013
PVP/VA 64 (2)	**2.5 wt% (a)**	**Z-Ave**	338.40 ± 2.71	341.07 ± 0.76
		PdI	0.174 ± 0.004	0.261 ± 0.015
	5 wt% (b)	**Z-Ave**	342.47 ± 2.05	345.53 ± 4.22
		PdI	0.218 ± 0.021	0.209 ± 0.012

For the carrier screening phase, a range of excipients was selected based on two key performance criteria: *i)* their ability to interact with water (*i.e.,* moisture-uptaking properties), which can affect granule formation, and *ii)* their potential impact on the granules technical and release performances when they are considered as such or, after further processing (*e.g.,* tableting). In this respect, granule-forming agents capable of modulating the release of CN, achieving both immediate and prolonged release patterns, were taken into account. Based on the above-mentioned considerations, the carriers selected for this work are detailed below:

- EXP: cross-linked sodium starch glycolate, a superdisintegrant that strongly swells upon contact with water (up to 300 times its volume), facilitating prompt disintegration and thus immediate drug release, while being suitable for both direct compression and wet granulation;
- SP: soy polysaccharides acting as disintegrants. Derived from non-genetically modified soy, this material ensures consistent disintegration times with minimal impact on tablet tensile strength;

- LT: monohydrate lactose, widely used as a filler in tablets and capsules, suitable for both wet and dry granulation due to its cohesive properties;
- ERL and EPO: methacrylate-based polymers commonly employed as coating agents for their release-modulating capabilities. More in detail, Eudragit® E is a cationic, pH-dependent polymer soluble at acidic pH (< 5), while Eudragit® RL is a cationic, water-insoluble but highly permeable material, enabling prolonged release.
- EC: ethylcellulose used as a coating and matrix former material in controlled-release formulations. It can modulate drug release by controlling diffusion;
- HPMCAS: hydroxypropyl methylcellulose acetate succinate with acetyl and succinyl groups, providing gastro-resistance. Insoluble in gastric fluids, it swells and dissolves in basic pHs, making it suitable for intestinal delivery.

3.2. Preliminary characterization of the placebo granules

As an initial step, placebo granules were manufactured using an aqueous-based placebo binder solution to assess the capability of different starting polymers to absorb water. This step was deemed essential due to the high-water content associated with the use of the CN NS. This approach allowed estimation of each material's water capacity per wetting before drying (2 h at 40 °C), and calculation of the number of granulation/drying cycles required to achieve the desired CN load.

Formulations containing SP, HPMCAs, EC, ERL, and EPO required at most two drying steps, which was consistent with their water-handling capabilities. In contrast, the LT-based formulation was observed as the most challenging for the WG process, due to the high solubility of the disaccharide. Variations in type or concentration of the binder generally had a limited impact on the process, except for EXP, which showed a shorter drying time when granulated PVP/VA 64 compared to PVP K-30. This screening was essential to identify interesting carrier/binder combinations for the subsequent preparation of NS-loaded granules. All the characterization results relevant to placebo formulations are summarized in Table 4.

Table 4. Physico-technological characteristics of placebo granules (355–500 μm particle size fraction)

	Yield (%)	Friability Mass loss (%)	Bulk density (g/ml)	Tapped Density (g/ml)	CI, %	Hausner ratio	Flowability*
SP1a	69.11	30.10	0.319	0.402	20.63	1.26	Passable
SP2a	48.86	30.05	0.271	0.314	13.51	1.16	Good
SP1b	59.58	10.04	0.379	0.436	13.21	1.15	Good
SP2b	58.11	4.63	0.386	0.446	13.46	1.16	Good
LT1a	40.23	5.47	0.469	0.576	18.60	1.23	Fair
LT2a	43.77	9.52	0.489	0.573	14.63	1.17	Good
LT1b	56.04	28.77	0.590	0.669	11.76	1.13	Good
LT2b	51.15	32.82	0.445	0.527	15.56	1.18	Good
EC1a	27.66	23.46	0.410	0.466	11.90	1.14	Good
EC2a	42.00	10.27	0.400	0.488	18.00	1.22	Fair
EC1b	32.82	10.12	0.427	0.467	8.51	1.09	Excellent
EC2b	50.19	27.55	0.392	0.455	13.73	1.16	Good
HPMCAs1a	88.63	2.50	0.477	0.572	16.67	1.20	Fair
HPMCAs2a	84.07	1.02	0.500	0.588	15.00	1.18	Good
HPMCAs1b	84.87	7.06	0.501	0.572	12.50	1.14	Good
HPMCAs2b	75.07	7.82	0.488	0.556	12.20	1.14	Good
EPO1a	88.43	8.98	0.445	0.541	17.78	1.22	Fair
EPO2a	81.41	8.80	0.400	0.488	18.00	1.22	Fair
EPO1b	86.43	10.29	0.501	0.556	10.00	1.11	Excellent
EPO2b	80.22	10.31	0.456	0.528	13.64	1.16	Good
EXP1a	29.13	12.52	0.485	0.563	13.89	1.16	Good
EXP2a	51.67	36.41	0.455	0.541	15.91	1.19	Fair
EXP1b	49.55	8.77	0.417	0.501	16.67	1.20	Fair
EXP2b	50.20	8.93	0.440	0.510	15.22	1.18	Good
ERL1a	91.16	36.97	0.36	0.46	21.43	1.27	Passable
ERL2a	82.61	44.42	0.27	0.36	24.32	1.32	Passable
ERL1b	94.16	51.27	0.33	0.44	25.00	1.33	Passable
ERL2b	93.21	70.07	0.34	0.44	23.73	1.31	Passable

*defined based on Eur. Ph. XI Ed., 2.9.36 - Powder flow

As highlighted in the table, reference criteria were set to facilitate the identification of the most promising formulations. By way of examples, these included: *i)* flowability, which needed to be "excellent" or "good", *ii)* friability < 15%, and *iii)* product yield > 50%.

Among SP-based samples, the use of PVP/VA 64 resulted in improved flowability, product yield, and mass loss compared to PVP K-30. LT formulations containing PVP/VA 64 showed higher friability but maintained yield above 50%, while flowability remained comparable to PVP K-30 batches. EC samples displayed variable results: most of them were characterized by yields below 50%, with EC2b as an exception, though with higher mass loss; EC1b had excellent flowability and acceptable friability but low overall yield. PVP K-30-based EC samples pointed out insufficient yield, and some showed high mass loss or poor flowability. HPMCAs and EPO formulations performed consistently, with yields around 80% and mass loss ≤10%. Flowability was slightly improved using PVP/VA 64, particularly in EPO samples. EXP granules showed comparable flowability. Differences were observed in product yield (~50% with PVP/VA 64) and mass loss, which remained <10% only in 1b and 2b samples. ERL formulations had analogous, though suboptimal, flowability, high mass loss, and excellent product yield (>90%).

Based on the above-mentioned results, PVP/VA 64 was selected as the binder for preparing drug-loaded granules: both minimum (2.5% w/w) and maximum (5% w/w) binder concentrations were employed.

3.3. Characterization of the CN NS-loaded granules

Based on placebo trials, CN NS containing granules were prepared and characterized, assessing the effect of using a NS-based wetting liquid on the key quality attributes previously defined (Table 5).

Table 5. Physico-technological characteristics of CN NS-loaded granules (355–500 μm particle size fraction)

	Yield (%)	**Particle size distribution (μm)**	**Friability**	**Bulk density (g/ml)**	**Tapped Density (g/ml)**	**CI, %**	**Hausner ratio**	**Flowability***
		D_{50} ± SD	**Mass loss (%)**					
SP1bNS	44.32	480 ± 3.2	1.40	0.334	0.395	15.38	1.18	Good
SP2bNS	41.97	478 ± 1.2	1.64	0.352	0.409	14.00	1.16	Good
LT1bNS	44.92	495 ± 9.0	7.55	0.557	0.67	16.67	1.20	Fair
LT2bNS	48.17	505 ± 2.3	7.94	0.557	0.67	16.67	1.20	Fair
EC1bNS	60.68	482 ± 1.7	1.40	0.392	0.435	9.80	1.11	Excellent
EC2bNS	58.71	466 ± 2.6	3.85	0.394	0.447	11.76	1.13	Good
HPMCAs1bNS	77.85	504 ± 6.2	2.42	0.513	0.572	10.26	1.11	Excellent
HPMCAs2bNS	75.71	517 ± 9.6	10.16	0.477	0.541	11.90	1.14	Good
EPO1bNS	55.98	529 ± 14.2	12.52	0.476	0.556	14.29	1.17	Good
EPO2bNS	61.93	519 ± 6.1	13.84	0.500	0.572	12.50	1.14	Good
EXP1bNS	41.41	425 ± 11.7	10.11	0.400	0.47	14.00	1.16	Good
EXP2bNS	52.06	490 ± 3.2	22.52	0.510	0.57	10.26	1.11	Excellent
ERL1bNS	44.28	430 ± 12.5	5.33	0.390	0.48	17.65	1.21	Fair
ERL2bNS	38.87	455 ± 5.5	7.34	0.390	0.45	13.46	1.16	Good

*defined based on Eur. Ph. XI Ed., 2.9.36 - Powder flow

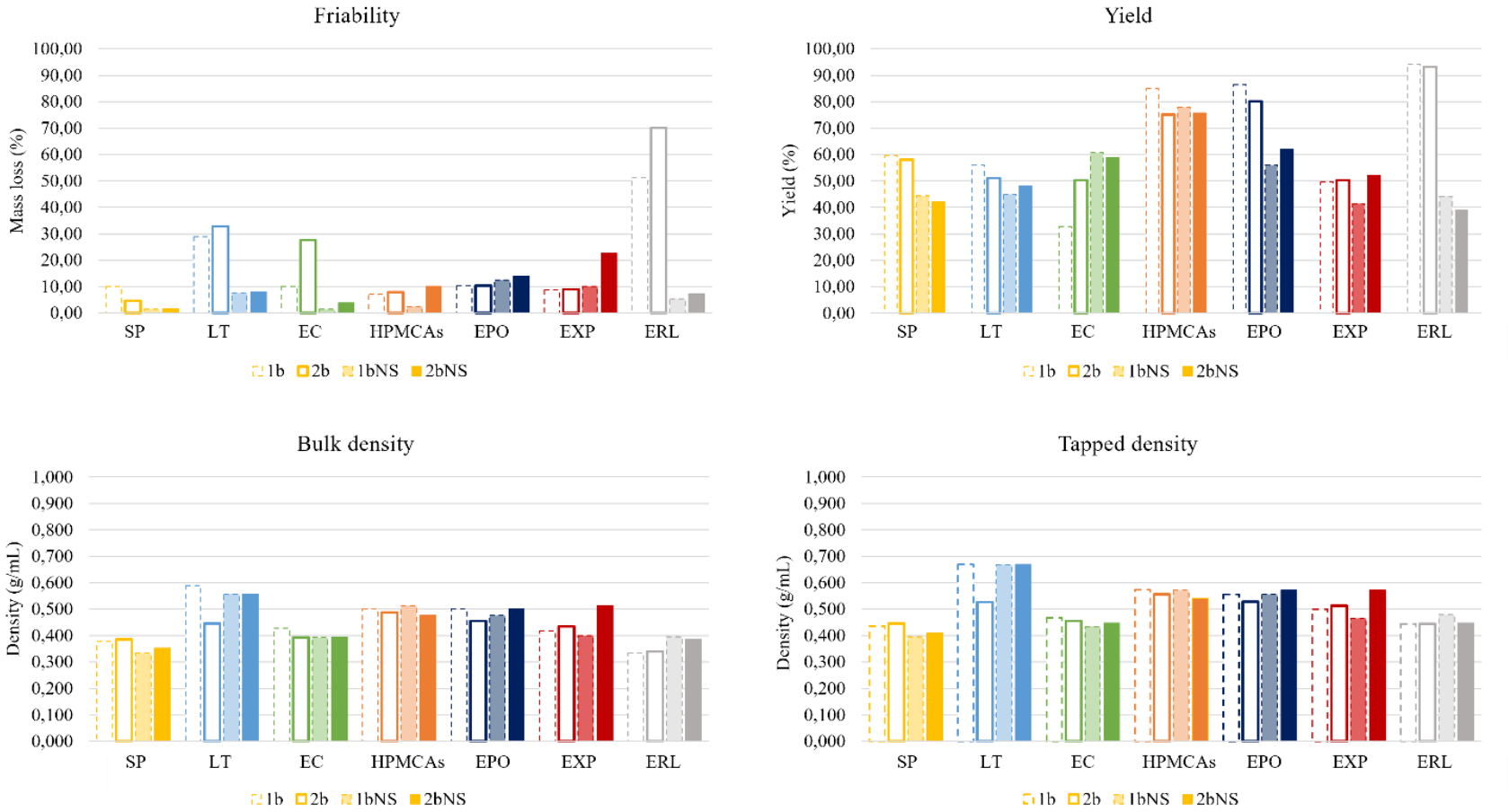

Figure 7. Comparative histograms illustrating the key physico-technological properties of granules.

Overall, the physico-technological characteristics of NS-loaded granules were preserved or even improved, particularly in terms of flowability and mass loss, with only minor reductions in product yield. More into details, WG using the CN NS generally resulted in granules with friability values markedly reduced (overall 10%, Figure 1a) with respect to their placebo counterparts. EXP2bNS sample represented the sole exception, exhibiting a mass loss of approximately 20%. A particularly striking example is provided by ERL1b and ERL2b, as placebo formulations showed mass losses of 51% and 70%, respectively, while the corresponding NS-loaded granules exhibited only 5% and 7%.

Regarding product yield % (Figure 1b), most granules exhibited values comparable to placebo samples. Indeed, in most cases, yields exceeded 50%, with only a few formulations showing slightly lower values, though never below 40%. The most pronounced difference was observed for ERL-based samples, which displayed a markedly reduced yield compared to the corresponding placebo granules, with a decrease of approximately 50%.

Interestingly, the use of the CN NS as the granulating liquid did not negatively affect the flowability of the resulting granules (Figure 1c and 1d). Except for the LT-based formulations, which exhibited only a slight deviation from their placebo analogues, all NS-loaded samples displayed flow properties comparable to the corresponding placebo and, in the case of EXP1bNS, EXP2bNS, ERL1bNS, and ERL2bNS, even improved performance.

As no major differences were observed between granules with different PVP/VA 64 concentrations, further analyses, including drug content, dissolution profile, and redispersibility index, were deemed essential to fully assess granule quality.

3.3.1. Drug content

Evaluating the actual CN content in granules was considered a critical step in this screening process. Indeed, it was a way to assess that the drug was effectively retained during the WG process and no marked loss occurred (Table 6).

Table 6. Drug content (%) of CN NS-loaded granules, including the coefficient of variation (CV, %)

	CN content, % (CV, %)
SP1bNS	105.05 (1.97)
SP2bNS	99.02 (11.36)
EC1bNS	93.56 (1.48)
EC2bNS	95.06 (4.72)
HPMCAs1bNS	97.68 (2.91)
HPMCAs2bNS	99.04 (4.07)
LT1bNS	98.94 (15.87)
LT2bNS	100.61 (2.52)
EXP1bNS	108.89 (5.76)
EXP2bNS	104.13 (3.48)
EPO1bNS	94.51 (7.75)
EPO2bNS	103.7 (7.87)
ERL1bNS	101.72 (2.16)
ERL2bNS	103.96 (3.96)

The analysis of the CN content confirmed an overall high loading efficiency, with most samples showing values above 95-105%.

3.3.2. *In vitro* performance

Assessing the release behavior of CN NS-loaded granules was a pivotal part of the characterization phase. Indeed, in products containing drug nanocrystals, dissolution performance serves not only as an indicator of the granulation efficiency but also offers valuable insights into two key aspects: *i)* whether the WG process preserves the nanoscale particle size of the drug, thereby enabling granules to exhibit a release profile comparable to the original NS, and *ii)* the capability of the selected carriers in achieving their intended function of modulating drug release (*e.g.,* ensuring controlled release even when dealing with granules containing drug nanocrystals that can easily escape entrapment within the polymeric network). By way of example, profiles relevant to granules containing the lowest binder concentration (*i.e.,* 1bNS formulations) are summarized in Figure 2.

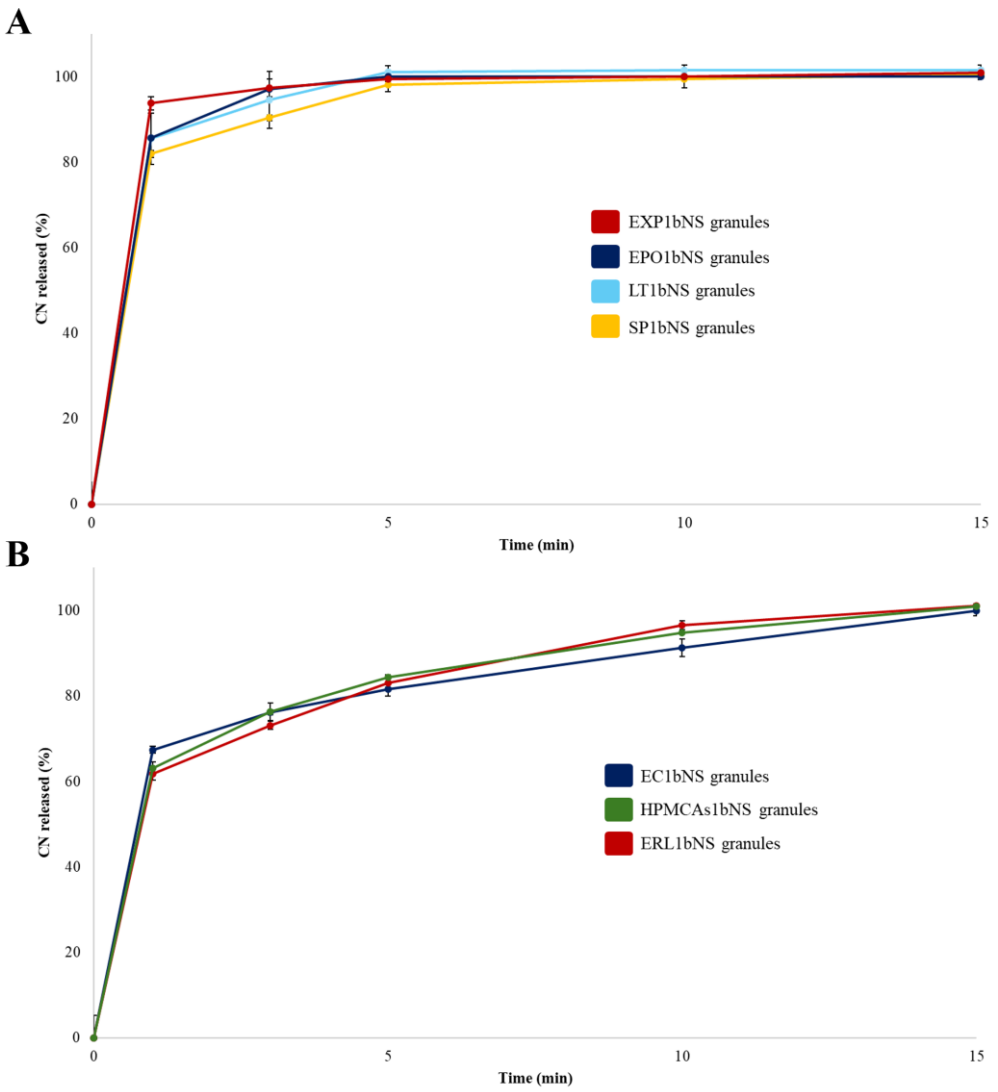

Figure 8. Release profiles relevant to (A) immediate- and (B) modified-release granules.

Granules based on EXP and EPO released nearly 100% of the CN within 3 min, while those containing LT and SP reached a plateau within 5 min. In contrast, granules prepared with EC, HPMCAs, and ERL did not exhibit the expected modified release behavior. Indeed, they released the entire drug content within 15 minutes. By way of example, profiles relevant to granules containing the lowest binder concentration (*i.e.,* 1bNS formulations) are summarized in Figure 2. Indeed, formulations with the highest concentration of binder (*i.e.,* 2bNs) pointed out an analogous release pattern.

The impossibility of obtaining the desired modified release appeared inconsistent with the intrinsic functional properties of the polymers selected, which are typically associated with prolonged release when used as matrix-forming material. A plausible

explanation is that the granulation process was not sufficiently effective in both providing appropriate densification of the product and achieving a homogeneous incorporation of the nanocrystals within the polymer matrix, thus leading to only a superficial drug deposition and prompt release. Additionally, the very high surface area coupled with the size as well as the fast dissolution kinetics of the CN nanocrystals in acidic environment might have overshadowed the controlling effect of the polymers, preventing the onset of controlled release.

3.3.3. Nanocrystals' redispersibility

The RDI of the CN nanocrystals from drug-loaded granules was assessed in comparison against the reference NS, to ensure that the manufacturing processes, and especially the drying phase, did not alter the starting particle size of CNS (Table 7). RDI values approaching 1.0 indicated optimal redispersion of nanocrystals from the granules, with values < 1.20 considered acceptable [9, 17].

Table 7. Z-average, PdI, and RDI values relevant to CN NS-loaded granules

Sample	Z-ave (d-nm) ± SD	PdI ± SD	RDI
SP1bNS	346.4 ± 4.42	0.210 ± 0.01	1.007
SP2bNS	345.1 ± 7.29	0.212 ± 0.02	1.003
LT1bNS	388.0 ± 4.76	0.345 ± 0.04	1.128
LT2bNS	344.5 ± 0.85	0.204 ± 0.02	1.001
EC1bNS	355.8 ± 3.59	0.239 ± 0.01	1.034
EC2bNS	320.0 ± 0.80	0.213 ± 0.01	0.930
HPMCAs1bNS	587.1 ± 6.84	0.382 ± 0.03	1.707
HPMCAs2bNS	475.9 ± 5.35	0.302 ± 0.04	1.383
EXP1bNS	357.2 ± 4.30	0.185 ± 0.02	1.038
EXP2bNS	349.3 ± 6.92	0.163 ± 0.01	1.015
EPO1bNS	401.4 ± 6.78	0.298 ± 0.03	1.167
EPO2bNS	392.5 ± 5.00	0.278 ± 0.02	1.141
ERL1bNS	379.3 ± 5.22	0.241 ± 0.01	1.103
ERL2bNS	415.6 ± 1.32	0.246 ± 0.02	1.208

All granules exhibited acceptable RDI values, indicating an effective redispersion of the nanocrystals and demonstrating the process ability to preserve the original CN NS particle size. Minor deviations were observed for HPMCAs-based samples. However, values falling outside the acceptable range can likely be attributed to the presence of

insoluble particle populations, dimensionally greater but indistinguishable from CN nanocrystals due to limitations of the analytical technique employed.

3.4. Tableting

As a further assessment of their performance, the granules were used to prepare mini-tablets of 4 mm in diameter. Besides exploring the suitability of granules for further processing, this step helps in evaluating whether *i*) the application of mechanical stress would compromise the physico-chemical and dimensional properties of the nanocrystals conveyed, and *ii*) the densification achieved could enhance the release behavior of products intended for controlled release. To this end, EC-based products served as a model system. More in detail, mini-tablets were produced starting from granules having the highest binder concentration (*i.e.,* EC2bNS), which were blended with either Mg St alone or in combination with HPMC K4M (Table 8), used as a matrix-forming polymer.

Table 8. Tableting parameters and physico-technological characteristics of the resulting tablets

	Tablet weight (mg) (± SD)	**Compression force (kN) (± SD)**		**Ejection force (kN) (± SD)**	**Thickness (mm) (± SD)**	**Hardness (N) (± SD)**
		Upper	**Lower**			
EC2bNS mini-tablet	25.20 ±2.20	4.87 ± 0.16	4.91 ± 0.15	21.06 ± 1.15	2.30 ± 0.06	14.3 ± 1.53
EC2bNS-HPMC K4M mini-tablet	25.32 ±2.12	3.78 ± 0.03	3.81 ± 0.03	23.36 ± 0.81	2.16 ± 0.02	4.0 ± 0.52

All tablets exhibited an acceptable weight and comparable average thickness. Prototypes containing HPMC K4M were characterized by a greater mechanical resistance.

3.4.1. *In vitro* performance

The *in vitro* performance of the EC-based tablets allowed to estimate whether the densification entailed by the tableting process effectively impacted the release behavior of the starting granules, and the presence of high viscosity HPMC further helped to control the release kinetics (Figure 3).

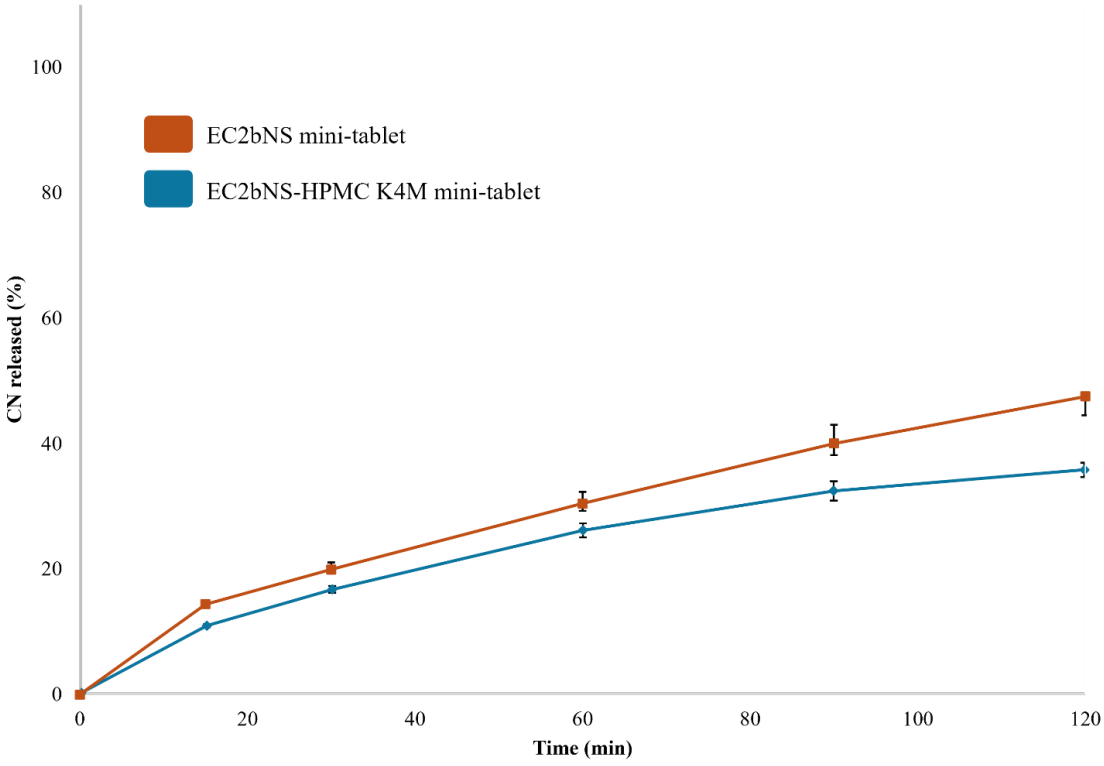

Figure 9. Release profiles relevant to EC2b mini-tablets with and without HPMC K4M.

The dissolution profiles of the EC-based mini-tablets clearly demonstrated that compaction of granules induced an effective modification in the release behavior compared to the corresponding uncompressed products (Figure 3). Specifically, EC2bNS specimens exhibited a slower release rate, achieving approximately 50% of drug release within 2 h. Adding HPMC K4M further slowed down the release rate, with samples releasing approximately 35% of the CN over the same timeframe. These

data highlighted the positive impact of a hydrophilic matrix-forming agent on the release pattern of tableted samples compared to formulations without the polymer.

Overall, the *in vitro* performance test confirmed that the granules, when used as intermediates, can implement the prolonged-release profile thanks to the densification provided by the tableting process, and the latter can be further fine-tuned by adding other release-controlling polymers.

3.4.2. Nanocrystals' redispersibility

Assessing the maintenance of the CN nanoscale dimensions was essential to determine the actual impact of an additional technological process (*e.g.,* tableting) on the original drug particle size (Table 9).

Table 9. Z-average, PdI, and RDI values relevant to CN NS-loaded mini-tablets

Sample	Z-ave (d-nm) ± SD	PdI ± SD	RDI
EC2bNS mini-tablet	368.8 ± 8.44	0.382 ± 0.06	1.072
EC2bNS-HPMC K4M mini-tablet	443.0 ± 10.08	0.395 ± 0.03	1.288

Also in this case, dimensional values were found to be consistent with those relevant to the starting NS, with RDI data falling within the optimal range. More in detail, the CN nanocrystals were effectively redispersed by the EC2bNS mini-tablets. On the other hand, EC2bNS-HPMC K4M samples displayed slightly higher-than-expected measurements.

4. Conclusion

This work represented a proof-of-concept study on the feasibility of transforming, at the lab-scale, a NS containing CN, a poorly water-soluble BCS class II model drug, into solid oral dosage forms while preserving the nano-dimensions of the drug. The WG strategy proved effective in producing granules containing drug nanocrystals that preserved their nanoscale dimensions and physicochemical integrity. Additionally, the granules exhibited technological attributes comparable to the placebo counterparts

and, when formulated with polymers with a prompt interaction with biological fluids, delivered the intended IR performance. To test the possible use of granules not only as a final dosage form but also as an intermediate for subsequent processing, they were used to produce mini-tablets. Tableting allowed to modulate the CN release by decreasing product porosity and reducing the area exposed to aqueous fluids, enabling the attainment of slower release profiles, particularly when hydrophilic polymers were added in the external phase. Importantly, neither granulation nor tableting altered the crystalline state or the size of the CN nanocrystals. Overall, this work confirmed the possibility of using WG with water-based NS as the granulation liquid for manufacturing solid oral dosage forms containing BCS class II drugs, offering a versatile platform for tailoring the product release performance through appropriate selection of formulation and processing parameters.

References

1. V. Patel and Y. Agrawal, "Nanosuspension: An approach to enhance solubility of drugs," *J Adv Pharm Technol Res*, vol. 2, no. 2, p. 81, 2011, doi: 10.4103/2231-4040.82950.
2. V. P. Chavda, D. A. Vaghela, H. K. Solanki, P. C. Balar, S. Modi, and N. R. Gogoi, "Nanosuspensions: A new era of targeted therapeutics," Mar. 01, 2025, *Editions de Sante*. doi: 10.1016/j.jddst.2025.106613.
3. S. Jacob, A. B. Nair, and J. Shah, "Emerging role of nanosuspensions in drug delivery systems," Jan. 15, 2020, *BioMed Central Ltd.* doi: 10.1186/s40824-020-0184-8.
4. R. M. Hanwate, R. H. Babu, A. A. Wadhave, and V. Mishra, "Advancements in Nanosuspension Technology for Drug Delivery," 2025, *Springer Nature*. doi: 10.1007/s44174-025-00368-4.
5. S. Jacob, F. S. Kather, S. H. S. Boddu, M. Attimarad, and A. B. Nair, "Nanosuspension Innovations: Expanding Horizons in Drug Delivery Techniques," Jan. 01, 2025, *Multidisciplinary Digital Publishing Institute (MDPI)*. doi: 10.3390/pharmaceutics17010136.
6. I. Aghrbi, V. Fülöp, G. Jakab, N. Kállai-Szabó, E. Balogh, and I. Antal, "Nanosuspension with improved saturated solubility and dissolution rate of cilostazol and effect of solidification on stability," *J Drug Deliv Sci Technol*, vol. 61, Feb. 2021, doi: 10.1016/j.jddst.2020.102165.
7. M. Malamatari, S. Somavarapu, K. M. G. Taylor, and G. Buckton, "Solidification of nanosuspensions for the production of solid oral dosage forms and inhalable dry powders," Mar. 03, 2016, *Taylor and Francis Ltd*. doi: 10.1517/17425247.2016.1142524.
8. N. C. Patel and H. A. Patel, "A Recent Solidification Approach for Nanosuspension: Formulation, Optimisation and Evaluation of Canagliflozin Immediate Release Pellets," *Folia Med (Plovdiv)*, vol. 64, no. 3, pp. 488–500, 2022, doi: 10.3897/folmed.64.e68866.
9. X. Zhang, J. Guan, R. Ni, L. C. Li, and S. Mao, "Preparation and solidification of redispersible nanosuspensions," *J Pharm Sci*, vol. 103, no. 7, pp. 2166–2176, 2014, doi: 10.1002/jps.24015.

10. A. K. Vadaga, S. S. Gudla, G. S. K. Nareboina, H. Gubbala, and B. Golla, "Comprehensive review on modern techniques of granulation in pharmaceutical solid dosage forms," Oct. 01, 2024, *KeAi Publishing Communications Ltd.* doi: 10.1016/j.ipha.2024.05.006.
11. P. Suresh, I. Sreedhar, R. Vaidhiswaran, and A. Venugopal, "A comprehensive review on process and engineering aspects of pharmaceutical wet granulation," 2017, *Elsevier B.V.* doi: 10.1016/j.cej.2017.07.091.
12. S. M. Iveson, J. D. Litster, K. Hapgood, and B. J. Ennis, "Nucleation, growth and breakage phenomena in agitated wet granulation processes: a review," 2001. [Online]. Available: www.elsevier.comrlocaterpowtec
13. S. Shanmugam, "Granulation techniques and technologies: Recent progresses," *BioImpacts*, vol. 5, no. 1, pp. 55–63, 2015, doi: 10.15171/bi.2015.04.
14. G. L. Amidon, H. Lennernäs, V. P. Shah, and J. R. Crison, "A theoretical basis for a biopharmaceutic drug classification: the correlation of in vitro drug product dissolution and in vivo bioavailability," *Pharm Res*, vol. 12, 1995.
15. E. Ragucci *et al.*, "Feasibility of Hot Melt Extrusion in Converting Water-Based Nanosuspensions into Solid Dosage Forms," *Pharmaceutics*, vol. 17, no. 5, p. 662, May 2025, doi: 10.3390/pharmaceutics17050662.
16. M. Wewers *et al.*, "Influence of formulation parameters on redispersibility of naproxen nanoparticles from granules produced in a fluidized bed process," *Pharmaceutics*, vol. 12, no. 4, Apr. 2020, doi: 10.3390/pharmaceutics12040363.
17. M. Wewers *et al.*, "Evaluation of the Formulation Parameter-Dependent Redispersibility of API Nanoparticles from Fluid Bed Granules," *Pharmaceutics*, vol. 14, no. 8, Aug. 2022, doi: 10.3390/pharmaceutics14081688.

Chapter II - Part II

The content of Chapter II - Part II is currently being prepared for submission to a scientific journal.

Twin-screw wet granulation: a novel continuous manufacturing approach for solidifying nanosuspensions

Abstract

Despite their widely recognized performance-related benefits, oral solid products containing nanosuspensions (NSs) present major challenges for the pharmaceutical sector, mainly due to their poor stability as well as the energy- and time-consuming nature of the manufacturing methods already in use. In this context, we assessed the potential of a lab-scale twin-screw wet granulation (TSWG) process, based on a dry binder approach, as a novel and scalable continuous manufacturing strategy for transforming NSs into solid orally administered dosage forms. To this end, a DoE considering soluble (lactose, LAC; mannitol, MAN) and insoluble (hydrated colloidal silicon dioxide, SYL; pregelatinized maize starch, PGS) fillers in different ratios was employed, using a model cinnarizine (CN)-based NS as the wetting liquid and powder blends comprising a fixed combination of disintegrant, lubricant, and glidant. The granules attained were checked for key quality attributes (*e.g.,* physico-technological properties, nanocrystal redispersibility, and release performance) and further evaluated as intermediates for tablet production. Overall, the strategy pursued in this work turned out to be effective in speeding up the identification of optimal formulations. Specifically, those containing lower amounts of SYL, irrespective of the paired soluble filler, yielded to granules with desirable characteristics in terms of CN load, porosity, redispersibility of drug nanocrystals, and compaction behavior. On the other hand, analogous formulations containing PGS exhibited suboptimal compressibility and CN content, while MAN emerged as a more effective soluble filler. Finally, the nanoscale size of the drug, which was successfully preserved during processing, showed improved dissolution rate and bioavailability in model Caco-2 cells.

Keywords: nanosize, granules, tableting, continuous manufacturing, design of experiment, poorly soluble drugs, Caco-2 cells.

1. Introduction

Over the past years, the continuous manufacturing (CM) approach has garnered significant interest in the pharmaceutical field [1-4]. In this approach, several unit operations involved in the production of a specific dosage form (*e.g.,* blending, granulation, drying, milling, dosing, and tableting) are integrated into a single, streamlined process. By leveraging process analytical technologies, it also enables real-time monitoring of the downstream manufacturing chain, supporting continuous optimization [5-7]. Due to these peculiar characteristics, CM allows overcoming the current limitations of the batch-wise manufacturing approach, such as unexpected inconsistency among batches, which are ruled out in a delayed manner with respect to the time of manufacturing, risk of contamination, and relatively long process times [8-11]. CM leads to substantial cost and time savings, facilitating shorter production cycles, reducing the number of processing steps, and minimizing energy consumption as well as waste, increasing the overall manufacturing efficiency while enhancing product consistency and reproducibility, which are critical for maintaining high-quality standards. The latter aspects are especially relevant today, as the pharmaceutical industry increasingly prioritizes sustainability and leaner manufacturing approaches. Its inherent flexibility in scaling either up or down allows for a more adaptable manufacturing process, which can quickly respond to changing market demands, even including the new ones associated with personalized medicine. In a wider perspective, all these features make CM an interesting tool in the field of medicinal products, and its application potential deserves to be further explored [7, 12-14].

In the framework of CM, twin-screw wet granulation (TSWG) stands out as a versatile, reliable, cost- and time-efficient method for producing solid oral dosage forms [15,16]. Indeed, it offers several advantages, including flexibility in formulation (*i.e.,* type and amount of excipients), equipment design (*i.e.,* screw elements and barrel configuration), and processing parameters (*i.e.,* screw speed, feed rate) [17]. As a CM-compatible technique, TSWG supports both small- and large-scale production by simply adjusting the processing time and/or throughput, without the need to change the equipment in use. Moreover, it enables robust in-line process controls, enhancing consistency and ensuring reliable product quality [18-22].

Being based on the addition of a granulation liquid (commonly water) to a powder stream and often used in combination with subsequent continuous fluid-bed drying, TSWG may represent an advantageous alternative to solidifying techniques, such as freeze- and spray drying, for particulate production. By way of example, the prolonged time required by spray-granulation methods not only increases production costs but can also lead to instability constraints, particularly when dealing with heat-sensitive materials, such as biopharmaceuticals, and with thermodynamically unstable systems, such as nanosuspensions (NSs) [21, 23-26]. NSs are submicron-sized, colloidal, heterogeneous aqueous dispersions containing poorly soluble active pharmaceutical ingredients (APIs), with particle sizes ranging from 1 to 1000 nm [27-29]. Overall, they are characterized by an increased specific surface area (SSA) of the drug which can led to *i)* improved saturation solubility [30], *ii)* a faster dissolution rate as described by the Noyes-Whitney equation [30, 31], and *iii)* enhanced mucoadhesive properties, which may prolong the residence time in the gastrointestinal tract, thus providing more time for the active molecule to completely dissolve [32-35]. However, all these features, which could in principle improve drug bioavailability, are accompanied by major challenges, mainly related to physical-chemical instability of the water-based NSs. In fact, as the surface area increases, Gibbs free energy rises, leading to a thermodynamically unstable system sensitive to sedimentation, aggregation, solid-state transformation, and crystal growth phenomena. As a result, dimensional changes of the API nanoparticles may occur, worsening their dissolution performance and, ultimately, bioavailability [36-39]. In this respect, transforming NSs into more convenient solid products by downstream processes, taking advantage of appropriate drying methods, was described as an interesting strategy to address the above-mentioned challenges. Indeed, this approach not only enhances NS stability and ease of handling but also contributes to improve compliance from the patients' perspective, as solid oral dosage forms remain the preferred route for drug administration [40, 41]. This study evaluates the feasibility of TSWG, considering its compatibility with the CM approach, for transforming a case-study NS into multiparticulate systems (*i.e.,* granules) intended for oral administration in a single processing step. More specifically, the TSWG approach relied on *i)* a NS containing cinnarizine (CN) as a model drug, and *ii)* on the use of a dry binder, overcoming possible issues related to

further addition of a binding solution. A 2^3 full-factorial design was performed to deepen the formulation parameters (*i.e.,* amount and type of fillers intended as carriers forming the powder bulk) and to evaluate robustness of the tested formulations towards the addition of high amounts of water, as necessarily entailed by the use of a NS as the starting material. During the work, major efforts were dedicated to verifying that the transformation process did not change the nanosized drug, given its impact on CN dissolution rate and, therefore, on final *in vivo* exposure.

2. Materials and Methods

2.1. Materials

EXP: sodium starch glycolate (EXPLOTAB® CLV; JRS PHARMA, Rosenberg, Germany); A200: colloidal anhydrous silica (Aerosil 200; Evonik, Essen, Germany); PVP K-30: polyvinylpyrrolidone (Plasdone K30; Ashland, Hamburg, Germany); SSF: sodium stearyl fumarate (PRUV®; JRS Pharma, Rosenberg, Germany); LAC: spray-dried mixture of crystalline and amorphous lactose (Sheffield™ Spray Dried Fast Flo® 316; Kerry Group, Tralee, Ireland); MAN: spray-dried mannitol (PEARLITOL 200SD; Roquette, Lestrem, France); SYL: hydrated colloidal silicon dioxide (SYLOID 244 FP; Grace, Columbia, MD, USA, USA); PGS: partially pregelatinized maize starch (MAISSTAERKE STA-RX 1500; Colorcon, Idstein, Germany).

CN: cinnarizine (mean particle size distribution, PSD: ~ 63.5 ± 1.2 μm) kindly provided by Novartis Pharma AG (Basel, Switzerland).

CN NS: CN nanosuspension (CN load, 10 wt%; d-a-tocopheryl polyethylene glycol 1000 succinate, TPGS, 2.5%; Z-average of ~ 500 nm and PdI of 0.4) kindly supplied by Novartis Pharma AG (Basel, Switzerland). It was manufactured and characterized as described before [42].

2.2. Methods

2.2.1. *Preparation of powder blends*

Powder blends were formulated based on a Design of Experiments (DoE) full factorial approach, involving 77% by weight of variable fillers and 23% of fixed components (Table 1). Powder batches (200 g) were prepared in a single-mixing step, using a Turbula® shaker mixer (type T2C, WAB AG, Maschinenfabrik, Muttenz,

Switzerland), operating for 4.30 min at 22.5 rpm. Before blending, starting materials were manually sieved through a 0.8 mm mesh sieve.

Table 1. Composition of the formulations tested and relevant identification codes.

Code	Materials							
	Fixed components (23%)				DoE variable components (77%)			
	EXP	PVP K30	SSF	A200	LAC	MAN	SYL	PGS
N1	15	2.5	5.0	0.5	23.10			53.90
N2					23.10		53.90	
N3						23.10		53.90
N4						23.10	53.90	
N5					53.90			23.10
N6					53.90		23.10	
N7						53.90		23.10
N8						53.90	23.10	

2.2.2. *TSWG*

TSWG was carried out in a co-rotating Pharma 11 mm twin-screw granulator (Thermo Scientific Pharma 11, Thermo Fisher Scientific, Karlsruhe, Germany). The design of the screws was previously defined to ensure proper formulation flow along the successive zones of the barrel. More into details, the resulting screws were composed of different elements ensuring: feeding (zone 1- 2), kneading (zone 3-6), and grinding (zone 7-8) [43]. Screws features were: diameter (D) 11 mm, length (L), 40 ¾ D. From inlet to outlet of the barrel the following elements were provided: 2 L/D conveying elements (CE), 4 L/D long helix CE, and 4 L/D CE in the feeding zone; a sequence of ¾ L/D at 30° stagger angle kneading elements (KE) [43], and 9 L/D CE in the kneading zone, repeated twice in the forward configuration; ¾ L/D at 30° stagger angle KE, 8 L/D CE, and 2 ½ L/D distributive flow elements (set to reduce oversized granules fraction [44].

The temperature was maintained constant (30 °C) along the different barrel zones. The setup of other TSWG parameters is discussed in the results and discussion section. Before the trials, the extruder was equilibrated for at least 1h to ensure temperature stabilization. Probes were plugged and connected for each zone to rule out any temperature changes during the process. A water-based cooling system (Thermo Scientific™, Accel 500 LC, Thermo Fisher Scientific, Karlsruhe, Germany) was used,

setting the water temperature at 15 °C. Feeding (zone 1) of powder blends into the twin-screw granulator was carried out using a gravimetric twin-screw feeder (K-Sampler, K-CL-SFS-MT12, Coperion K-Tron, GmbH, Niederlenz, Switzerland), which was previously calibrated to ensure the desired feeding rate (*i.e.,* 250 g/h). The liquid feeding port was placed at zone 2, dispensing the NS by means of a peristaltic pump (Ismatec Reglo ICC ISM4308, Cole-Parmer, Barrington, Illinois, United States; inner diameter tube, 0.06 mm; tube wall, 0.03 mm). The NS flow rate was purposely calibrated. Each trial lasted approximately 40 min. Every 10 min, wet granules were collected at the barrel outlet for visual inspection and checked for moisture content, verifying the achievement of the desired L/S ratio.

2.2.3. *Fluidised-bed drying*

Drying of wet granules was carried out using a fluidised-bed dryer (Mini Glatt 5, Glatt, Binzen, Germany) pre-heated for at least 1h, allowing stabilization of the exhaust air temperature at 40 °C. After equilibration, the fluid bed was filled with the resulting total amount of wet granules (approximately between 300 and 550 g). For each drying process, the inlet air flow rate was increased until appropriate fluidisation, ranging between 0.4 and 0.5 bar. Parameters were adjusted according to Section 3 Results and discussion. The process time varied between 20 and 50 min. A two-step process control was applied based on the achievement of a product with a temperature around 40 °C and a loss of drying content (LOD) of ≤5%. Prior to further characterization, dried granules were milled through a 0.71 mm mesh sieve.

2.2.4. *Characterization*

2.2.4.1. *Particle size measurements*

Particle size distribution and specific surface area (m^2/kg) were determined through a laser diffraction system, using a Mastersizer 3000 (n = 3; Malvern Instruments, Worcestershire, UK), equipped with either an Aero S dry dispersion unit or a Hydro SV liquid dispersion unit. The dispersion conditions (% air pressure and % feed rate) were adjusted depending on the different product flowability. Results were expressed as median particle size (D50), which represents the diameter at which 50% of the total particle volume consists of smaller particles. The span was also calculated using the

following formula (Span = $(D_{90}-D_{10})/D_{50}$), referring to the width of the particle size distribution. X_{10} and X_{90} were determined, representing the particle diameters below which 10% and 90% of the total particle volume, respectively, were found.

2.2.4.2. *LOD analysis*

Granules' LOD was measured using a thermobalance moisture analyzer (HX204, Mettler Toledo, Greifensee, Switzerland), by drying approximately 2-4 g of samples at 105 °C, until the weight loss rate was less than 1mg/50s. LOD data were employed both for checking the applied L/S ratio during the wet granulation process and defining the final point of fluidised-bed drying.

2.2.4.3. *Density measurements*

True density (ρ_{true}) of the granules was determined using a helium gas pycnometer Ultrapyc 5000 (Anton Paar GmbH, Graz, Austria, n = 3, 10 purging runs, 2.0 g sample size, and 19.000 psi target pressure).

Granules bulk (ρ_{bulk}) and tap (ρ_{tapped}) densities were evaluated according to the USP-Method I procedure. Before measurements, granules were sieved through a 1.0mm sieve to break up agglomerates that may have formed during storage. ρ_{bulk} of granules was determined by gently introducing approximately 15 mL of product into a graduated cylinder as the ratio of the mass of the powder to the volume occupied. Afterward, the cylinder was mechanically tapped (volumetric analyzer; JEL Stampfvolumeter STAV 2003, Engelsmann, Germany) 10, 500, and 1250 times, determining the ρ_{tapped}. The tapped density was calculated by dividing the mass of the granules by their tapped volume.

Granules cohesiveness was assessed using the Hausner ratio (HR), calculated on their bulk and tapped density (Eq. 1). Moreover, Carr's index (CI) was used to determine the flowability of the granules (Eq. 2).

$$HR = \frac{\rho tapped}{\rho bulk} \qquad \text{(Eq. 1)}$$

$$CI = \frac{(\rho tapped - \rho bulk)}{\rho tapped} * 100 \qquad \text{(Eq. 2)}$$

From ρ_{true} and ρ_{bulk} values, fractional granule porosity (ε) was finally calculated as (Eq. 3):

$$\varepsilon = 1 - \frac{\rho bulk}{\rho true} \qquad \text{(Eq. 3)}$$

2.2.4.4. *Drug content*

CN content (n = 3) was determined using high-performance liquid chromatography (HPLC-UV; Agilent 1260, Agilent Technologies, Santa Clara, CA, USA) equipped with an UV-Vis detector and a reverse-phase column (IYMC-Pack ODS, 50 × 4.6 mm, 3 µm, YMC Co., Ltd., Kyoto, Japan), maintained at 30 °C. The mobile phase, *i.e.* a mixture of methanol and pH 3.5 phosphate buffer in water for HPLC (70:30, *v*/*v*) [45], was filtered before use (0.45 µm membrane filter) and pumped at a flow rate of 1 mL/min at 30 °C. The time of the run was set at 4 min. The sample to be evaluated (20 mg) was initially dispersed in 250 mL of mobile phase and then ultrasonicated for 30 min to ensure complete CN dissolution. The resulting liquid, filtered through a 0.45 µm PVDF syringe filter, was transferred into an HPLC vial kept at 30 °C. From the latter10 µL were automatically injected into the HPLC system for being assayed spectrophotometrically (retention time = 1.6 min, λ_{MAX} = 250 nm).

2.2.4.5. *Two-stage biorelevant dissolution performance*

Two-stage biorelevant dissolution test (n = 3) was performed according to an already standardized protocol [46, 47]. A USP apparatus II was used with paddles rotating at 75 rpm. Samples containing nominal 20 mg of CN were poured into 250 mL of Fasted State Simulated Gastric Fluid (FaSSGF, pH 1.6) kept at 37 °C. 2 ml of the dissolution medium was manually withdrawn at pre-defined times (5, 10, 20, and 30 min). After 30 min, 250 mL of concentrated Fasted State Simulated Intestinal Fluid (FaSSIF, pH 7.5) was added to attain a final volume of 500 mL (pH 6.5). After this addition, 2 ml of the dissolution medium were collected at 40, 50, and 60 min. After 60 min and before taking the last sample of the dissolution media (75 min), the paddle rotation speed was increased (150 rpm). All the liquid specimens were filtered using 0.1 µm 25 mm syringe filter and assayed for CN content as described in Section 2.2.4.4. Drug content.

2.2.4.6. *Nanocrystals' redispersibility*

Nanocrystals redispersibility (n =3) was measured by means of dynamic light scattering (DLS), using a Zetasizer Nano ZS DLS instrument (Malvern Instruments, Worcestershire, UK). Samples were dispersed in 0.1 mM NaCl solution (magnetic stirrer rotating at 200 rpm). The resulting dispersions were centrifuged for 10 min, calculating centrifugal force (RCF) and rotor rpm to be able to separate finer excipient particles from the nanocrystals. Z-average (z-avg.) and polydispersity index (PdI) were used as characteristic values for differentiating the redispersibility of the tested granules. Data were compared to the original NS dimension through the redispersibility index (RDI) [41]. RDI was calculated (Eq. 4) by normalizing the mean particle size of the redispersed nanocrystals (z-avg.redisp) to the mean NS particle size (z-avg.orig):

$$RDI = \frac{\text{z-avg.redisp}}{\text{z-avg.orig}} \qquad \text{(Eq. 4)}$$

2.2.4.7. *Compaction study*

Round flat face compacts (11.28 mm diameter, compact mass 550 mg) were manufactured, using a single punch tableting machine (STYL'one nano PV-S6-005, Medelpharm, Beynost, France) equipped with an automatic feeding system. Increasing compaction pressures were applied (50 MPa, 100 MPa, 150 MPa, 200 MPa, 300 MPa, and 400 MPa), using a standard V-shape compression profile at 10 mm/s punch speed. For each compaction pressure, 10 compacts were manufactured for further characterization.

Compacts were checked for weight, height, and diameter, out-of-die porosity, hardness, and disintegration time. Their weight, height, diameter, and hardness were assessed immediately after compaction using a semi-automatic tablet tester (Sotax MT50, Aesch, Switzerland). The out-of-die porosity was calculated on 10 compacts produced at each compaction pressure:

$$Porosity\ (\%) = \left(1 - \frac{\text{Tablet density}}{\text{True density}}\right) * 100 \qquad \text{(Eq. 5)}$$

where the tablet density was calculated taking into account its weight and the theoretical volume. Tensile Strength (σ, MPa) [48] of the compacts was calculated using the following equation:

$$\sigma = \frac{2*\text{hardness (N)}}{\pi*\text{diameter (mm)}*\text{thickness (mm)}} \quad \text{(Eq. 6)}$$

2.2.5. *DoE*

The DoE approach was applied to set the experimental trials, and the collected data were subsequently analyzed using multiple linear regression (Table 2) (OriginLab Corporation, Northampton, MA, USA). The same program was used to calculate the regression coefficients of the statistical models as well as their significant values and to attain descriptive plots. When the *p-values* were less than 0.05, the differences were considered statistically significant.

Table 2. Levels of the independent variables considered in the DoE.

Factors	**Level**	
	-1	**1**
X_1 = insoluble filler	PGS	SYL
X_2 = soluble filler	LAC	MAN
X_3 = filler ratio	70:30	30:70

2.2.5.1. Statistical model

A Full Factorial Design (2^3) was set up, considering 3 factors, each to be evaluated on 2 different levels, resulting in a total of 8 runs. The type of fillers (X_1, insoluble; X_2, soluble) and their ratio within the blends (X_3) were assigned to be the independent parameters (Table 3). The selected dependent responses were CN amount (mg/100mg), RDI, ε of the granules, out-of-the-die porosity for tablets obtained under 50 MPa, and tensile strength for tablets obtained at 200 MPa. The results were analyzed by multiple linear regression analysis, enabling the calculation of the coefficients of the mathematical model correlating factors and responses, which was described by the following equation:

$$y = \beta_0 + \beta_1 X_1 + \beta_2 X_2 + \ldots \beta_i X_i + \varepsilon \quad \text{(Eq. 7)}$$

Where y is the dependent variable or response, X_1, X_2, and Xi are the independent variables or factors, β_0 is the intercept, β_1, β_2 and β_i are the coefficients of independent values, and ε is the residual error.

Table 3. Experimental matrix of the full factorial design

Code	**Insoluble filler**	**Soluble filler**	**Filler ratio**
	X_1	**X_2**	**X_3**
N1	-1	-1	-1
N2	1	-1	-1
N3	-1	1	-1
N4	1	1	-1
N5	-1	-1	1
N6	1	-1	1
N7	-1	1	1
N8	1	1	1

The interaction plot was employed as a qualitative graphical tool to explore potential interactions between the parameters investigated. The results were statistically analyzed using OriginPro, Version 2025 (OriginLab Corporation, Northampton, MA, USA), which performed three-way analysis of variance (ANOVA). When the *p-values* were less than 0.05, the differences were considered statistically significant. In addition, the OriginPro software was also used to plot the data as interaction and radar charts, as discussed in the Results Section.

2.2.6. *Permeability/Bioavailability study*

2.2.6.1. *Caco-2 cell culture and differentiation*

Human intestinal Caco-2 cells, obtained from INSERM (Paris, France), were routinely cultured in Dulbecco's Modified Eagle Medium (DMEM) containing 25 mM of glucose, 3.7 g/L of $NaHCO_3$, 4 mM of stable L-glutamine, 1% nonessential amino acids, 100 U/L of penicillin, and 100 µg/L of streptomycin (complete medium), supplemented with 10% heat-inactivated fetal bovine serum (FBS; Hyclone Laboratories, Logan, UT, USA). For differentiation, they were seeded on polycarbonate filters, 12 mm diameter, 0.4 µm pore diameter (Transwell, Corning Inc., Lowell, MA, USA) at a 3.0 × 105 cells/cm^2 density in complete medium supplemented

with 10% FBS in both apical (AP) and basolateral (BL) compartments to allow the formation of a confluent cell monolayer. After 2 days, cells were then supplemented with 10% Hyclone FBS and allowed to differentiate for 21 days with regular medium changes three times weekly.

2.2.6.2. *3-(4,5-Dimethylthiazol-2-yl)-2,5-diphenyltetrazolium bromide (MTT) assay*

The MTT experiments were conducted on human intestinal Caco-2 cells. Briefly, a total of 3×10^4 cells/well were seeded in 96-well plates and, after 24 h, treated with cinnarizine nano 0.000001 to 1.0 mg/mL, or vehicle, in complete growth media for 48 h at 37 °C under 5% CO_2 atmosphere. Subsequently, the treatment was aspirated, and 100 µL/well of MTT filtered solution was added. After 2 h of incubation at 37 °C under a 5% CO_2 atmosphere, 0.5 mg/mL solution was aspirated, and 100 µL/well of the lysis buffer (8 mM HCl + 0.5% NP-40 in dimethyl sulfoxide, DMSO) was added. After 10 min of slow shaking, the absorbance at 575 nm was read on the Synergy H1 fluorescence plate reader (Biotek, Bad Friedrichshall, Germany).

2.2.6.3. *Cell monolayers integrity evaluation and intestinal absorption experiments*

The trans-epithelial electrical resistance (TEER) of differentiated Caco-2 cells was measured at 37 °C using the voltmeter apparatus Millicell (Millipore Co., Billerica, MA, USA), immediately before, at time 0, 30, 60, and 120 min until the end of the transport experiments. According to previously published conditions [49], CN intestinal absorption was assessed in differentiated Caco-2 cells in transport buffer solution (137 mM NaCl, 5.36 mM KCl, 1.26 mM CaCl2, and 1.1 mM $MgCl_2$, 5.5 mM glucose). The AP solutions were kept at pH 6.0 (buffered with 10 mM morpholinoethane sulfonic acid), and the BL solutions were kept at pH 7.4 (buffered with 10 mM N-(2-Hydroxyethyl)piperazine-N'-(4-butanesulfonic acid)) to replicate the pH conditions found *in vivo* in the small intestinal mucosa. Before the transport assay, cells were equilibrated in Hanks' Balanced Salt Solution (HBSS) for 15 min at 37 °C. CN-containing samples were added to the AP compartment by dissolving it in AP transport solution (500 µL) at the final concentration of 3.7 µg/mL (corresponding to 1.0 µM of CN), while in the BL compartment was added the BL transport solution (700 µL). At the end of the absorption experiment carried out for 120 min at 37 °C, the

BL solutions were collected and kept at −80°C before analysis. Transport experiments were performed in duplicate.

The CN-containing samples used to treat the AP compartment at time 0 (t_0 sample) was retained and used as a reference for compound identification by mass spectrometry in BL solution after 2 hours of the absorption experiment.

2.2.6.4. *Mass spectrometry analysis (UHPLC-MS/MS)*

All samples were dried and then dissolved in 100 µL of a solution of 90% water and 10% acetonitrile. Then, they have been analyzed at UNITECH OMICs (University of Milano, Italy) using Agilent 1290 Infinity II LC (Agilent) connected to an Agilent 6495 LC/TQ (Agilent). Chromatographic separation was achieved on a ZORBAX ECLIPSE PLUS C18 (Agilent) 50 mm (Length) x 2.1 mm (ID) x 1.8 µm (Particle Size) using mobile phase A (water with formic acid 0,1%) and mobile phase B (acetonitrile with formic acid 0,1%) at a flow rate of 400 µL/min. The column and autosampler temperatures were set at 40°C and 15°C, respectively. The sample injection volume was 1 µL. Data processing was performed using MassHunter Workstation LC/MS Data Acquisition software version 10.1 (Agilent).

3. Results and discussion

3.1 Manufacturing

In this work, we investigated the feasibility of a lab-scale twin-screw wet granulator (TSWG) in combination with a fluid-bed dryer (FBD) in converting a liquid NS into multiparticulate products in a single step, thus coupling advantages of nanotherapeutics (*i.e.,* increased solubility and dissolution rate of the drug) with those associated with a CM-compliant solidification technique, while improving processing sustainability. The core idea behind the study design was to directly feed a model NS containing CN (CN NS) into a twin-screw granulator. To avoid the need to modify the NS formulation, which would require additional stability testing, this study explored the use of TSWG with dry binder addition [50]. In this set-up, the liquid NS served not only as a dispersion medium for the nanoscale API, but also as an *in situ* binder solvent. A combination of different soluble and insoluble hygroscopic fillers was selected for the experiments. This method is designed to allow the formulations to absorb

substantial amounts of water while supporting granule compactability and promoting rapid disintegration and dissolution in the final product. Alongside a spray-dried lactose (LAC) traditionally used for tableting [51], mannitol (MAN) was tested as an alternative option, being highly water-soluble, giving a pleasant feeling in the mouth, and having different mechanical properties (*i.e.,* greater brittleness) coupled with well-known good compactability behavior [52, 53]. On the other hand, insoluble fillers with highly specific surface area, such as a silica-based mesoporous carrier (SYL) and pregelatinized maize starch (PGS) were chosen considering their capability to absorb high volumes of liquids [54-56]. PVP K30 was employed as the dry binder to be *in situ* solubilized during the manufacturing process [50]. To ensure further processing (*i.e.,* tableting, glidant (A200), superdisintegrant (EXP), and a lubricant (SSF) were also included in the granule formulation.

A 2^3 full factorial design was applied to investigate the effect of LAC, MAN, SYL, and PGS included in different quantities and combinations on the properties of the resulting granules. The DoE outputs evaluated were: API loading (*i.e.,* CN amount, mg/100mg), NS dimensional stability (*i.e.,* RDI), and physical-technological properties of the prepared granules (*i.e.,* ε). Moreover, following the idea of directly tabletting the granules, a compression study was carried out evaluating the features of the final tablets. In this respect, the tensile strength at 200 MPa and tablet porosity at 50 MPa were selected as the key outputs.

Prior to TSWG trials, the water uptake threshold for each formulation (*i.e.,* the L/S ratio leading to a slurry paste) was experimentally defined. The selected final L/S ratio values turned out to be dependent on the type and amount of insoluble filler added. Moreover, it impacted the granulation liquid throughput and thus the pump rate to be set during processing. In particular, SYL showed better moisture uptake ability with respect to PGS, regardless of the soluble filler selected. The different NS formulations tested required modifying fluidised bed drying conditions, which led to varying drying times. Dried granules quali-quantitative compositions, and the processing parameters are reported in Tables 4 and 5, respectively.

Table 4. Nominal composition (amount, wt%) of the dry granules defined by the DoE

	N1	**N2**	**N3**	**N4**	**N5**	**N6**	**N7**	**N8**
LAC	21.4	20.1	-	-	51.3	47.9	-	-
MAN	-	-	21.4	20.1	-	-	51.3	47.9
SYL	-	46.9	-	46.9	-	20.5	-	20.5
PGS	49.8	-	49.8	-	22.0	-	22.0	-
EXP	13.9	13.0	13.9	13.0	14.3	13.3	14.3	13.3
A200	0.5	0.4	0.5	0.4	0.5	0.5	0.5	0.5
PVP K30	2.3	2.2	2.3	2.2	2.4	2.2	2.4	2.2
SSF	4.6	4.4	4.6	4.4	4.7	4.5	4.7	4.5
CN	6.0	10.4	6.0	10.4	3.8	8.9	3.8	8.9
TPGS	1.5	2.6	1.5	2.6	1.0	2.2	1.0	2.2
L/S ratio	0.65	1.2	0.65	1.2	0.4	1.0	0.4	1.0

Table 5. Processing parameters set

	N1	**N2**	**N3**	**N4**	**N5**	**N6**	**N7**	**N8**
Granulation liquid throughput (g/h)	162.5	300	162.5	300	100	250	100	250
Granulation liquid pump rate (rpm)	19.0	35.5	19.0	35.5	11.6	29.5	11.6	29.5
Dryer inlet air temperature (°C)	65	65	65	80	80	80	80	80
Dryer inlet air flow rate (bar)	0.5	0.5	0.4	0.4	0.4	0.5	0.5	0.5

3.2. Characterization

All the TSWG trials were successful, leading to multi-particulate systems with good physical-technological characteristics in terms of dimensions, flowability, and mechanical strength, visualized by a minimum dust loss during handling, and a granular porosity (ε) in the 0.6-0.8 range. This was deemed particularly promising in view of the sought dissolution release performance. In Table 6, data relevant to the multiple linear regression for all the analyzed samples are summarized.

Table 6. Multiple linear regression results and significance values (F, p) for model terms

Response	Intercept (β_0)	X_1	X_2	X_3	X_1*X_2	X_1*X_3	X_2*X_3	$X_1*X_2*X_3$	R^2	Adj. R^2	F-value (model)	p-value (model)
API loading	95.36708	13.28375 (F = 559.34) (p < 0.0001)	3.74625 (F = 44.49) (p < 0.0001)	–12.26125 (F = 476.55) (p < 0.0001)	–0.97542 (F = 3.02) (p = 0.1017)	–11.09292 (F = 390.06) (p < 0.0001)	–4.70708 (F = 70.23) (p < 0.0001)	1.41625 (F = 6.36) (p = 0.0227)	0.98978	0.98531	221.43	<0.0001
RDI	1.26875	0.07125 (F = 5.83) (p = 0.0281)	–0.09042 (F = 9.39) (p = 0.0074)	–0.06542 (F = 4.92) (p = 0.0414)	0.09208 (F = 9.74) (p = 0.0066)	–0.23292 (F = 62.32) (p < 0.0001)	–0.08792 (F = 8.88) (p = 0.0088)	0.07125 (F = 5.83) (p = 0.0281)	0.86983	0.81288	15.27	<0.0001
Fractional Porosity (ε)	0.69875	0.04817 (F = 551.29) (p < 0.0001)	0.01125 (F = 30.07) (p < 0.0001)	–0.01642 (F = 64.04) (p < 0.0001)	–0.003 (F = 2.14) (p = 0.163)	–0.0485 (F = 558.95) (p < 0.0001)	0.00425 (F = 4.29) (p = 0.0548)	0.00417 (F = 4.13) (p = 0.0592)	0.98700	0.98131	173.56	<0.0001
Porosity (50 MPa)	35.975	9.11667 (F = 17536.06) (p < 0.0001)	–0.11667 (F = 2.87) (p = 0.1095)	–3.50833 (F = 2596.94) (p < 0.0001)	–0.45833 (F = 44.32) (p < 0.0001)	–1.45 (F = 443.60) (p < 0.0001)	0.91667 (F = 177.29) (p < 0.0001)	–0.14167 (F = 4.23) (p = 0.0563)	0.99923	0.99890	2972.19	<0.0001
Tensile Strength (200 MPa)	2.60417	1.22083 (F = 300.17) (p < 0.0001)	0.17917 (F = 6.47) (p = 0.0217)	0.1875 (F = 7.08) (p = 0.0171)	–0.00417 (F = 0.0035) (p = 0.9536)	–0.5625 (F = 63.72) (p < 0.0001)	0.2125 (F = 9.09) (p = 0.0082)	0.02917 (F = 0.17) (p = 0.6844)	0.96027	0.94289	55.24	<0.0001

Responses were also plotted in the following Figures. The degree of non-parallelism between lines indicates the extent of interaction: non-parallel lines suggest an interaction, while crossing lines imply a strong interaction between factors. By way of example, interaction plots for the X_1*X_2*X_3 factors, which were shown to be statistically significant, are reported in Figure 1.

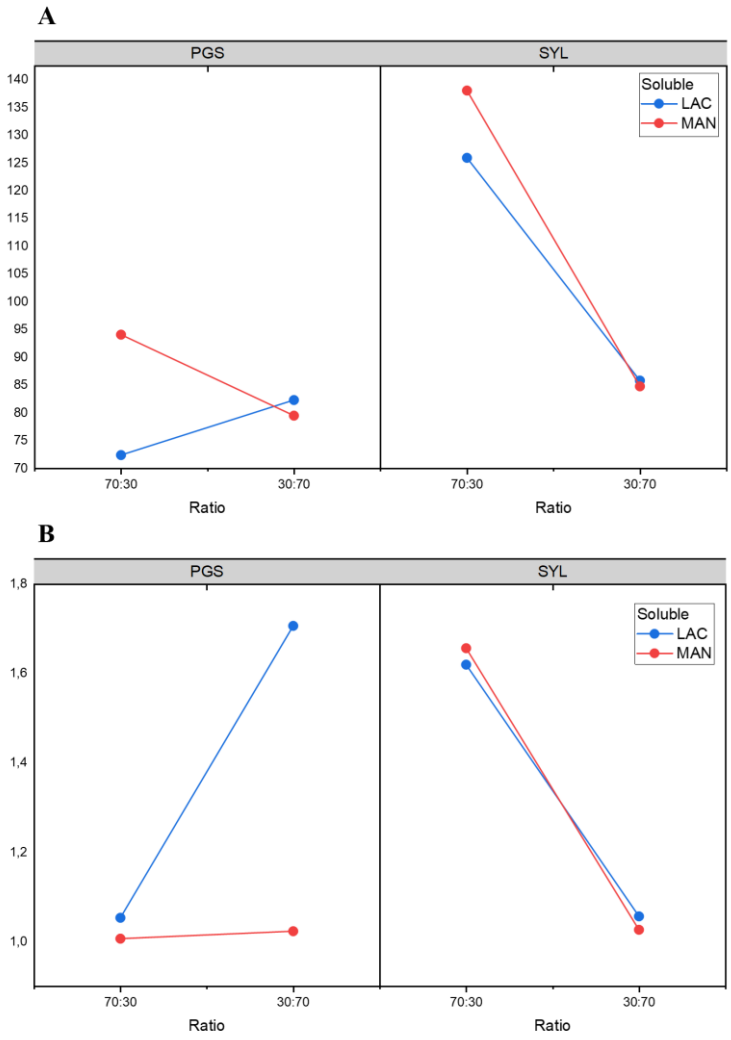

Figure 1. Graphical illustration for the significant factors interaction (X_1*X_2*X_3) influence on A) API loading, and B) RDI.

The CN load was expressed as a percentage relative to the nominal L/S ratio, enabling more precise assessment of process quality and NS load accuracy, and serving as a baseline for further optimization. According to the DoE interaction plots (Figure 1A, 1B), SYL showed higher drug loading than PGS, likely because its greater surface area and moisture uptake enabled more efficient NS incorporation (Table 7). Additionally,

higher proportions of insoluble material, regardless of the type, consistently led to an increased drug retention, confirming that the absolute quantity of water-absorbing matrix played a critical role. As for the soluble carrier, MAN exhibited a slightly more favourable aptitude than LAC, further supporting its suitability in facilitating the integration of liquid-based systems within the granulation matrix.

Table 7. CN content and RDI of the granules

	N1	**N2**	**N3**	**N4**	**N5**	**N6**	**N7**	**N8**
CN Loading (%)	72.41 ± 0.32	125.94 ± 0.99	94.09 ± 1.01	138.73 ± 5.78	82.32 ± 0.54	85.81 ± 0.62	79.51 ±1.08	84.78 ± 0.79
RDI	1.06 ± 0.06	1.63 ± 0.1	1.00 ± 0.02	1.52 ± 0.12	1.17 ±0.05	1.04 ± 0.08	1.04 ± 0.02	1.06 ± 0.01

The preservation of CN nanoscale dimensions after the TSWG process was preliminarily assessed by redispersing the granules attained and checking nanocrystals for average particle size and distribution in comparison with the values relevant to the NS. A near 1 RDI value would suggest that the nanocrystals were optimally redispersed from granules, considering a RDI <1.20 acceptable [57, 58]. CN nanocrystals were generally redispersible, and only minor differences were observed based on the type of moisture-absorbing carrier material utilized (see Table 7). Granules with PMS showed good redispersibility (RDI < 1.17). In contrast, SYL effect depended on concentration: lower SYL levels resulted in optimal RDI, while higher amounts led to poorer nanocrystal dispersion. However, a relatively low correlation coefficient was calculated for this feature. To this end, the above-mentioned findings could also be ascribed to specific constraints of the analytical protocol. Indeed, laser diffraction data relevant to samples containing SYL revealed finer particle size (D10 < 3 μm, relevant to Span values), which can be hard to separate from the CN nanocrystals during sample preparation. On the other hand, the polydispersity index of the NS was maintained after redispersion of N1 and N3 formulations, while in all the other cases showed a tendency to increase, even over 0.5, which was associated to a broad particle size distribution [59]. According to this hypothesis, the statistical significance of the model turned out to be poor for the RDI parameter.

Recognising that solid CN NS stability may affect drug dissolution, this impact was carefully assessed. Since CN is a weak organic base (pK_{a1} = 1.94 and pK_{a2} = 7.47), showing a pH-dependent solubility (2 µg/ml at pH 6.5, increasing up to 2110 µg/ml at acidic pH) [60], a two-stage dissolution test using biorelevant media was set up to assess the performance of the micronized DS, compared to initial NS and compared to relevant formulations in different conditions. CN dissolution profiles from nanocrystal-containing granules, having diverse L/S ratios, are reported in Figure 2B, alongside those relevant to drug powder as such and to the starting NS, for comparison purposes (Figure 2A).

As expected, CN NS showed a faster dissolution rate than the micronized API, being completely dissolved within 10 min. With respect to CN micronized powder ($t_{90\%}$ ~ 30 min), CN NS displayed a better performance, even in a dissolution medium that was expected to be poorly discriminating for a weak-base compound (FaSSGF, pH 1.6). Considering that the solid dissolution rate is a function of the surface area exposed to the aqueous fluids, as described by the Noyes-Whitney equation [28, 31], data turned out consistent with the higher CN nanocrystals' specific surface area (SSA, 10'520 m^2/kg) compared to the micronized CN (SSA, 167,07 m^2/kg).

On the other hand, simulated intestinal conditions represented an unfavourable environment for CN to dissolve. Irrespective of the particle size, being transferred from a highly acidic environment into FaSSIF adjusted to pH 6.5, both micronized CN and CN NS showed a tendency to supersaturate and precipitate [61, 62], having an erratic lower amount of drug dissolved displayed in the profiles. Granules release performance turned out to be consistent with the NS data. Considering NS $t_{90\%}$ ~ 5 min, different formulations were capable of releasing more than 90% of the loaded nanosized drug substance within 5 min. Finally, changing the media pH, a deflection of the CN dissolution profile could also be appreciated for granules.

To this end, granule porosity has probably played a pivotal role. This feature turned out to be correlated with the formulation parameters, even if interactions were less significant. In all tested formulations, product porosity was sufficient so that solvent-wetted area did not limit dissolution performance.

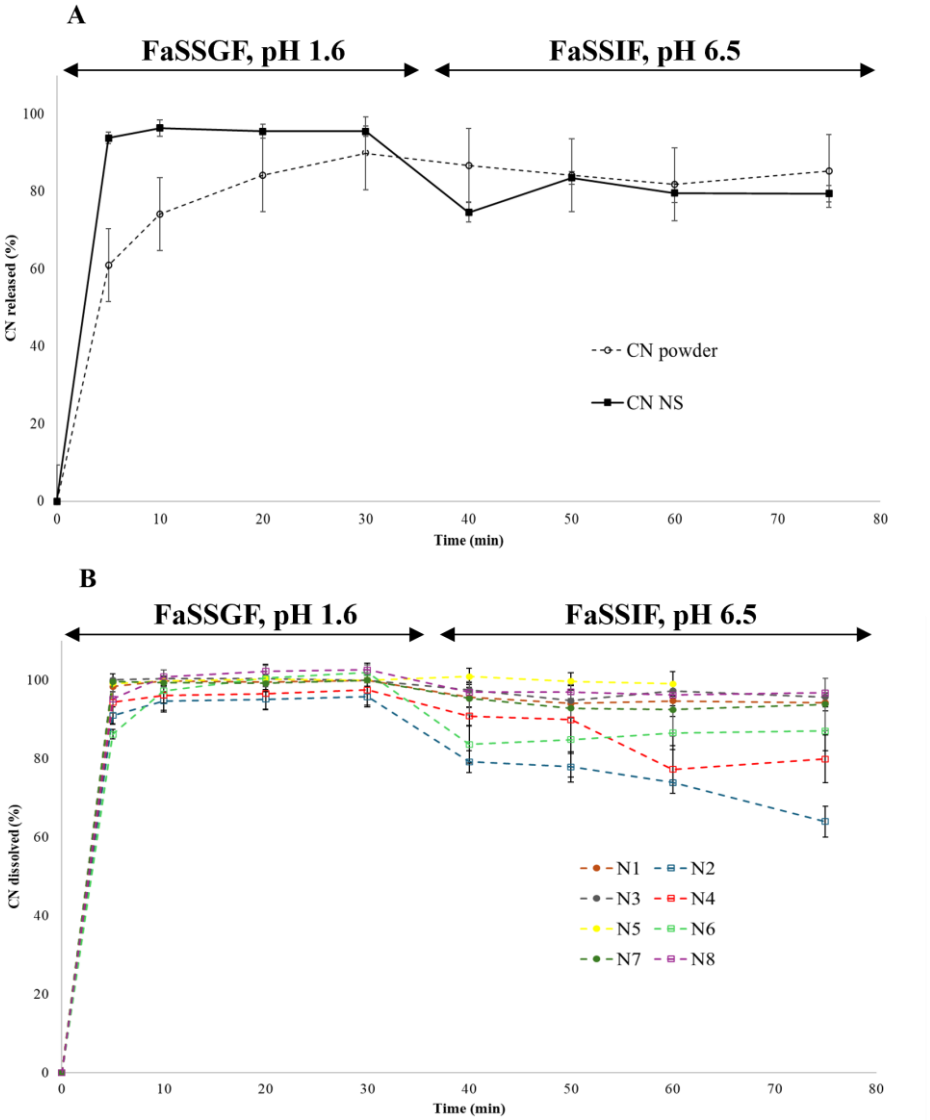

Figure 2. Comparative dissolution profiles relevant to (A) CN powder *versus* CN NS, and (B) CN NS-containing granules.

3.3. Bioavailability study

To further check the impact of the TSWG process in solidifying the NS, preliminary data relevant to CN NS bioavailability on human intestinal Caco-2 cells were collected [63-65]. This experiment was intended to preliminarily demonstrate the ability of the CN NS to permeate the epithelial barrier, rather than to perform a kinetic study.

Before performing experiments at cellular level, MTT assays were performed to evaluate any samples cytotoxic effect on Caco-2 cells (Figure 3). According to the

results in Figure 3A, CN NS did not negatively impact on Caco-2 cells viability up to 10 μg/mL (0.01 mg/mL). Conversely, the findings revealed a reduction in cells viability of 12.42 ± 0.56 %, and 23.93 ± 5.59 %, at 0.1 and 1 mg/mL, respectively. According to MTT results, a safe concentration of 3.7 μg/mL of CN in the nanosize, corresponding to 1 μM of CN, was employed for bioavailability studies on differentiated Caco-2 cells. As reported in Figure 3B and C, CN NS-containing samples did not alter the TEER values during transport experiments, suggesting that the NS did not cause any damage to the differentiated Caco-2 cells monolayer integrity. Finally, mass spectrometry analysis was carried out on the BL sample, revealing a peak at a retention time of tR = 2.94 min (Figure 4). This peak is attributable to the presence of CN, confirming the detection of this molecule in the BL compartment. This finding suggested that the molecule has been successfully transported across the Caco-2 cell monolayer.

Overall, the bioavailability study revealed that the nanosized CN was able to be absorbed and to cross the cell monolayer without impacting the viability of the Caco-2 cells and the monolayer integrity.

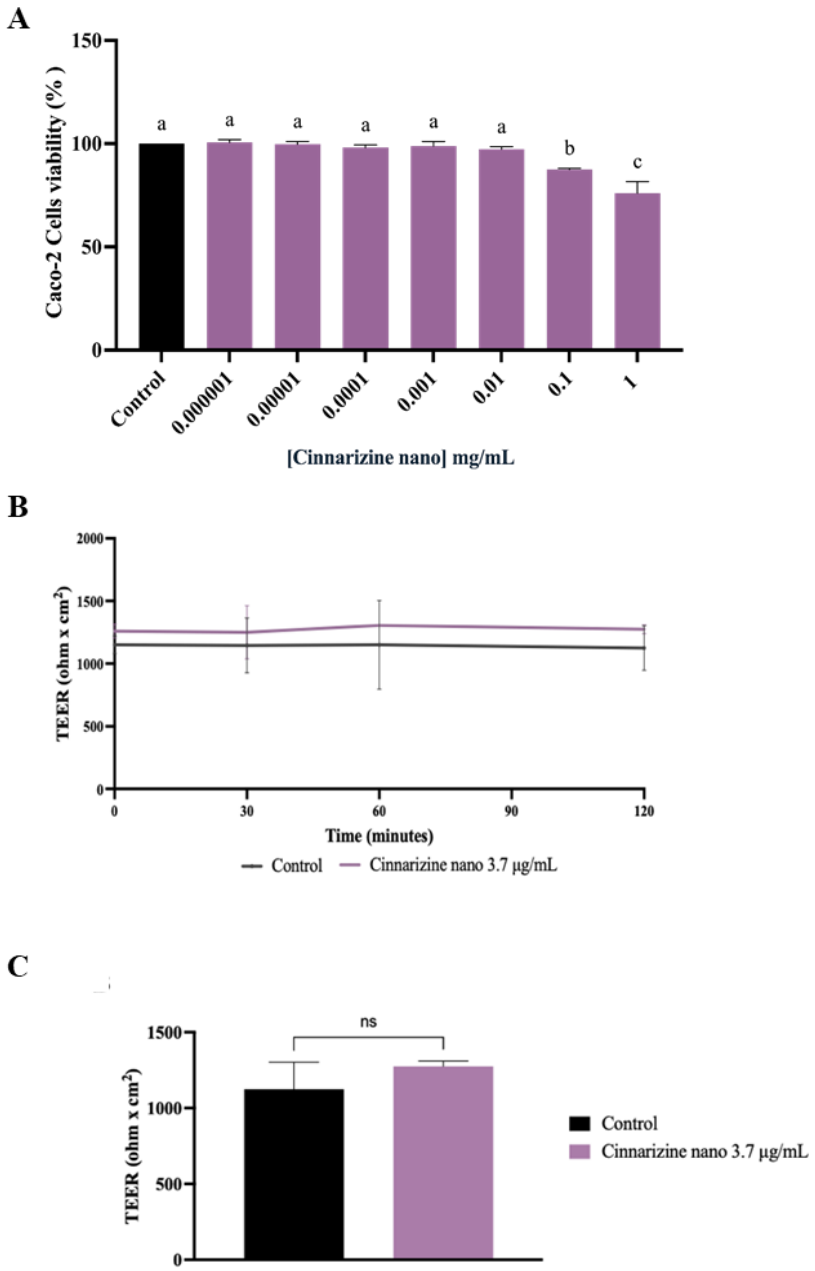

Figure 3. Preliminary assays on Caco-2 cells: (A) MTT assay: bars represent the mean ± s.d. of three independent experiments performed in triplicate and statistically analyzed by One-way Anova followed by Tukey's post-hoc test; statistical differences among different concentrations of treatment are indicated by different letters ($p < 0.05$). TEER measurements in differentiated Caco-2 monolayer during trans-epithelial transport experiments: (B) time course of TEER changes recorded in 2 h in untreated (control) and treated with CN-containing sample; (C) TEER values after 120 min; data are the mean ±S.D. of an experiment performed in duplicate; ns: not significant.

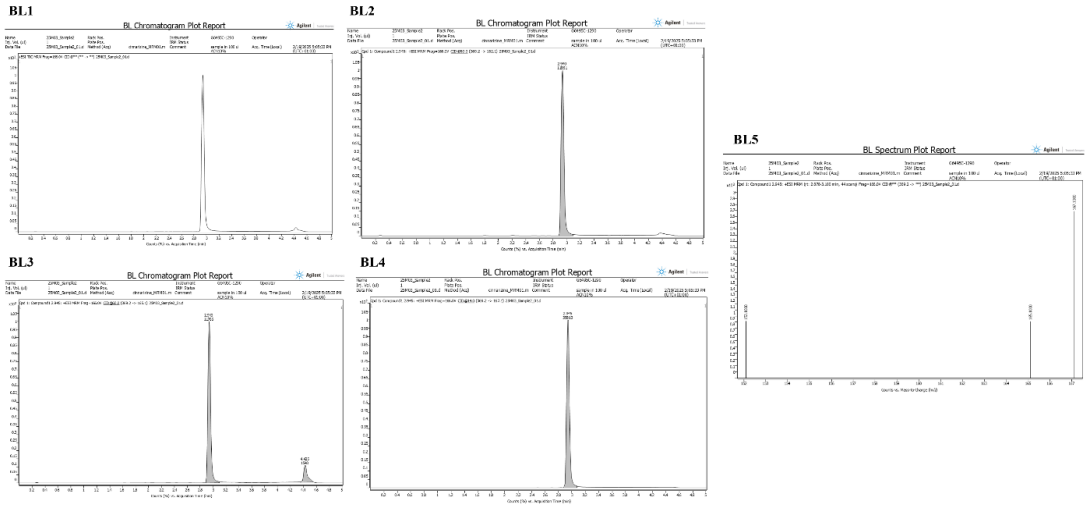

Figure 4. MS spectra of different BL samples.

3.4. Compaction studies

TSWG granules were also used as intermediates for tablet production, to explore their potential towards further processing, especially considering that tablets are the most common and preferred dosage form for oral administration. To achieve this, the effects of formulation parameters on the compaction characteristics of granules were examined by measuring tablet porosity and tensile strength.

The DoE analysis showed that porosity values mainly depended on the amount and type of insoluble excipient. Increasing compaction pressure lowered tablet porosity, but SYL-based granulates still had over 15% porosity with high amounts of insoluble filler (Figure 5A). At 50 MPa, only the soluble filler type and ratio significantly affected porosity.

Figure 5B shows the tabletability of N1-8 formulations. A tensile strength (σ) of 1.6 MPa is reported as the benchmark for adequate cohesion [66]. In terms of tabletability, PGS proved to be the most promising filler. Only when combined with MAN in relatively lower quantities, SYL succeeded in achieving a similar tabletability profile. Such findings could be ascribed to different materials' behavior when compacted, being PGS a plastic-deforming material and having a viscoelastic component [67]. Statistical evaluation of the tensile strength parameter at 200 MPa confirmed these observations. Indeed, σ varied depending on the ratio and the type of soluble used

(LAC or MAN) for both PGS and SYL. For PGS, tensile strength increased when moving from the 70:30 to the 30:70 ratio, with MAN showing a higher tensile strength compared to LAC at both ratios. Conversely, for SYL, tensile strength decreased as the ratio shifted from 70:30 to 30:70. Overall, MAN tended to provide better tensile strength compared to LAC in both materials, but the effect of the ratio was opposite for PGS (*i.e.,* increasing strength) and SYL (*i.e.,* decreasing strength).

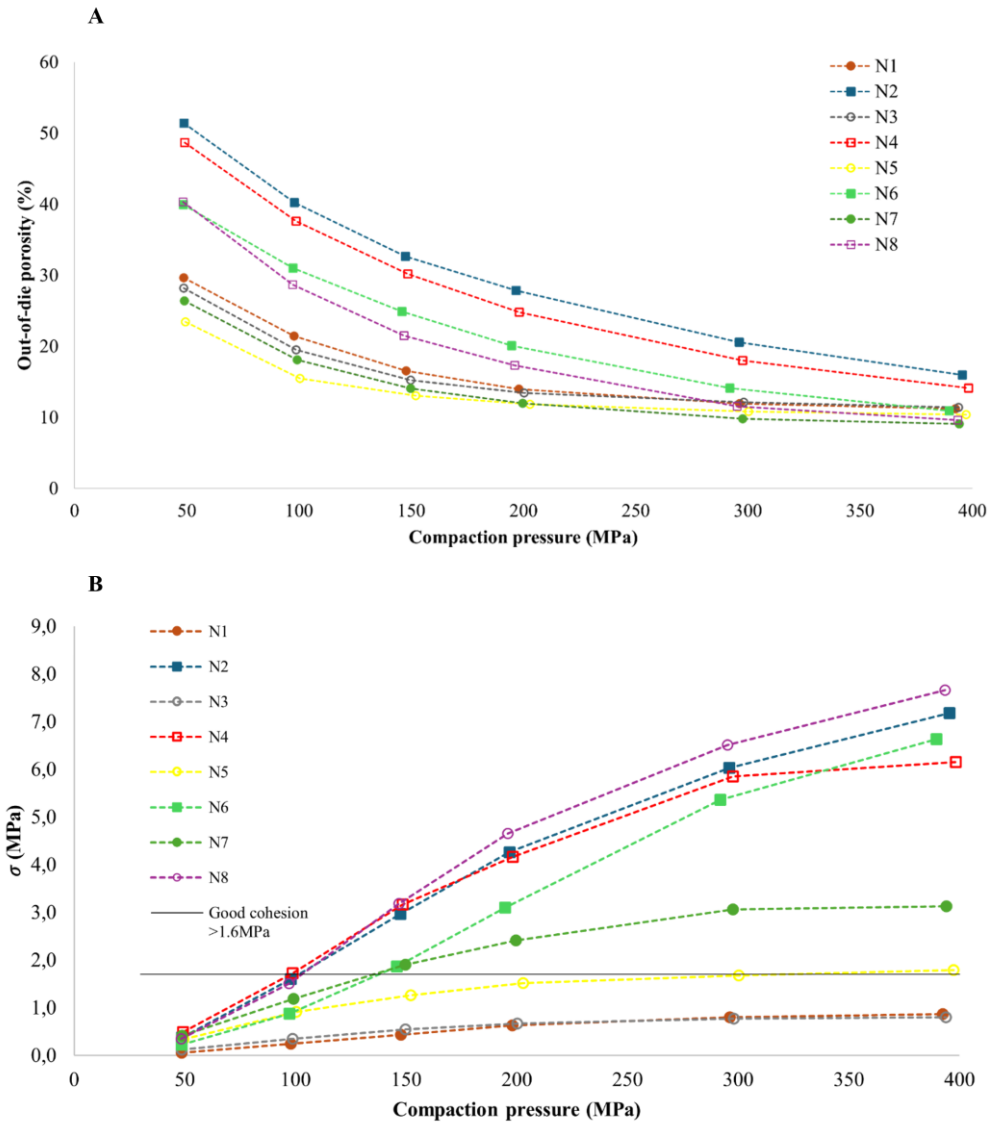

Figure 5. Overall, A) compressibility and B) tabletability profiles relevant to N1-8 batches.

Radar charts relevant to formulations with different filler ratios were finally built (Figure 6) for visually assessing the overall quality and balance of each formulation,

highlighting overall strengths and weaknesses across the key characterization responses. Specifically, these radar charts enabled a holistic comparison of multiple critical quality attributes simultaneously, providing a visual tool to identify promising formulations. More into details, the findings were converted into five-dimensional radar charts and standardized between 0 and 2, where the highest score corresponded to the most desirable value. The 2 value was attributed to: an RDI equal to 1, an API loading equal to 100%, a porosity (ε) equal to 0.6, a tensile strength >2 MPa, and a tablet porosity equal to 60% at 50 MPa.

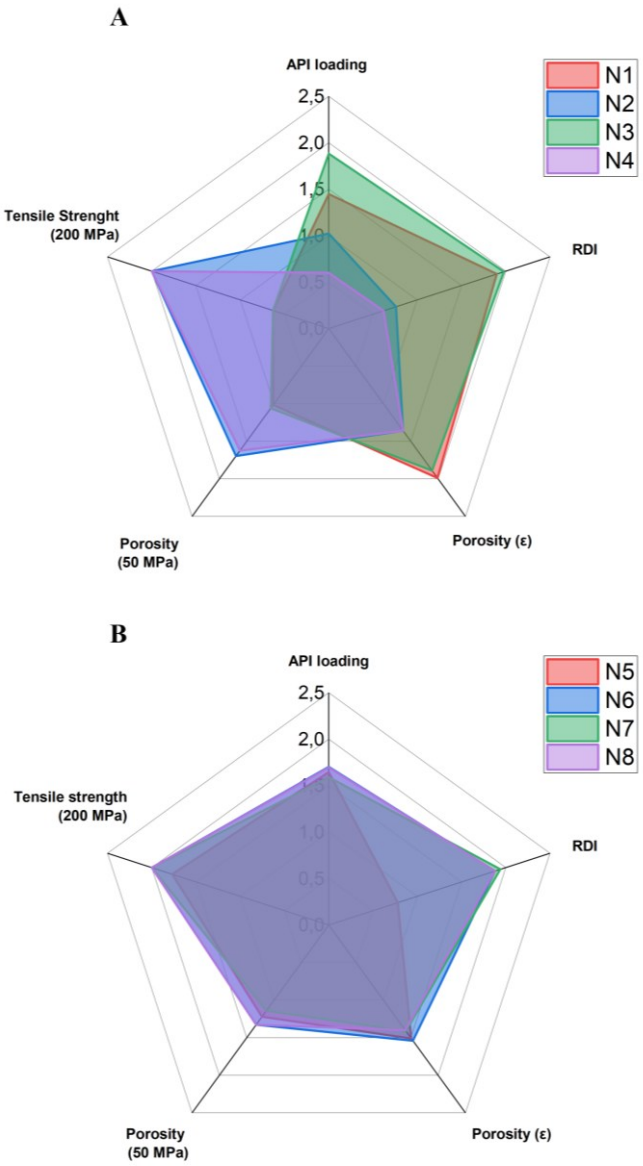

Figure 6. Radar chart showing the multivariate comparison of granule formulations based on (A) 30:70 and (B) 70:30 ratio between soluble and insoluble fillers across key performance attributes. Data were normalized (0–2) on the set optimal values to allow visual comparison across different units and scales.

Overall, the results showed that the type of insoluble filler (X_1) and the ratio between soluble and insoluble fillers (X_3) in the formulation of granules had the major impact on the selected outputs. Indeed, formulations N1-N4 (*i.e.,* with higher X_1) exhibited more variable and less balanced profiles, while N5-N8 (*i.e.,* with lower X_1) presented a more uniform and optimized landscape, pointing out superimposable X_1-dependent profiles.

These trends can be mechanistically rationalized by considering the distinct physicochemical behavior of the insoluble components and, thus, their different mechanism of interactions with the liquid NS during the manufacturing process. PGS undergoes partial hydration and swelling upon contact with the aqueous NS, promoting plastic deformation and cohesive wet mass formation. This behavior supports effective granule growth and drug distribution but may limit internal densification during subsequent drying and sieving, resulting in comparatively lower mechanical strength and less efficient consolidation upon compaction. Conversely, SYL, a mesoporous silica, primarily absorbs and retains liquid within its internal pore network rather than swelling, leading to granules that maintain a rigid internal structure after drying. This liquid-retentive and porous architecture would favor higher tensile strength, improved compaction behavior, and well-defined compact porosity, without negatively impacting drug incorporation.

More specifically, N1 and N3 PGS-based formulations were characterized by similar compressed polygons, with a limited radial extension in compacts relevant responses and with CN load, RDI, and ε values pointing to the optimal values. The presence of MAN as the soluble filler in N3 resulted in a modest improvement compared to N1, suggesting a beneficial contribution of the soluble filler to granule consolidation within PGS-based systems. In contrast, N2 and N4 granules with SYL had symmetric profiles and showed better mechanical strength when compacted, but only moderate porosity and CN loading, reflecting enhanced mechanical performance upon compaction, although the overall balance across all normalized parameters remained moderate.

From this evaluation, the standout formulations were those containing lower amounts of SYL irrespective of the soluble filler coupled (*i.e.,* N6 and N8). Indeed, relevant granules showed nearly overlapping, expansive profiles, reflecting strong balance and optimal responses across all parameters. Formulations containing PGS and MAN (*e.g.,* N7) also performed well, as the combination of plastic insoluble filler with a highly soluble filler facilitated uniform drug distribution and moderate densification, supporting both mechanical integrity and CN loading. While structurally presenting a regular polygon, N5 and N7 analogous formulations containing PGS slightly diverged from the other profiles, mainly displaying suboptimal out-of-die porosities and drug content, likely reflecting the reduced contribution of insoluble filler to structural

reinforcement compared to SYL-based counterparts. In this case, the presence of MAN as the soluble filler (formulation N7) turned out to be advantageous.

4. Conclusion

In this study, the downstream processing of nanosuspension containing poorly soluble DS using the TSWG process was demonstrated, successfully maintaining biopharmaceutical quality attributes such as an enhanced dissolution rate and bioavailability in model Caco-2 cells. Formulation factors (*e.g.,* the combination of fillers with different solubility and the presence of mesoporous silica and mannitol) for manufacturing granules with good technological properties suitable for further processing steps were identified. More importantly, a DoE-based method was demonstrated as a strategic tool to identify the formulations worth of further assessment. Overall, the results suggest considerable potential for the pharmaceutical industry, as the TSWG approach appears adaptable to different production scales, from clinical research to large-scale manufacturing.

References

1. G. Fülöp *et al.*, "Integrated twin-screw wet granulation, continuous vibrational fluid drying and milling: A fully continuous powder to granule line," *Int J Pharm*, vol. 594, Feb. 2021, doi: 10.1016/j.ijpharm.2020.120126.
2. M. Jelsch, Y. Roggo, P. Kleinebudde, and M. Krumme, "Model predictive control in pharmaceutical continuous manufacturing: A review from a user's perspective," *European Journal of Pharmaceutics and Biopharmaceutics*, vol. 159, pp. 137–142, Feb. 2021, doi: 10.1016/j.ejpb.2021.01.003.
3. H. Leuenberger, "New trends in the production of pharmaceutical granules: batch versus continuous processing," *European Journal of Pharmaceutics and Biopharmaceutics*, vol. 52, pp. 289–296, Jun. 2001.
4. S. M. Ooi, S. Sarkar, G. Van Varenbergh, K. Schoeters, and P. W. S. Heng, "Continuous processing and the applications of online tools in pharmaceutical product manufacture: Developments and examples," 2013, *Newlands Press Ltd*. doi: 10.4155/tde.13.11.
5. V. Vanhoorne and C. Vervaet, "Recent progress in continuous manufacturing of oral solid dosage forms," *Int J Pharm*, vol. 579, Apr. 2020, doi: 10.1016/j.ijpharm.2020.119194.
6. M. Fonteyne *et al.*, "Process Analytical Technology for continuous manufacturing of solid-dosage forms," Apr. 01, 2015, *Elsevier B.V.* doi: 10.1016/j.trac.2015.01.011.
7. S. L. Lee *et al.*, "Modernizing Pharmaceutical Manufacturing: from Batch to Continuous Production," Sep. 07, 2015, *Springer New York LLC*. doi: 10.1007/s12247-015-9215-8.
8. K. Plumb, "Continuous processing in the pharmaceutical industry: Changing the mind set," *Chemical Engineering Research and Design*, vol. 83, no. 6 A, pp. 730–738, 2005, doi: 10.1205/cherd.04359.
9. C. V. Rossi, "A Comparative Investment Analysis of Batch Versus Continuous Pharmaceutical Manufacturing Technologies," *J Pharm Innov*, vol. 17, no. 4, pp. 1373–1391, Dec. 2022, doi: 10.1007/s12247-021-09612-y.
10. K. P. Kashinath, L. R. Sanjay, M. K. Ashokbhai, S. Roy, M. S. Sardar, and S. Kaity, "Continuous manufacturing based paradigm shift in pharmaceuticals

production and current regulatory framework," Mar. 01, 2025, *Institution of Chemical Engineers*. doi: 10.1016/j.cherd.2025.01.003.

11. M. S. Kerr and K. P. Cole, "Sustainability case studies on the use of continuous manufacturing in pharmaceutical production," *Current Research in Green and Sustainable Chemistry*, vol. 5, Jan. 2022, doi: 10.1016/j.crgsc.2022.100279.
12. S. Mascia *et al.*, "End-to-end continuous manufacturing of pharmaceuticals: Integrated synthesis, purification, and final dosage formation," *Angewandte Chemie - International Edition*, vol. 52, no. 47, pp. 12359–12363, Nov. 2013, doi: 10.1002/anie.201305429.
13. K. P. Kashinath, L. R. Sanjay, M. K. Ashokbhai, S. Roy, M. S. Sardar, and S. Kaity, "Continuous manufacturing based paradigm shift in pharmaceuticals production and current regulatory framework," Mar. 01, 2025, *Institution of Chemical Engineers*. doi: 10.1016/j.cherd.2025.01.003.
14. L. Rogers and K. F. Jensen, "Continuous manufacturing-the Green Chemistry promise?," *Green Chemistry*, vol. 21, no. 13, pp. 3481–3498, 2019, doi: 10.1039/c9gc00773c.
15. M. R. Thompson and J. Sun, "Wet granulation in a twin-screw extruder: Implications of screw design," *J Pharm Sci*, vol. 99, no. 4, pp. 2090–2103, 2010, doi: 10.1002/jps.21973.
16. E. I. Keleb, A. Vermeire, C. Vervaet, and J. P. Remon, "Twin screw granulation as a simple and efficient tool for continuous wet granulation," *Int J Pharm*, vol. 273, no. 1–2, pp. 183–194, Apr. 2004, doi: 10.1016/j.ijpharm.2004.01.001.
17. C. Vervaet and J. P. Remon, "Continuous granulation in the pharmaceutical industry," in *Chemical Engineering Science*, Jul. 2005, pp. 3949–3957. doi: 10.1016/j.ces.2005.02.028.
18. R. M. Dhenge, R. S. Fyles, J. J. Cartwright, D. G. Doughty, M. J. Hounslow, and A. D. Salman, "Twin screw wet granulation: Granule properties," *Chemical Engineering Journal*, vol. 164, no. 2–3, pp. 322–329, Nov. 2010, doi: 10.1016/j.cej.2010.05.023.
19. J. Zhao, G. Tian, and H. Qu, "Pharmaceutical Application of Process Understanding and Optimization Techniques: A Review on the Continuous Twin-

Screw Wet Granulation," Jul. 01, 2023, *Multidisciplinary Digital Publishing Institute (MDPI)*. doi: 10.3390/biomedicines11071923.

20. A. Schmidt, H. de Waard, K. P. Moll, P. Kleinebudde, and M. Krumme, "Simplified end-to-end continuous manufacturing by feeding API suspensions in twin-screw wet granulation," *European Journal of Pharmaceutics and Biopharmaceutics*, vol. 133, pp. 224–231, Dec. 2018, doi: 10.1016/j.ejpb.2018.09.026.
21. S. Shirazian *et al.*, "Continuous twin screw wet granulation: The combined effect of process parameters on residence time, particle size, and granule morphology," *J Drug Deliv Sci Technol*, vol. 48, pp. 319–327, Dec. 2018, doi: 10.1016/j.jddst.2018.09.016.
22. A. S. El Hagrasy, J. R. Hennenkamp, M. D. Burke, J. J. Cartwright, and J. D. Litster, "Twin screw wet granulation: Influence of formulation parameters on granule properties and growth behavior," *Powder Technol*, vol. 238, pp. 108–115, Apr. 2013, doi: 10.1016/j.powtec.2012.04.035.
23. G. Bano, R. De-Luca, E. Tomba, A. Marcelli, F. Bezzo, and M. Barolo, "Primary Drying Optimization in Pharmaceutical Freeze-Drying: A Multivial Stochastic Modeling Framework," *Ind Eng Chem Res*, vol. 59, no. 11, pp. 5056–5071, Mar. 2020, doi: 10.1021/acs.iecr.9b06402.
24. N. O. Chung, M. K. Lee, and J. Lee, "Mechanism of freeze-drying drug nanosuspensions," *Int J Pharm*, vol. 437, no. 1–2, pp. 42–50, Nov. 2012, doi: 10.1016/j.ijpharm.2012.07.068.
25. E. Jakubowska, M. Bielejewski, B. Milanowski, and J. Lulek, "Freeze-drying of drug nanosuspension– study of formulation and processing factors for the optimization and characterization of redispersible cilostazol nanocrystals," *J Drug Deliv Sci Technol*, vol. 74, Aug. 2022, doi: 10.1016/j.jddst.2022.103528.
26. A. Ziaee, A. B. Albadarin, L. Padrela, T. Femmer, E. O'Reilly, and G. Walker, "Spray drying of pharmaceuticals and biopharmaceuticals: Critical parameters and experimental process optimization approaches," Jan. 15, 2019, *Elsevier B.V.* doi: 10.1016/j.ejps.2018.10.026.
27. B. E. Rabinow, "Nanosuspensions in drug delivery," Sep. 2004. doi: 10.1038/nrd1494.

28. S. Jacob, A. B. Nair, and J. Shah, “Emerging role of nanosuspensions in drug delivery systems,” Jan. 15, 2020, *BioMed Central Ltd.* doi: 10.1186/s40824-020-0184-8.
29. F. Kesisoglou, S. Panmai, and Y. Wu, “Nanosizing - Oral formulation development and biopharmaceutical evaluation,” Jul. 30, 2007. doi: 10.1016/j.addr.2007.05.003.
30. M. Bisrat and C. Nyström, “Physicochemical aspects of drug release. VIII. The relation between particle size and surface specific dissolution rate in agitated suspensions,” *Int J Pharm*, vol. 47, pp. 223–231, 1988.
31. Noyes Arthur A. and Wihtney Willis R., “Per cent. 2 1. 7 7 THE RATE OF SOLUTION OF SOLID SUBSTANCES IN THEIR OWN SOLUTIONS,” *Journal of the American Chemical Society*, no. 19, pp. 930–934, Oct. 1897.
32. V. Patel and Y. Agrawal, “Nanosuspension: An approach to enhance solubility of drugs,” *J Adv Pharm Technol Res*, vol. 2, no. 2, p. 81, 2011, doi: 10.4103/2231-4040.82950.
33. E. Merisko-Liversidge, G. G. Liversidge, and E. R. Cooper, “Nanosizing: A formulation approach for poorly-water-soluble compounds,” 2003. doi: 10.1016/S0928-0987(02)00251-8.
34. E. Merisko-Liversidge and G. G. Liversidge, “Nanosizing for oral and parenteral drug delivery: A perspective on formulating poorly-water soluble compounds using wet media milling technology,” 2011. doi: 10.1016/j.addr.2010.12.007.
35. S. M. Dizaj, Z. Vazifehasl, S. Salatin, K. Adibkia, and Y. Javadzadeh, “Nanosizing of drugs: Effect on dissolution rate,” 2015.
36. Y. Wang, Y. Zheng, L. Zhang, Q. Wang, and D. Zhang, “Stability of nanosuspensions in drug delivery,” 2013, *Elsevier B.V.* doi: 10.1016/j.jconrel.2013.08.006.
37. A. Bitterlich *et al.*, “Process parameter dependent growth phenomena of naproxen nanosuspension manufactured by wet media milling,” *European Journal of Pharmaceutics and Biopharmaceutics*, vol. 92, pp. 171–179, 2015, doi: 10.1016/j.ejpb.2015.02.031.
38. M. Malamatari, S. Somavarapu, K. M. G. Taylor, and G. Buckton, “Solidification of nanosuspensions for the production of solid oral dosage forms and inhalable

dry powders," Mar. 03, 2016, *Taylor and Francis Ltd*. doi: 10.1517/17425247.2016.1142524.

39. L. Wu, J. Zhang, and W. Watanabe, "Physical and chemical stability of drug nanoparticles," May 30, 2011. doi: 10.1016/j.addr.2011.02.001.
40. B. Van Eerdenbrugh, L. Froyen, J. Van Humbeeck, J. A. Martens, P. Augustijns, and G. Van den Mooter, "Drying of crystalline drug nanosuspensions-The importance of surface hydrophobicity on dissolution behavior upon redispersion," *European Journal of Pharmaceutical Sciences*, vol. 35, no. 1–2, pp. 127–135, Sep. 2008, doi: 10.1016/j.ejps.2008.06.009.
41. M. Wewers *et al.*, "Influence of formulation parameters on redispersibility of naproxen nanoparticles from granules produced in a fluidized bed process," *Pharmaceutics*, vol. 12, no. 4, Apr. 2020, doi: 10.3390/pharmaceutics12040363.
42. E. Ragucci *et al.*, "Feasibility of Hot Melt Extrusion in Converting Water-Based Nanosuspensions into Solid Dosage Forms," *Pharmaceutics*, vol. 17, no. 5, p. 662, May 2025, doi: 10.3390/pharmaceutics17050662.
43. S. Van de Steene, J. Van Renterghem, V. Vanhoorne, C. Vervaet, A. Kumar, and T. De Beer, "Identification of continuous twin-screw melt granulation mechanisms for different screw configurations, process settings and formulation," *Int J Pharm*, vol. 630, Jan. 2023, doi: 10.1016/j.ijpharm.2022.122322.
44. C. Portier, C. Vervaet, and V. Vanhoorne, "Continuous twin screw granulation: A review of recent progress and opportunities in formulation and equipment design," May 01, 2021, *MDPI*. doi: 10.3390/pharmaceutics13050668.
45. B. Van Eerdenbrugh *et al.*, "A screening study of surface stabilization during the production of drug nanocrystals," *J Pharm Sci*, vol. 98, no. 6, pp. 2091–2103, 2009, doi: 10.1002/jps.21563.
46. J. Mann *et al.*, "Validation of Dissolution Testing with Biorelevant Media: An OrBiTo Study," *Mol Pharm*, vol. 14, no. 12, pp. 4192–4201, Dec. 2017, doi: 10.1021/acs.molpharmaceut.7b00198.
47. P. Berben *et al.*, "Biorelevant dissolution testing of a weak base: Interlaboratory reproducibility and investigation of parameters controlling in vitro precipitation," *European Journal of Pharmaceutics and Biopharmaceutics*, vol. 140, pp. 141–148, Jul. 2019, doi: 10.1016/j.ejpb.2019.04.017.

48. M. C. I. Amin and J. T. Fell, “Tensile strength and bonding in compacts: A comparison of diametral compression and three-point bending for plastically deforming materials,” *Drug Dev Ind Pharm*, vol. 28, no. 7, pp. 809–813, 2002, doi: 10.1081/DDC-120005626.
49. C. Lammi *et al.*, “Trans-epithelial transport, metabolism and biological activity assessment of the multi-target lupin peptide lilpkhsdad (P5) and its metabolite lpkhsdad (p5-met),” *Nutrients*, vol. 13, no. 3, pp. 1–17, Mar. 2021, doi: 10.3390/nu13030863.
50. L. Vandevivere *et al.*, “Influence of binder attributes on binder effectiveness in a continuous twin screw wet granulation process via wet and dry binder addition,” *Int J Pharm*, vol. 585, Jul. 2020, doi: 10.1016/j.ijpharm.2020.119466.
51. C. Shi, H. Zhao, Y. Fang, L. Shen, and L. Zhao, “Lactose in tablets: Functionality, critical material attributes, applications, modifications and co-processed excipients,” Sep. 01, 2023, *Elsevier Ltd*. doi: 10.1016/j.drudis.2023.103696.
52. A. Megarry, A. Taylor, A. Gholami, H. Wikström, and P. Tajarobi, “Twin-screw granulation and high-shear granulation: The influence of mannitol grade on granule and tablet properties,” *Int J Pharm*, vol. 590, Nov. 2020, doi: 10.1016/j.ijpharm.2020.119890.
53. S. Paul, P. Tajarobi, C. Boissier, and C. C. Sun, “Tableting performance of various mannitol and lactose grades assessed by compaction simulation and chemometrical analysis,” *Int J Pharm*, vol. 566, pp. 24–31, Jul. 2019, doi: 10.1016/j.ijpharm.2019.05.030.
54. W. Xu, J. Riikonen, and V. P. Lehto, “Mesoporous systems for poorly soluble drugs,” 2013, *Elsevier B.V.* doi: 10.1016/j.ijpharm.2012.09.008.
55. M. Kovačević, I. German Ilić, K. Bolko Seljak, and A. Zvonar Pobirk, “High-Shear Wet Granulation of SMEDDS Based on Mesoporous Carriers for Improved Carvedilol Solubility,” *Pharmaceutics*, vol. 14, no. 10, Oct. 2022, doi: 10.3390/pharmaceutics14102077.
56. J. Zhang *et al.*, “Water absorption behavior of starch: A review of its determination methods, influencing factors, directional modification, and food applications,” Feb. 01, 2024, *Elsevier Ltd*. doi: 10.1016/j.tifs.2023.104321.

57. M. Wewers *et al.*, "Evaluation of the Formulation Parameter-Dependent Redispersibility of API Nanoparticles from Fluid Bed Granules," *Pharmaceutics*, vol. 14, no. 8, Aug. 2022, doi: 10.3390/pharmaceutics14081688.
58. X. Zhang, J. Guan, R. Ni, L. C. Li, and S. Mao, "Preparation and solidification of redispersible nanosuspensions," *J Pharm Sci*, vol. 103, no. 7, pp. 2166–2176, 2014, doi: 10.1002/jps.24015.
59. B. Hoseini, M. R. Jaafari, A. Golabpour, A. A. Momtazi-Borojeni, M. Karimi, and S. Eslami, "Application of ensemble machine learning approach to assess the factors affecting size and polydispersity index of liposomal nanoparticles," *Sci Rep*, vol. 13, no. 1, Dec. 2023, doi: 10.1038/s41598-023-43689-4.
60. M. Maghsoodi, A. Nokhodchi, M. Azhdarzadeh, and S. Heidari, "Formulation of cinnarizine for stabilization of its physiologically generated supersaturation," *AAPS PharmSciTech*, vol. 20, no. 3, p. 139, Mar. 2019, doi: 10.1208/s12249-019-1338-7.
61. M. Berlin, K. H. Przyklenk, A. Richtberg, W. Baumann, and J. B. Dressman, "Prediction of oral absorption of cinnarizine - A highly supersaturating poorly soluble weak base with borderline permeability," *European Journal of Pharmaceutics and Biopharmaceutics*, vol. 88, no. 3, pp. 795–806, 2014, doi: 10.1016/j.ejpb.2014.08.011.
62. C. H. Gu, D. Rao, R. B. Gandhi, J. Hilden, and K. Raghavan, "Using a novel multicompartment dissolution system to predict the effect of gastric pH on the oral absorption of weak bases with poor intrinsic solubility," *J Pharm Sci*, vol. 94, no. 1, pp. 199–208, 2005, doi: 10.1002/jps.20242.
63. M. Fanzaga *et al.*, "Bioavailability Assessment of an Iron Formulation Using Differentiated Human Intestinal Caco-2 Cells," *Foods*, vol. 12, no. 16, Aug. 2023, doi: 10.3390/foods12163016.
64. T. Lea, "Caco-2 cell line," in *The Impact of Food Bioactives on Health: In Vitro and Ex Vivo Models*, Springer International Publishing, 2015, pp. 103–111. doi: 10.1007/978-3-319-16104-4_10.
65. T. Lenhardt, G. Vergnault, P. Grenier, D. Scherer, and P. Langguth, "Evaluation of nanosuspensions for absorption enhancement of poorly soluble drugs: In vitro

transport studies across intestinal epithelial monolayers," *AAPS Journal*, vol. 10, no. 3, pp. 435–438, 2008, doi: 10.1208/s12248-008-9050-7.

66. A. Sauer, S. Warashina, S. M. Mishra, I. Lesser, and K. Kirchhöfer, "Downstream processing of spray-dried ASD with hypromellose acetate succinate – Roller compaction and subsequent compression into high ASD load tablets," *Int J Pharm X*, vol. 3, Dec. 2021, doi: 10.1016/j.ijpx.2021.100099.
67. J. Rojas, Y. Uribe, and A. Zuluaga, "Powder and compaction characteristics of pregelatinized starches," *Pharmazie*, vol. 67, no. 6, pp. 513–517, 2012, doi: 10.1691/ph.2012.1118.

Conclusions

This Ph.D. project originated from the need to identify novel industrially viable solidification strategies for converting liquid NSs into solid dosage forms as alternative approaches to the well-established spray drying technology followed by conventional powder-based processes. In particular, the research aimed at exploring the feasibility of multi-particulates systems (*e.g.,* pellets or granules, to be employed as such or further processed into capsules or tablets) capable of preserving the nanosized characteristics of the employed NSs and achieving different release performance (*i.e.,* ranging from immediate to modified release), while enhancing their long-term stability, manufacturability, and patient compliance.

The participation of a leading international pharmaceutical company -with a portfolio of active ingredients that present significant challenges in terms of dissolution behavior and bioavailability- profoundly shaped the trajectory of the research. This partnership introduced a pronounced industrial orientation, prioritizing not only process feasibility but also scalability, thereby supporting the advancement of innovative therapeutic candidates from early-stage development through to commercial deployment. Within this context, CN and NAP were selected as representative poorly soluble drugs, due to the potential biopharmaceutical benefits from nanosizing as well as the availability of a well-established scientific background supporting the preparation of relevant NSs. Among the various solidification techniques described in the scientific literature, hot-melt extrusion (HME) and wet granulation (WG) were selected, not only in view of their technological relevance and peculiar advantages but also considering relevant scalability and adaptability to an industrial framework. For this purpose, a wide range of polymers, potentially suitable for either hot- or wet-processing, was extensively investigated. Special emphasis was placed on evaluating their suitability as carriers in the formulation of both immediate- and modified-release products, with the objective of identifying materials that offer robust processability while preserving the nanoscale characteristics of the embedded drug. Initial feasibility trials were manually carried out to evaluate the potential of HME and WG at the lab scale, identifying their respective strengths and limitations. As a step forward, either automated or larger processing equipment was employed for both processes. To complement the experimental work and to better interpret the data collected while guiding further process optimization, a rational, model-based approach

was integrated into the investigation. In the case of HME, a model describing drug-polymer interactions (*i.e.,* T-C phase diagram) was designed, built, and tested across different processing scales. The model-based strategy turned out highly valuable in rationalizing formulation composition and processing parameters, thereby providing an in-depth understanding of the key requirements for successful scale-up and industrial translation. For WG, a full factorial formulative design of experiments (2^3) was employed to identify compositions worth further evaluation. This experimental design not only enabled a visual and systematic interpretation of the factors exerting the most significant influence on the outcomes but also demonstrated that WG *via* twin-screw extrusion would represent a promising and versatile approach for NS solidification.

Overall, the findings collected during this work suggest the considerable versatility, potential, and applicability of both HME and WG techniques across different processing scales for converting NSs into solid dosage forms. At the same time, several formulation- and process-dependent sensitivities emerged, suggesting that the methods may not be directly transferable to all APIs or equipment configurations and should be interpreted in light of the specific materials, scales, and conditions investigated.

In parallel, this study emphasized the importance of advancing the current understanding by critically examining all the variables involved, integrating rational, model-driven methodologies with a systematic exploration of both process and formulation parameters that could influence the outcomes.

Building upon this perspective, the work highlighted the need for continued research aimed at deepening the mechanistic understanding of how formulation components, drug properties, and process parameters interact to affect critical quality attributes. A more cautious and comprehensive evaluation of these interdependencies is required before robust industrial translation can be fully supported. Therefore, embracing a more comprehensive and integrative outlook was deemed crucial in this framework. This expanded perspective paves the way for several strategic directions for future research, including:

- Implementing complementary manufacturing strategies by integrating insights from the T-C model applied in hot-processing techniques with granulation method (*e.g.,* high-shear mixing), may enable the production of larger batches

suitable for subsequent scale-up through HME, targeting both immediate and modified release performances for the final product. Based on these insights, future studies could investigate hybrid strategies that combine HME and WG techniques or incorporate novel excipients, which may contribute to further optimizing NSs solidification and enabling the achievement of tailored drug release profiles, while critically assessing the practicality, scalability, and robustness of these strategies across different APIs;

- Expanding the range of NSs to validate the applicability of the investigated carriers and transformation processes, ensuring that the developed approaches are robust and broadly applicable across different poorly soluble compounds. This step is necessary to determine whether the observations made for CN and NAP can be generalized or whether compound-specific behaviour may impose further constraints;
- Systematically evaluating key process parameters for each piece of equipment considered, potentially integrating in-line process analytical technologies, can help assess their influence across the entire manufacturing chain, provide real-time monitoring of critical quality attributes, and support consistent, reproducible production as well as more efficient scale-up, ensuring overall product performance consistency. Such evaluations may also help identify where the processes show inherent robustness and where they remain sensitive to variability, thus informing their realistic industrial applicability.

Acknowledgements

I would like to express my sincere gratitude to all the people and research groups who have contributed to this doctoral work.

My deepest appreciation goes to the PhormulaMi research group at the University of Milan, for their continuous support, valuable scientific discussions, and for providing an inspiring and collaborative research environment throughout this journey. Their guidance and encouragement have been fundamental in shaping my research and professional growth.

I would also like to thank the teams of Novartis PHAD Materials Science and PHAD Continuous Manufacturing, as well as all the researchers and colleagues with whom I had the privilege to collaborate. Their expertise, commitment, and enthusiasm have greatly enriched both my scientific and personal experience. Moreover, the opportunity to conduct part of my research within an industrial environment has been particularly valuable, providing me with unique insights into the translation of scientific knowledge into practical applications and strengthening my understanding of the link between academic research and industrial innovation.

Furthermore, I am deeply grateful to the research groups of the Institute for Particle Technology (iPAT), the Center of Pharmaceutical Engineering (PVZ), and the Institute of Pharmaceutical Technology and Biopharmaceutics at Technische Universität Braunschweig (Germany). Their openness, collaboration, and scientific insight have been essential to the success of this work and have provided a valuable international perspective.